BAKU STATE UNIVERSITY

7th INTERNATIONAL CONFERENCE MTP-2021: MODERN TRENDS IN PHYSICS

DECEMBER 15-17, 2021
BAKU STATE UNIVERSITY, BAKU, AZERBAIJAN

BOOK OF ABSTRACTS

Book of Abstacts. 7th International Conference MTP-2021: Modern Trends in Physics, December 15-17, 2021, Baku State University, Baku, Azerbaijan. 220 p.

ISBN: 978-9952-546-24-8

ORGANIZING COMMITTEE:

Chairman:

Elchin Babayev	Rector of Baku State University (BSU)

Deputy chairman:

Huseyn Mammadov	Vice rector for Science and Innovations, BSU, Azerbaijan

Members:

Ali Nagiyev	Rector's advisor for Strategic Development and Relations, BSU, Azerbaijan
Sadiyar Rahimov	Director of Institute for Physical Problems under BSU, BSU, Azerbaijan
Mustafa Muradov	Deputy Director for Education, Programs and Cooperation of BSU Excellence Center, BSU, Azerbaijan
Mahir Pirguliyev	Head of the Rector's Secretariat, BSU, Azerbaijan
Maarif Jafarov	Professor, Department of Semiconductor Physics, BSU, Azerbaijan
Zohrab Aghamaliyev	Deputy Director for R&D and Innovations of BSU Excellence Center, BSU, Azerbaijan
Goncha Eyvazova	Leading researcher, BSU EC Nano Research Lab, BSU, Azerbaijan
Vusal Mammadov	Deputy Dean for Academic Affairs of the Physics Faculty, BSU, Azerbaijan
Shahla Hacıyeva	Deputy Dean for Scientific Affairs of the Physics Faculty, BSU, Azerbaijan
Majid Gojayev	Associate Professor, Theoretical Physics Department, BSU, Azerbaijan
Mehdi Mahmudov	Associate Professor, Solid State Physics Department, BSU, Azerbaijan
Rovshan Mammadov	Associate Professor, Semiconductor Physics Department, BSU, Azerbaijan
Ilyas Nasibov	Director of the Student Scientific-Technical Creativity Center, BSU, Azerbaijan

PROGRAM COMMITTEE:

Chairman:

Aydin Kazimzade	Rector's advisor for Science and Education, BSU, Azerbaijan

Members:

Arshad Saleem Bhatti	Rector of the Pakistan Virtual University, Pakistan
Zoltan Konya	Vice rector for Science and Innovations of Szeged University, Hungary
Mursal Aliyev	Director of the Scientific Research Institute of the Ministry of Defense Industry, Azerbaijan
Akos Kukovecz	Director of the Institute for Chemistry of Szeged University, Hungary
Mais Suleymanov	Director of the Center for Organization of Scientific Activity and Innovations, BSU, Azerbaijan
Alexander Cheplakov	Scientific Secretary of VBLHEP of Joint Institute for Nuclear Research, Russian Federation
Namig Dzhalilov	Director-General of Shamakhy Astrophysical Observatory of Academy of Sciences Azerbaijan (named after N. Tusi), Corresponding member of ANAS, Azerbaijan
Ahmad Abdinov	Head of the Department of Physical Electronics, BSU, Azerbaijan
Mirzayusuf Musachanov	Professor, National University of Uzbekistan, Uzbekistan
Eldar Masimov	Head of the Department of Matter Structure, BSU, Azerbaijan
Vagif Salmanov	Head of the Department of Semiconductor Physics, BSU, Azerbaijan
Mammad Aliyev	Head of the Department of Solid State Physics, BSU, Azerbaijan

Rena Gasimova	Head of the Department of Optics and Molecular Physics, BSU, Azerbaijan
Faig Pashayev	Head of the Department of Chemical Physics of Nanomaterials, BSU, Azerbaijan
Mammad Rajabov	Acting Head of the Department of Theoretical Physics, BSU, Azerbaijan
Kamala Alisheva	Acting Head of the Department of Astrophysics, BSU, Azerbaijan
Eldar Alakbarov	Acting Head of the Department of General Physics and Methods of Teaching Physics, BSU, Azerbaijan
Alexander Vodopiyanov	Head of VBLHEP division of Joint Institute for Nuclear Research, Russian Federation
Farhad Rustamov	Head of Condensed Matter department, Institute for Physical Problems under BSU, BSU, Azerbaijan
Gennady Zinovjev	Head of the Department at the Institute of Theoretical Physics of the National Academy of Sciences of Ukraine, Ukraine
Namig Ahmedov	Head of Biophysics department, Institute for Physical Problems under BSU, BSU, Azerbaijan
Shahin Agayev	Head of the Department Theoretical physics under BSU, Institute for Physical Problems, BSU, Azerbaijan
Sajida Abdulvahabova	Professor, Department of Matter Structure, BSU, Azerbaijan
Sofiya Figarova	Professor, Department of Solid State Physics, BSU, Azerbaijan
Ali Huseynov	Professor, Department of Semiconductor Physics, BSU, Azerbaijan
Gulnara Akverdieva	Leading researcher, Institute for Physical Problems under BSU, BSU, Azerbaijan
Sajid Qamar	Professor, COMSATS University, Pakistan
Boris Belashev	Professor, Karelian Research Center of the Russian Academy of Sciences, Russian Federation

SPECTROSCOPIC ELLIPSOMETRY AND FREE CARRIER PLASMA EDGE: TOPOLOGICAL INSULATORS CASE

Mamedov N.T.
Institute of Physics, Azerbaijan National Academy of Sciences, Azerbaijan
n.mamedov@physics.ab.az; mamedov@pe.osakafu-u.ac.jp

Spectroscopic ellipsometry is commonly recognized as one of the most powerful tools for optical studies of the various excitations in solids and liquids. Being a self-referring optical technique, it is superior over optical reflection and allows more accurate determination of such a fundamental material constant as dielectric function in a broad photon energy range.

Quantum phases of matter continue to be among the hottest spots of condensed matter physics. Especially strong interest is attracted to topological insulators, rapidly growing worldwide after the recent discovery of the first magnetic topological insulator.

The purpose of this paper is to overview the current status of the research on topological insulators, focusing on free carrier plasma edge and plasmons of non-magnetic and magnetic topological insulators.

The author acknowledges the support of the Science Development Foundation under the President of the Republic of Azerbaijan (grant number EİF-BGM-4-RFTF-1/2017-21/04/1-M-02).

MAGNETOHYDRODYNAMIC SEISMOLOGY OF THE CORONA OF THE SUN

Nakariakov Valery
University of Warwick, United Kingdom
Special Astrophysical Observatory of RAS, St. Petersburg, Russia
v.nakariakov@warwick.ac.uk

Processes operating in the outer part of the atmosphere of the Sun, the fully-ionized and magnetically-dominated plasma of the solar corona,

remain one of the major puzzles of the Solar System. The intensively debated research topics are enigmatic problems of coronal heating, rapid release of a huge amount of magnetic energy in solar flares and coronal mass ejections, microphysical processes responsible for effective acceleration of charged particles and anomalous values of transport coefficients, and so on. The solar physics research community is well supported by a number of ground-based and spaceborne observational facilities providing us with a wealth of high-precision data throughout the electromagnetic wave spectrum, from radio to gamma-rays. However, several key parameters of the solar corona, such as the magnetic field and coronal heating function, as well as effective coefficients of thermal conduction, viscosity and resistivity, are not open to direct observations. The method of magnetohydrodynamic (MHD) seismology, based on the estimation of plasma parameters by MHD waves, provide us with a paradigm changing diagnostic tool for probing the plasma in the corona. Modern MHD seismology utilizes confidently detected kink, sausage and slow MHD modes of various plasma structures to reveal key parameters of the corona, and processes operating there. In the talk, we present the current state-of-the-art in MHD seismology.

GLUONS, LIGHT AND HEAVY QUARKS IN THE INSTANTON LIQUID MODEL OF QCD VACUUM

Musakhanov Mirzayusuf
National University of Uzbekistan
musakhanov@gmail.com

Outline
1. Instanton Liquid Model (ILM);
2. Light quarks in ILM;
3. Gluons in ILM;
4. Heavy quark correlators with perturbative corrections in ILM;
5. Heavy quarks-light quarks interactions in ILM;
6. Discussion.

Talk is based on the following publications:
1. MM, N. Rakhimov, U. Yakhshiev, e-Print: 2103.16628 [hep-ph];
2. MM, N. Rakhimov, U. Yakhshiev, Phys. Rev. D102(2020)076022;
3. MM, Sh. Baratov, N. Rakhimov, Phys. Rev. D 99 (2019) 7, 074005;
4. MM, O. Egamberdiev, Phys. Lett. B 779 (2018) 206;
5. MM, EPJ Web Conf. 137 (2017) 03013;
6. U. Yakhshiev, H. C. Kim, MM, E. Hiyama, B. Turimov, Chin.Phys.C41(2017)083102.

MODELING AND SIMULATION OF STRUCTURE-PROPERTY RELATIONS IN FE-BASED NANOALLOYS VIA COMPUTATIONAL MATERIALS SCIENCE

Mekhrabov A.O., Irmak E.A., Akdeniz M.V.
Novel Alloys Design and Development Laboratory (NOVALAB)
Department of Metallurgical and Materials Engineering, METU, Ankara, Turkey
amekh@metu.edu.tr

The presentation will be an overview of the main research thrusts at the "Novel Alloys Design and Development Lab" (NOVALAB) of MetE-METU in the designing and development of advanced metallic materials for technological applications. Fundamental principles and main aspects of *Computational Materials Science (CMS)* for *modeling and simulation based "alloy design"* which has been developed over 25 years at NOVALAB, will be presented**.** Main goals of CMS are the establishments of principles and also algorithms for providing of computer-based modeling and simulation studies replicating experimental conditions as nearly as possible, or in other words to provide computer-based experiment for materials design.

Application of this new approach for the designing and utilization of advanced Fe-based nanoalloys with enhanced physico-chemical properties will be discussed. Nanoalloys are present very complex structures and

properties, which crucially depend on their size, composition and chemical ordering, and which can therefore be tailored for specific and industrially relevant applications - as in data storage, optical devices, catalysis etc. So, controlling and tailoring the structure and properties of nanoalloys, and determining their phase diagrams, require the concerted effort of experiment and computer modeling and simulation. This lecture will address the problem of integrating computation and experiment into a new coherent methodology of widespread applicability aimed at designing structure of nanoalloys, determining their phase diagrams and their magnetic, optical and catalytic properties in view of new technological applications. Special emphasis will be given on the modeling and simulation of structural stability and local structural evolutions in 6 nanometer $FeNi_3$ nanoparticles at a wide temperature range (300-1700 K) by using classical molecular dynamics (MD) simulation method combined with embedded atom model (EAM) in Large-scale Atomic/Molecular Massively Parallel Simulator (LAMMPS).

WHY QUANTUM FIELD THEORY IN EARLY UNIVERSE IS FAR FROM BEING WELL UNDERSTOOD

Akhmedov E.T.
Moscow Institute of Physics and Technology, Russia
akhmedov@itep.ru

We discuss equilibration process in expanding universes as compared to the thermalization process in Minkowski space--time. The final goal is to answer the following question: Is the equilibrium reached before the rapid expansion stops and quantum effects have a negligible effect on the background geometry or stress--energy fluxes in a highly curved early Universe have strong effects on the expansion rate and the equilibrium is reached only after the drastic decrease of the space--time curvature? We argue that consideration of more generic non--invariant states in theories with invariant actions is a necessary ingredient to understand quantum field dynamics in strongly curved backgrounds. We are talking about such states in which correlation functions are not functions of such isometry

invariants as geodesic distances, while having correct UV behavior. The reason to consider such states is the presence of IR secular memory effects for generic time dependent backgrounds, which are totally absent in equilibrium. These effects strongly affect the destiny of observables in highly curved space--times.

DEVELOPMENTS AND CHALLENGES İN SOLAR CELL TECHNOLOGY: MATERİALS AND PROCESSES

S. Ismat Shah
Department of Materials Sceince and Physics
University of Delaware, Newark, Delaware, USA
Ismat@udel.edu

Recent developments in solar cells materials and relevant technologies have made the Levelized Cost of Electricity (LCOE) of PV comparable to the cost of electricity produced from natural gas burning or by land-based wind turbines. Although the vast majority of commercial production is still based on Si (polycrystalline and thin films), there are some exciting developments in alternative materials and device designs. These materials and devices have much better quantum efficiencies than silicon-based solar cells and provide easier manufacturing routes. However, there are still challenges related to the stability and longevity of materials and devices. For example, perovskite-based solar cells are still of interest but the problem related to their temporal instability has slowed down the progress of developing perovskite-based solar cells modules in the last couple of years. Polymer-based solar cells still have continued interest but they too suffer the air and moisture-related degradation and can only be suitable for some niche applications. I will give a review of the latest developments in solar cell technology. I will also describe the challenges that still need to be tackled for this technology to continue pace with the alternative technologies, especially wind, that are simultaneously being pursued.

OBSERVATION OF DIFFERENT SCENARIOS IN DIFFERENT TEMPERATURES IN SMALL AND LARGE COLLISION SYSTEMS AT HIGH ENERGIES

Muhammad Ajaz
Abdul Wali Khan University, Pakistan
muhammad.ajaz@cern.ch

We used the modified Hagedron function and analyzed the experimental data measured by the BRAHMS, STAR, PHENIX and ALICE Collaborations in Copper-Copper, Gold-Gold, deuteron-Gold, Lead-Lead, proton-Lead and proton-proton collisions, and extracted the related parameters (kinetic freeze-out temperature, transverse flow velocity, kinetic freeze-out volume, mean transverse momentum and initial temperature) from the transverse momentum spectra of the particles (non-strange and strange particles). We observed that all the above parameters decrease from central to peripheral collisions, except transverse flow velocity which remains unchanged from central to peripheral collisions. The kinetic freeze-out temperature depends on the cross-section interaction of the particle such that larger cross-section of the particle corresponds to smaller T0, and reveals the two kinetic freeze-out scenario, while the initial temperature depends on the mass of the particle and it increase with the particle mass. The transverse flow velocity and mean transverse momentum depends on the mass of the particle and the former decrease while the later increase with the particle mass. In addition, the kinetic freeze-out volume also decreases with particle mass which reveals the volume differential freeze-out scenario and indicates different freeze-out surfaces for different particles. We also extracted the entropy index-parameter n and the parameter N0, and the former remains almost unchanged while the later decrease from central to peripheral collisions. Furthermore, the kinetic freeze-out temperature, transverse flow velocity, kinetic freeze-out volume, initial temperature, mean transverse momentum and the parameter N0 at LHC are larger than that of RHIC, and they show their dependence on the collision cross-section as well as on collision energy at RHIC and LHC.

SEARCH FOR ASSOCIATED PRODUCTION OF A HIGGS BOSON AND A SINGLE TOP QUARK USING P-P COLLISIONS AT 13 TeV WITH THE ATLAS DETECTOR IN THE H→bb FINAL STATE

Huseynov Nazim, Igor Boyko, Oksana Koval
Joint Institute for Nuclear Research, Russia
nguseynov@jinr.ru

The Yukawa coupling of the Higgs boson to the top quark is a key parameter of the Standard Model (SM). It can be determined from the ratio of the top quark mass and Higgs field vacuum expectation value, from the cross section of gg→H production through a top quark loop, from the cross sections of the processes gg/qq→ttH, or from the cross sections of the processes gq→t(t)Hq, which is a tree-level process at lowest order in perturbation theory. Comparison of these measurements has the potential to identify and disambiguate new physics effects that can modify the tHq production cross section relative to the SM expectation.

STUDY OF THE ASSOCIATED PRODUCTION OF HIGGS BOSON WITH VECTOR BOSON

Ahmadov F.N.
Institute of Physics of ANAS, Baku, Azerbaijan
Joint Institute for Nuclear Research, Dubna, Russia
fahmadov@jinr.ru

The associated production of the Higgs boson with vector boson (where the Higgs boson decays into $b\bar{b}$ and vector bosons into leptons) was studied in two stages: 1. at the level of event generation and 2. at the level of event reconstruction. Analysis at the level of event generation, signal events were generated using three generators CompHEP, PYTHIA and POWHEG. The first two generators were used to generate the main background processes VV and $Vb\bar{b}$ (where *V* is either a W or *Z* boson). The distributions of the kinematic variables for the signal process ($VHb\bar{b}$), ob-

tained from different generators were compared. The distributions obtained from CompHEP and PYTHIA are in good agreement with each other. The slight difference between the distributions obtained from POWHEG and the other two is due to the use of different parton distribution functions (PDF). CompHEP and PYTHIA use leading order PDF, while POWHEG use next to leading order PDF.

The main goal of analyzing generated events is to find variables that improve the signal-to-background ratio. The cosine of the angle between the direction of the lepton in the rest frame of the vector boson and the direction of the vector boson in the center of mass system of VH can become such a variable. The distribution of this variable for the signal has a different shape than for the background processes. By cutting out events with a higher absolute value of this variable, we can significantly improve the signal-to-background ratio.

The analysis of the reconstructed events is carried out using various algorithms of the multivariate analysis method. After a preliminary check, two algorithms were selected that gave the best results (BDT and ANN). Later, these two algorithms were compared using higher statistics of signal and background events. It turned out that BDT gives slightly better results and faster than ANN. The angular variable mentioned above was used as one of the input variables for BDT and ANN. Despite the improvement in the results of both WH and ZH channels when analyzing the generated events, in the case of reconstructed events this variable does not give the expected improvement for the WH channel due to the inaccuracy of the neutrino reconstruction.

TO OBSERVE THE PRODUCTİON OF Φ MESONS AT SPS ENERGİES

Uzma Tabassam, Mujtaba Ali
COMSATS University Islamabad Campus, Pakistan
uzma.tabassam@comsats.edu.pk

The study of ϕ meson help us to understand the properties of QGP via strangeness enhancement, which is the main observable to study the properties of hot and dense medium produced as a result of heavy ion collision. ϕ meson is one of the most interesting hadrons, because it consists of an s and an $\bar{s}$ valence

quark with solely small admixtures of mild valence quarks. Its strangeness vanishes, which make it a pure hadron scenario, ϕ production is insensitive to strangeness-related effects. On the other hand, if partonic levels of freedom are significant, the ϕ will behave like a doubly-strange particle. Therefore, ϕ mesons are expected to play a key role in studies of phenomena related to the phase transition separating the confined hadron and deconfined parton phase, the quark-gluon plasma. The transition is considered to occur in heavy ion collisions in the lower CERN SPS energy regime. Such parton matter may (can) be detected in the final state of nuclear collisions by studying the onset of medium effects which cannot be explained by hadron processes. Doubly-strange hadrons are considered to be sensitive to those medium effects.

The ϕ vector meson, lightest bound state of strange and anti-strange quarks, is considered as a good probe for the study of QCD matter formed in heavy-ion collisions. We have reported the transverse momentum (p_T) and rapidity (y) distributions of ϕ mesons in pp collisions at SPS, LHC and RHIC energies in the kinematic interval of $0 < p_T < 1.5$ GeV/c over a wide rapidity region. The results of Monte Carlo Simulation using PYTHIA8 event generator are compared to NA61/SHINE, ALICE and STAR data based on LHC and RHIC respectively. The PYTHIA 8 is tuned to color reconnection mode 0 and 1 (CR0, CR1). The CR0 is MPI based default tune while CR1 is QCD based tune. CR0 provides a good description of the ALICE data, while CR1 tune explains the ALICE data better than CR0. There are seen some deviations at low p_T values. The observed deviations in the distribution are due to the kinematics involved in the model. In case of PYTHIA8 default (CR0) the deviations are due to the multi parton interactions and for CR1 tune the non-perturbative QCD effects are more dominant which are due to parton fragmentation as discussed in Lund string model used in PYTHIA8. PYTHIA8, does not explain the STAR data. The quantitative analysis has also been performed by taking the ratio of Monte Carlo data to experiment data and deviations are within the uncertainty limit.

CHARMED Λ_c^+ BARYON PRODUCTION IN PP AND P-PB COLLISIONS AT 5.02 TeV

Yasir Ali, Hifza Zeenat
COMSATS University Islamabad Campus, Pakistan
yasir_ali@comsats.edu.pk

The main goal of relativistic heavy-ion collision is to create and explore the properties of a new strongly interacting hot and dense state of matter, called Quark-Gluon Plasma (QGP). The QGP consists of de-confined quarks and gluons, that contribute as separate degrees of freedom, created at extremely high temperatures and energy densities [1]. In high energy hadronic collisions, heavy flavor hadrons containing charm or beauty quarks play a key role in understanding the QCD: from the investigation of their production mechanisms in proton-proton (pp) collisions to the Cold Nuclear Matter (CNM) effects in proton-nucleus (p–A) collisions and their suppression in the presence of Quark-Gluon Plasma (QGP) in nucleus-nucleus (A–A) collisions. To get better understanding of the charmed hadron formation processes and charm-quark hadronisation, it is very crucial to study the relative production of baryons and mesons (heavy-flavour hadrons). The charmed baryon-to-meson ratio (Λ_c^+/D^0) in heavy-ion collisions is sensitive to the charm hadronisation mechanisms after the QGP phase because the hadronisation process of charm quark can be affected by its interaction with the QGP medium constituents.

We are presenting the spectra for p_T-differential production cross section of charmed Λ_c^+ baryon in pp and p–Pb collisions at 5.02 TeV in the transverse momentum range of $1<p_T<12$ GeV/c and $1<p_T<24$ GeV/c respectively. For this analysis we have used Monte Carlo simulation Model PYTHIA 8.303. The transverse momentum spectra are plotted in the rapidity interval of $|y|<0.5$ for pp collisions, and $-0.96 < y < 0.04$, $1.5 < y < 4.0$ (Forward) and $-2.5 < y < -4.0$ (Backward) for p-Pb collisions. Baryon to meson ratio Λ_c^+/D^0 as a function of transverse momentum and rapidity is also plotted to understand the charmed Λ_c^+ baryon enhancement relative to D^0 meson. The nuclear modification factor R_{pPb} for Λ_c^+ and D^0 at mid-rapidity calculated from the cross sections in pp and in p–Pb collisions, is also presented. The transverse momentum distributions of Λ_c^+ and Λ_c^+/D^0 ratios as a function of p_T

are well explained by PYTHIA 8 CR tunes that implements color reconnection beyond leading color approximations. PYTHIA 8 with MPI and QCD based CR Model mimic flow-like features which gives enhanced Λ_c^+ baryon production relative to D^0 meson at low p_T.

PYTHIA8 AND HIJING2 PREDICTIONS FOR THE Xe − Xe COLLISIONS AT $\sqrt{s}_{NN}$ = 5.44 T eV

Zain Ul Abidin, Uzma Tabassum
Department of Physics, COMSATS University Islamabad Campus, Park Road Chak Shahzad, Islamabad, Pakistan
zain15101991@gmail.com

In the current analysis we have studied the minimum bias differential yield of primary charged particles $\pi^+ \pi^-$, $K^+ K^-$, pp, strange particles K_s^0, $\Lambda^+ \Lambda^-$, $\Xi^+ \Xi^-$ and Ω, produced in Xe − Xe collisions at $\sqrt{s}_{NN}$ = 5.44 TeV as a function of p_T in kinematics range of $0 < p_T < 6$ GeV /c in pseudorapidity region of $|\eta| < 0.8$ using PYTHIA8 and HIJING2 models. The simulation data is compared with ALICE data at LHC. The PYTHIA8 predictions describe the ALICE data at low p_T values, while underestimates than ALICE data at high p_T values. The HIJING2 shows the same behavior as predicted by the ALICE data. We have found that the integrated yield of strange and multi-strange hadrons, relative to pions, kaons and protons increases significantly with p_T.

PROPERTIES OF TWO-BARRIER SCHOTTKY DIODES

Mamedov R., Aslanova A.
Baku State University, Baku, Azerbaijan
rasimaz50@yahoo.com

By measuring the scanning probe microscopy (SPM) methods, an additional electric field (AEF) was discovered in the edge region of the contact, which is well used for unambiguous interpretation of many features

of real Schottky diodes (SDs) that are difficult to interpret with the theory of ideal rectifying contacts metal - semiconductor (CMS). The AEF, which arises due to the potential difference between the interface surface and adjacent free surfaces of the semiconductor and metal, exists in almost all real CMS. Unfortunately, the effect of AEF on the properties of SD is still poorly understood.

AEF of SD penetrates into the peripheral near-contact region of the semiconductor and covers the edge part of the contact interface. The AEF intensity is directed from the edge part of the metal contact surface to the free surfaces of the contacting materials. The common contact surface of the SD consists of an inner part with a potential barrier height Φ_{B1} and an edge part with a AEF and a potential barrier height Φ_{B2}, where $\Phi_{B1} > \Phi_{B2}$. Under the influence of AEF, a redistribution of charge carriers occurs in the peripheral near-contact region and a voltage drop ($-U_C$) occurs. When the external circuit of the SD is short-circuited, I_o flows through the edge part of the contact, which is determined by the following formula:

$$I_O = SAT^2 \, exp(-\frac{\Phi_{B2}}{kT}) \left[exp(-\frac{qU_C}{kT}) - 1 \right]$$

The results of measurements of the dimensional dependences of the current passage into the metal - nSi SD with a potential barrier height of about 0.7 eV and different diameters (6-1000 μm) show that the contribution of the current I_o to the total diode current becomes insignificant at forward bias. In the case of reverse bias, it noticeably affects the current-voltage characteristic of the SD and causes a premature electrical breakdown of the junction. The breakdown voltage of the SD decreases with an increase in the contact diameter. The study of the current passage into the metal - nGaAs SD with a potential barrier height of about 1.1 eV and different diameters (5-500 μm) shows that the contribution of the current I_o to the total SD current significantly affects both the forward and reverse directions. The forward branches of the I - V characteristic of the Au - nGaAs SD are shifted by the U_C of the AEF in the direction of increasing voltage. The reverse branches of the I – V characteristic of the SD almost entirely consist of the edge currents of the contact. The reverse branches of the I – V characteristic of the SD almost entirely consist of the edge currents of the contact. The saturation currents of the SD in the forward

and reverse directions differ significantly from each other and the difference between them increases with a decrease in the contact diameter and for a SD with a diameter of 5 μm it is about 2 orders of magnitude.

PAULI FORM FACTOR $N + \gamma^* \to R(1710)$ TRANSITION IN THE HARD-WALL AdS/QCD MODEL

Taghiyeva Sh.I.
Baku State University, Baku, Azerbaijan
shahnaz.ilqarzadeh.92@mail.ru

The hard-wall and soft-wall models are the typical ones in the bottom-up approaches in holographic QCD. I define Pauli form factor of the $N + \gamma^* \to R(1710)$ transition in the hard-wall model framework. I define Pauli form factor within vacuum expectation of the nucleon's vector current is compared with electromagnetic current as following:

$$F_{Pauli}(Q^2) = \eta_V \frac{M}{2} \int_0^{z_m} dz z^2 V(Q,z) \sum_\tau c_\tau^{RN} \left(f_{\tau,0}^L(z) f_{\tau,1}^R(z) + f_{\tau,1}^L(z) f_{\tau,0}^R(z)\right) \quad (1)$$

Where, $M = m_{nuc.} + m_{Rop.}$, the functions $f_{\tau,n=0,1}^{L/R}(z)$ are the bulk profiles of fermions with specific $n = 0$ or $n = 1$. My result is close to the results of different theoretical approaches.

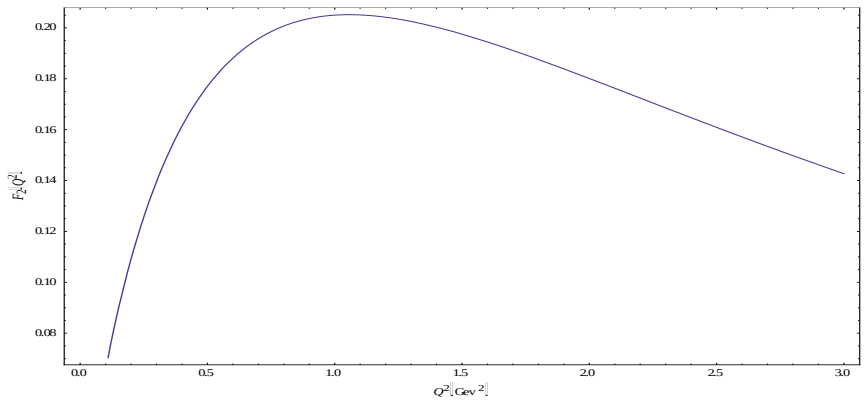

Fig. 1. F_{Pauli}^P form factor for $p + \gamma \to R_p$ transition

SEARCH FOR THE EXPERIMENTAL SIGNAL OF THE "BASIC" OBJECT OF UNIVERSE- OSCILLATING STRINGS AT THE LHC

Suleymanov Mais
Baku State University, Azerbaijan
mais.suleymanov@bsu.edu.az

We have discussed the experimental results obtained from the analysis of the p_T distributions of the charged and neutral particles produced in the p+p; Pb+Pb collisions at LHC energies. It was observed these distributions contained several p_T regions with special properties. Observation of the p_T regions for both *pp* and for Pb–Pb collisions suggests that these regions can reflect the fragmentation and hadronization properties of partons.

The regions could be characterized by the length L^c_K and two free fitting parameters a^c_K and b^c_K (upper indexes *c* show the type of events to which the region applies and lower ones *K* indicate the number of the region).

For Pb+Pb collisions, there were observed that the values of the fitting parameters strongly depend on the characteristics of the collisions (medium effect) in the region of $p_T < 4-6\ GeV/c$ (I region). The dependences become weaker inthe second region of $4-6\ GeV/c < p_T < 17-20\ GeV/c$ and almost disappered in the *III* region of $p_T > 17-20\ GeV/c$ (except centrality dependences for the parameter a^c_K).

In the case of central collisions, the ratio of the values of the parameters a^c_K for Pb+Pb collisions to the values of a^c_K for the pp collisions multiplied by the average number of participant nucleons have the minimum values for the second region and, it becomes less than 1 for the most central events - a suppression.

The values of the L^c_K increase with p_T and

$L^c_{III}: L^c_{II} \cong 5$; $L^c_{II}: L^c_I \cong 3$ (Pb − Pb);
$L^1_{III}: L^1_{II} \cong 5$; $L^1_{II}: L^1_I \cong 5$ (pp)

It was found that the ratio of the lengths (in case of the II regions) for the η-mesons (< $L_{\pi 0}$ >) to one for the π^0- mesons (<L_η >) produced in the pp collisions at 8 TeV is approximately equal to the ratio of their

masses (m_η and $m_{\pi 0}$ respectively): $< L_\eta >:< L_{\pi 0} > \cong m_\eta : m_{\pi 0}$. Assuming that the values of the LcK are directly proportional to the string tension, the result could be considered as a smoking gun for parton/string fragmentation dynamics. We propose this explanation since in string theory the masses of elementary particles and their energies are defined by the intensity of string vibration and strangeness of the string stretch, which are depend by the tension of strings. The parameter b_k^c could be represented as: $b_K^c \cong \frac{1}{\tilde{p}_T}$ (here $\tilde{p}_T$ is some average p_T for parton system) and with considering $-\tilde{p}_T \cong t \cong -q^2$ (t is Mandelstam variable) we can write that $b_K^c \cong \frac{1}{\sqrt{q^2}}$.

Using the expression $\alpha_S \cong \left[ln\left(\frac{q^2}{\Lambda^2}\right)\right]^{-1}$ (at Λ=0.2 GeV/c) one can get that:$\alpha_S \cong 1$ for the I region; ~ 0.25 for the II region and ~ 0.13 for the III region. The increasing of the α_s with decreasing of the p_T is similar to the dependence of the α_s on p_T which is characteristics of the QCD quark string: $\frac{1}{r^2} \sim Q^2 = -q^2$ (in which r is a distance between quarks in the string). This result together with the above result on the ratios of lengths can be clue that the fragmentation and hadronization of the partons occurs through the string dynamics, and the values of the L_K^c can be related to the string tension. So one can conclude that the meaning behind observed p_T regions at LHC energies is parton fragmentation and hadronization through parton strings (as in the below figure): the region III is the domain of creation of first generation partons/strings during collisions, where the most energetic hadrons /partons/ strings (with highest tension) are produced and weakly modified by the medium; The region II is the one with highest density of the strings decayed from ones in region III.

The high density causes string fusion and a collective phenomenon, which is as a result of the new string formation in the most central Pb-Pb interactions. It can explain the anomalous behavior of the Nuclear Modification Factor in this region; the region I is the one with the maximum number of hadrons and minimum number of strings.

PROMPT PHOTONS PRODUCTION IN PROTON-PROTON COLLISION AT HIGH ENERGIES

Alizada M.R.[1], Ahmadov A.I.[2,3], Arbuzov A.B.[2]
[1] Baku State University, Baku, Azerbaijan
[2]Joint Institute for Nuclear Research, Dubna, Russia
[3]Institute of Physics, ANAS, Baku, Azerbaijan
mohsunalizade@gmail.com

At present investigation of prompt photon production at heavy-ion collision on the RHIC and LHC experiments is actual. Photons play a special role in the study of hadron properties and nuclear interactions. Their free path is large not only in very dense hadron matter, but also in the medium of confined quarks and gluons. The experiments planned at the NICA collider will have a great advantage, since the energy obtained for colliding heavy ions will reduce the number of additionally production elementary particles.

It is known, the production of hard photons in high energy collisions is one of the most important and fundamental processes to be observed at a hadron collider. Photons produced from the underlying partonic interaction are called direct photons. They can probe the structure of the hadron at very small distance scales, so they are sensitive both to the details of the Standard model and to possible new physics scenarios. At the leading order, there are two partonic processes which can produce direct photons. The first is the annihilation channel and the second is the Compton channel. We constructed Feynman diagrams of these processes and wrote matrix elements.

Calculation of the matrix elements are preformed using FeynCalc. Expression for the differential cross-section of the subprocesses has been obtained. The differential cross-section of the subprocesses depend of the energy of colliding protons, mass quark and etc. The differential cross-section of the subprocesses decreases with increasing energy of colliding protons. The differential cross-section of the subprocesses without and with polarization of colliding protons were evaluated. It has been shown that, polarization of colliding protons may increase or decrease value of the differential cross-section of the subprocess. The double spin asymmetry of

the subprocesses has been obtained as a function of the center of mass energy and scattering angle. The value of the double spin asymmetry of Compon scatterin of quark-gluon process is zero. The value of the double spin asymmetryof annihilation of quark antiquark process linearly depends on the product of the polarization degrees of colliding protons and maximal when the polarization of colliding protons is opposite and minimal when they are identically directed.

ELECTRIC QUADRUPOLE TRANSITIONS IN NEUTRON CLUSTER TRANSFER REACTIONS

Abdulvahabova S.G.[1], Afandiyeva I. G.[2]
[1]Baku State University, Baku, Azerbaijan
[2]Azerbaijan State University of Oil and Industry, Baku, Azerbaijan
sacidaabdulvahabova@bsu.edu.az; afandiyeva.irada@asoiu.edu.az

In this article in the frameworks of clusters model, the electric quadrupole transitions in (p,t) reactions are discussed . The study of nuclear states built on clusters bound by valence nucleons in their configurations is a field of large interest, which is being renewed by the availability of exotic beams: clustering is, in fact, predicted to become very important at the drip-line, where weakly bound systems will prevail. Our interests are mainly related to the nuclei of average mass, in which pair correlation and collective movement are important. Reactions were considered in which transitions occur from the ground state of an even target nucleus to the ground state of an even residual nucleus, and the spins of the initial and final states are equal to zero. In this case, the most important residual interaction is the pair interaction. These motions enhance the electric quadruple matrix elements and give the events a unique signature, which can be used for identification. The study shows a strong population in (p,t) reactions of the 0^+ excited states in the rare-earth regions can be associated with the density distribution of single - particle levels and the alignment of the corresponding quadrupole moments in the vicinity of the Fermi surface of these nuclei. We limited by the fact that the internal states incident proton, emitted triton and any intermediate state clusters are fully

balanced S-states, so that the corresponding sequential interaction of transmission are diagonal in the spin states of nuclei. In the neutron clusters transfer reactions, the low-lying 0+ levels will be more strongly excited in nuclei in which the single-particle quadrupole transitions near the Fermi surface have the same sign. Violation of E2-additivity occurs for strongly interacting protons and neutron clusters. Only in the weak-coupling limit can the empirical quadrupole moment for the composite state of the proton-neutron cluster be described as a linear combination of the corresponding quadrupole moments of the proton and neutron cluster.

APPLICATION OF THE METHOD OF NON-CLASSICAL APPROACH TO CERTAIN PROBLEMS OF THE THEORY OF ANISOTROPIC SPACE PLAZMA IN FLUID DESCRIPTION

Nurmammadov A. Mahammad, Dzhalilov S. Namiq
Shamakhy Astrophysical Observatory named after N. Tusi, Azerbaijan National Academy of Sciences, Azerbaijan
dnamig@gmail.com

The new well-posed boundary value problem to the system of singular nonlinear differential equations is considered, which describes the stationary radial outflow of anisotropic plasma from the Sun (solar wind). These equations are obtained on the basis of 16-moment MHD (magnetohydrodynamic) transport equations for a collisionless magnetized plasma, which takes into account the temperature anisotropy relative to the direction of the magnetic field and the heat flux carried by the wind. This is a generalization of the classical isotropic Parker model taking into account the effects of anisotropy. In this paper, the equations under study are characterized as a nonautonomous nonlinear system of ordinary differential equations the coefficients in which degenerate and simultaneously have singularities. These equations are related to an unsolved problem in the general theory of ODEs (Ordinary Differential Equations). At first, according to the conditions of the coefficients of the equations, a non-classical boundary value problem is set, and the solvability is established for

the same non-autonomous and nonlinear system of equations under consideration. The found analytical solution reconstructs numerical solutions, which are simultaneously automatically established by classical formulation of boundary value problem. Parker's solutions are also partially included in this obtained class of solutions, which is presented with strictly proves. Further, by means of the methods of "ε -regularization" and "fixed point" the theorem of solvability for the considered differential equations is obtained. After constructed nonsingular system equations with well-posed boundary value problem, the analytical solutions are founded. Using the sketch of graph of these solutions their family is established.

EFFECTIVE "GREEN" SYNTHESIS OF STABLE SILVER AND MAGNETITE NANOPARTICLES USING OF ARTEMISIA ANNUA "HAIRY" ROOT EXTRACTS

Kobylinska N.G.[1], Klymchuk D.[2], Matvieieva N.A.[3]
[1] A.V.Dumansky Institute of Colloid Chemistry and Water Chemistry, NAS of Ukraine, Ukraine
[2] M.G.Kholodny Institute of Botany, NAS of Ukraine, Ukraine
[3] Institute of Cell Biology and Genetic Engineering, NAS of Ukraine, Ukraine
kobilinskaya@univ.kiev.ua

The necessity of modern science and technology in novel materials with specific properties increases the interest of the global industrial and scientific community in nanomaterials. In recent decades, a large amount of scientific data allows a synthesis of nanoparticles (NPs) with required morphological, physical and chemical properties. NPs can be generated by chemical routs using the various chemical components; it isn't safe for environment. So, biosynthesis of NPs can be an alternative way for metal nanoparticles synthesis without special equipment and toxic chemicals. Plant genetic transformation using *Agrobacterium rhizogenes* is the method for obtaining of "hairy" root cultures. At the same time, it is possible to obtain the samples of "hairy" roots characterized by the increased reducing power due to the incorporation bacterial *rol* genes into plant genome. Presence of these genes in plant cells can lead to the activation of

the synthesis of secondary metabolites with high activity and bioactive compounds.

In this work, the possibility for "green" synthesis of silver (AgNPs) or magnetite (Fe_3O_4NPs) NPs using the ethanol extracts of *Artemisia annua* "hairy" roots is reported. The total flavonoid content and reducing power of the extracts are studied. Also, the effect of the Fe(II, III) salts (chlorides, sulphates, etc.) on the process of NPs biosynthesis is evaluated.

Composition of the extracts was studied by means of HPLC and UPLC-ESI-UHR-Qq-TOF-MS methods. Flavonoids and phenolic acids were found to be the main groups of bioactive compounds available in the *A. annua* "hairy" root extracts. The AgNPs and Fe_3O_4NPs were successfully synthesized using this ethanol extracts. TEM data confirm the as-synthesis AgNPs and Fe_3O_4NPs have been characterized spherical shape with predominant average size of 10-50 nm and 8-25 nm, respectively (Fig. 1).

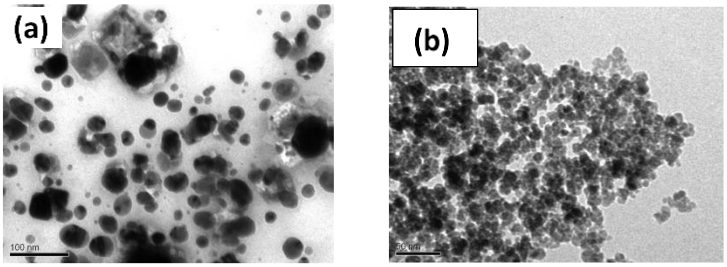

Fig. 1. TEM images of AgNPs(a) and Fe_3O_4NPs(b) obtaining by *A. annua* "hairy" root extracts.

The obtained NPs were succefully applied for environmental remediation and medical application. The data testify the importance of further study to use these NPs asantimicrobial agent against pathogenic microorganisms (*Escherichia coli*, Staphylococcus *aureus*, etc.)

GASEOUS PHASE SYNTHESIS OF BORON NITRIDE NANOSHEETS FOR MEDICAL AND TECHNICAL USE

Dvali N., Chirakadze A., Jishiashvili D., Jishiashvili A., Gorgadze K.
Georgian Technical University, Tbilisi, Georgia
achirakadze@gtu.ge

Boron nitride (BN) volume and nano-sized materials can be used for many different urgent purposes - from creation of hypersonic civil aircraft (due to high stability and integrity at high temperatures) to the development of effective cancer treatment methods (due to high values of thermal neutron capture cross section of ^{10}B isotope and high energy proton cross section of ^{11}B isotope). Nanostructured hexagonal boron nitride (h-BN) is a highly prospective material for the tumor localized boron neutron and boron-proton capture therapy characterized by high biocompatibility and significant efforts have been made to reduce the conventional synthesis and annealing temperature and improve the crystalline structure. The most advanced methods of synthesis of the isotopic enriched h-BN nanoparticle require synthesis and annealing temperatures higher than 900-1000 ^{O}C and quite expensive precursor materials like amorphous boron powder. The newly developed method being reported, utilizes gaseous ammonia and boron trifluoride at synthesis temperatures up to 250 ^{O}C and easily available cheap raw materials: gaseous boron trifluoride, gaseous ammonia and potassium chloride. The synthesis by-product undergoes farther processing, finally yielding again in boron trifluoride and ammonia. The XRD and Raman spectra of the obtained samples are given in figures 1 and 2.

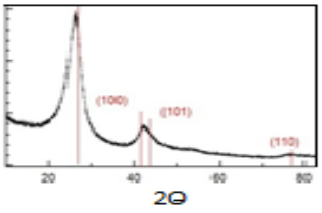

Fig. 1. XRD of the samples

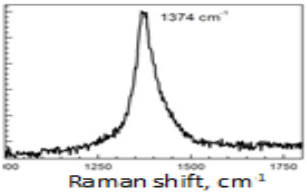

Fig. 2. Raman spectra of the samples

Despite of the extremely low temperature of synthesis (150-200^{O}C) samples of BN nanosheets and nanoparticles with a clearly defined hexagonal structure have been synthesized using cheap and easily available raw materials and a simple technological method.

DEGRADATION OF THE MAGNETOCALORIC EFFECT IN CYCLIC MAGNETIC FIELDS NEAR THE MAGNETOSTRUCTURAL PHASE TRANSITION

Gamzatov A.G.[1], Aliev A.M. [1], Qiao Kaiming[2], Zhou H.B. [2], Hu Feng-xia[2]
[1]Amirkhanov Institute of Physics, DFRC, RAS, 367003, Makhachkala, Russia
[2]Beijing National Laboratory for Condensed Matter Physics, Institute of Physics, Chinese Academy of Sciences, Beijing 100190, P. R. China
gamzatov_adler@mail.ru

Magnetic cooling technology based on the magnetocaloric effect (MCE) is one of the typical applications of magnetic materials in energy saving and reducing harmful emissions. In recent years, several new types of magnetocaloric materials with gigantic effect values discovered in the world have greatly contributed to the development of magnetic cooling technology at room temperature (these are compounds FeRh, Gd-Si-Ge, Ni-Mn-Ga and La(Fe,Si), MnAs1-xSbx and MnFePyAs1-y). In almost all these materials, giant values of the MCE are observed due to magnetostructural phase transitions (MSPT).

Despite the fact that the process of creating solid-state magnetic refrigerators goes to the practical plane the technology of magnetic cooling has faced many problems requiring further research. As is known, the prototypes of magnetic refrigeration machines created to date operate at relatively low frequencies of 4-10 Hz. One of the main problems hindering the beginning of mass production of magnetic refrigerators is the lack of an experimental basis for the study of the properties of magnetic materials in conditions of long-term cyclic influence of the magnetic field. In addition, such studies are of great interest from a fundamental point of view.

This report presents the influence of the long-term cyclic effect of magnetic fields (0.62, 1.2, 1.8 and 8 T) on the magnetocaloric effect in the $La_{1-x}Pr_xFe_{13.7}Si_{1.3}$ and $Fe_{50}Rh_{50}$ by directly measuring the adiabatic temperature change.

Our results show that despite high MCE values in studied samples ($La_{1-x}Pr_xFe_{13.7}Si_{1.3}$ and $Fe_{50}Rh_{50}$), the samples with MSPT may have some problems in cyclic fields. Therefore, we distinguish three types of degradation under long-term action of cyclic magnetic field: 1) degradation is associated with incompleteness of the MSPT. When the field induces a MSPT not in the entire volume of the sample (when the value of the cyclic field is less than the saturation field). In our case, in fields from 0.6 to 1.8 T; 2) MCE degradation due to temperature hysteresis. The reversibility of which depends both on the width of the hysteresis and on the value of the magnetic field; 3) Irreversible degradation, including mechanical destruction of the sample due to giant magnetostriction. As a rule, observed at high magnetic fields.

ENHANCING PERFORMANCE OF TRIBOELECTRIC NANOGENERATORS BY USING TITANIUM OXIDE/POLYVINYLCHLORIDE NANOCOMPOSITE FILMS

Gulahmadov O.G., Muradov M.B., Kim J.
Baku State University, Baku, Azerbaijan
kjiseok@bsu.edu.az

In this study, nanocomposite films which are made of polyvinylchloride (PVC) and titanium oxide (TiO_2) nanoparticles are used as triboelectric films for triboelectric nanogenerators (TENGs) to convert wasted mechanical energy into electrical energy. Nanocomposite films are fabricated by the hot-pressing method in which a mixture of melted PVC and TiO_2 nanoparticles are compressed with heating. TENGs are fabricated by assembling the PVC nanocomposite film and a nylon film. And performance of TENGs is investigated according to the concentration of TiO_2 nanoparticles in the PVC nanocomposite film. TiO_2 nanoparticles with high dielectric

constant and high mechanical strength provide positive effect for performance of TENGs. As a result, the charge density on the surface of the PVC nanocomposite triboelectric film is enhanced according to the concentration of TiO_2 nanoparticles. And electrical outputs of TENGs such as the open-circuit voltage and the short-circuit current increase as the concentration of TiO_2 nanoparticles that are dispersed into the PVC matrix. TiO_2/PVC nanocomposite films show enhancement of the mechanical property of TENGs because of the strong interfacial interaction between TiO_2 nanoparticles and the polymer matrix through the hot-pressing method. Mechanically robust TENGs with high electrical outputs are demonstrated by using TiO_2/PVC nanocomposite films.

DEVELOPMENT OF MAGNETIC NANOLIQUIDS UTILIAZING CURIE TEMPERATURE CONTROLLED NANOPARTICLES AND LIQUID CRYSTALLS

Mitagvaria N., Chirakadze A., Jishiashvili D., Petriashvili G., Chichua T. Chubinidze K., Chigogidze K., Khuskivadze N., Gulashvili M.
Georgian Technical University
nanakhuskivadze53@gmail.com

Compositions of liquid crystals (LCs) and nanoparticles form soft condensed systems via combining two extremely useful features of fluidity and space order with various unusual specific physical and biological properties of incorporate nanoparticles and nano-composites like ferromagnetic, antimicrobial, anti-inflammatory and anti-carcinogenic features. They can play an important role in several kinds of cancer therapy in the form of appropriate combinations of nano-fluids for magnetic hyperthermia and chemical-, photodynamic-, neutron capture-, hadron-, and conventional radio-therapy according to a novel concept and strategy being developed in Georgia in collaboration with colleagues from Germany, USA, Russia, Ukraine, Azerbaijan and other countries. They can also be used for developing of cancer treatment modalities with a controlled and prolonged release of active anticancer agents. That is why the toxicity of mixtures must be accurately assessed, when used for bio-sensing and

as a main component of a smart delivery system of nano-drugs, containing a mixture of different magnetic and nonmagnetic nanoparticles providing the controlled hyper-thermal, chemical, radiation and photodynamic therapeutic impact. 324 various compositions of nine magnetic nanoparticles and their mixtures and nine liquid crystals controllable by temperature, optic radiation and pH and their mixtures were composed and their Curie temperatures and nematic-isotropic phase transition temperatures were determined. The Curie and nematic-isotropic phase transition temperatures of the most mixtures can be accurately matched to the so-called therapeutic interval of hyperthermia treatment interval of 41-45 C^0 while their acute toxicity is only for 30-40 % higher compared to the toxicity of saline solution.

ELECTRICAL PROPERTIES OF p-Si/$Cd_{1-x}Zn_xS(Se)_{1-y}Se(Te)_y$/ZnO HETEROJUNCTIONS

Mamedov H.M., Jafarov M.A., Nasirov E.F., Rasulova A.R., Piriyeva D.N., Ganbarova S.V.
Baku State University, Baku, Azerbaijan
dilara.piriyeva@bsu.edu.az

Electrical properties of p-Si/$Cd_{1-x}Zn_xS(Se)_{1-y}Se(Te)_y$/ZnO heterojunctions deposited by the method of electrodeposition from aqueous solution were analyzed. The results indicate that optimizing the composition of $Cd_{1-x}Zn_xS(Se)_{1-y}Se(Te)_y$ films, substrate surface and heat-treatment conditions, one can obtain *p*-Si/$Cd_{1-x}Zn_xS(Se)_{1-y}Se(Te)_y$ heterojunctions suitable for the fabrication of rectifier diodes with high rectification coefficient. However, the increase in band width with the addition of Zn leads to an increase in the contact potential difference in the p-Si/$Cd_{1-x}Zn_xS$ heterostructures and a decrease in the conduction band difference in the transition region (in thin layers with x=0.8, ΔE_c=2.22 eV, Si with CdS contact ΔE_c=2.7 eV) which increases their applicability in solar energy converters.

The investigation of p-Si/$Cd_{1-x}Zn_xS(Se)_{1-y}Se(Te)_y$ heterostructures by a scanning electron microscope shows that after 11-13 minutes of

heat treatment in an argon environment at 410^0C the near transition part becomes sharper and the metal/semiconductor excess in the transition region decreases sharply. Electron-molecular processes and recrystallization occur not only on the surface of thin layers, but also throughout the volume during heat-treatment that has been established.

EFFECT OF ELECTROLYTE SOLUTION ON OPTICAL PROPERTIES OF CdS NANOPARTICLES

Muradov M.B., Gahramanli L.R., Eyvazova G.M., Balayeva O.O., Nasibov İ.N., Mirsultanova R.M.
Baku State University, Baku, Azerbaijan
lalagahramanli@bsu.edu.az

Semiconductor nanomaterials have attached much interest due to interesting physical and chemical properties. Cadmium sulfide (CdS) is an important direct intermediate bandgap (2.42 eV at 300 K) with excellent thermal and chemical stability and strong optical absorption and is used in solar cells, photodetectors, light emitting diodes, and lasers.

Thus, when nanoparticles are immersed in an electrolyte solution, as a result of the interaction of electrons in a nanoparticle and ions in electrolyte solutions, the potential energy of charge carriers' changes, which should lead to a change in their energy spectrum. In addition, as a result of the interaction of nanoparticles with the environment, the defect and crystal structure may change. The study of these factors has a great scientific and practical interest.

The purpose of this paper is to determine the effect of various electrolyte concentrations to its optical properties of cadmium sulfide nanoparticles. The obtained nanoparticles were placed in different ambient solutions (Cd $(NO_3)_2 \bullet 4H_2O$; Cd $(CH_3COO)_2 \bullet 2H_2O$; NaCl) to determine the influence of ambience and different electrolyte concentration (0.01M; 0.1M; 1M; and 2M) on the optical properties of pure CdS nanoparticles.

The band gap value of pure CdS in water is 2.51 eV.

Table.1. Band gap values (E_g) of nanoparticles.

Salts	E_g, eV			
	0.01 M	0.1 M	1 M	2 M
CdS+$Cd(NO_3)_2$•$4H_2O$	3.73	3.69	3.64	3.61
CdS+$Cd(CH_3CO_2)_2$•$2H_2O$	2.44	2.38	2.29	2.25 AQ
CdS+NaCl	4.13	3.77	3.17	3.17

As can be seen from the table, the band gap of nanoparticles strongly depends on the nature of the environment. Adding CdS into $Cd(CH_3CO_2)_2$ solution the band gap decreased slightly by increasing the concentration of electrolyte solution. But the band gaps of CdS in cadmium nitrate and sodium chloride solutions were decreased significantly by increasing the concentration of electrolyte solution.

Ab INITIO STUDIES OF ELECTRONIC BAND STRUCTURE OF DEFECTS IN CdMnS

Mehrabova M.A. [1], Panahov N.T. [2], Hasanov N.H.[3]
[1] Institute of Radiation Problems, ANAS, Baku, Azerbaijan
[2] Azerbaijan University of Architecture and Construction, Baku, Azerbaijan
[3]Baku State University, Baku, Azerbaijan
m.mehrabova@science.az

Room temperature CdS based semimagnetic semiconductors (SMSC), such as Mn doped CdS is a very good photo-luminance compound due to *d* states at the top of the valence band and intra-*d* shell transitions. The ternary nature of CdMnS SMSC gives us the possibility of tuning the lattice constant and band parameters by varying the composition of the material. The substitutional Mn atoms in the CdS lattice are also characterized by highly efficient electroluminescence, which makes this material important in the context of optical flat panel display applications.

The Mn-CdS sheet with 16 atom supercells is analyzed by Kumar et al. The investigated electronic and magnetic properties of Mn doped CdS

in wurtzite phase, using ab-initio calculations based on LDA, GGA and LDA + U exchange and correlation functionals. Ahmed et al. investigated electronic band structure of $Cd_{1-x}Mn_xS$ (x = 6.25 %) using spin-polarized Density Functional Theory (DFT) within the framework of GGA, its extension via on-site Hubbard U interactions (GGA + U) and a model for exchange and correlation potential TB-mBJ.

The purpose of this work was to calculate the electronic band structure of defective $Cd_{1-x}Mn_xS$ SMSC. Supercell of $Cd_{1-x}Mn_xS$ of 64 atoms with interstitial Cd atom or interstitial S atom was constructed. Ab initio calculations are performed in the Atomistix Toolkit program within the DFT and LSDA on DZDP basis. We have used Hubbard U potential U_{Mn} = 3.59 eV for *3d* states for Mn atoms. After the construction of $Cd_{1-x}Mn_xS$ (*x*=6.25 %) supercell with interstitial atom, atom relaxation and optimization of the crystal structure were carried out. Electron band structure, density of states was calculated, total energy has been defined.

It has been established that interstitial Cd or S atom in the crystal structure of $Cd_{1-x}Mn_xS$ SMSC leads to the change of band gap, formation of deep levels in the band gap, shifting of Fermi level towards the valence or conduction band.

CARBON NANOTUBES DECORATED WITH NICKEL NANOPARTICLES FOR AMMONIA DETECTION

Ahmadova S.A.[1], Musayeva N.N.[1], Trevisi G.[2]
[1] Institute of Physics, ANAS, Baku, Azerbaijan
[2] IMEM-CNR Institute, Italy
e-shahla.ahmadova05@gmail.com

The paper reports influance of decoration of carbon nanotubes (CNTs) with nickel nanoparticles on their sensory properties. Multi-walled carbon nanotubes (MWCNTs) were synthesized by the Aerosol Chemical Vapor Deposition method (ACVD). After purification from pyrolytic carbon, which are formed during synthesis, the surface of MWCNTs is functionalized with carboxyl groups (-COOH) for activation them to environ-

ment. The decoration of the functionalized multi-walled carbon nanotubes (f-MWCNTs) with nickel nanoparticles was carried out at Angstrom Engineering (Canada, Kitchener Ontario). Nickel (99.99%) was deposited in a vacuum 10^{-2} Torr at 14K temperature by electron-beam evaporation (grow rate was 0.13Å/sec) on the surface of f-MWCNTs networks, which dispersed on the glass substrate. The thickness of nickel layer on the CNTs in the range of 5-10 nm was confirmed by the ellipsometric method (Ellipsometer J.A.Woolam/M2000-DI, USA). The morphology of pristine, functionalized and nickel-coated MWCNTs was observed by Scanning Electron Microscopy (SEM) and the effects of CNTs functionality and nickel decoration were analyzed by Raman spectroscopy.

The results of Raman spectroscopic analysis indicate that nickel decoration of the f-MWCNTs caused blue shift of D (defective) and G (graphite) peaks and increase the I_D/I_G ratio (from 0.33 to 0.41). This proves that nickel decoration creates additional defects in the outer walls of MWCNTs.

Based on f-MWCNTs and Ni/f-MWCNTs, a sensor element was prepared on a dielectric substrate and its sensitivity in vapor medium of ethanol (CH_3CH_2OH), methanol (CH_3OH), ammonia (NH_3) and acetone (CH_3COCH_3) was investigated. The operating temperature was room temperature. The response of the sensor is defined by the resistance, that is $\Delta R/R_0=(R-R_0)/R_0$, where R_0 is the resistance before contact with the gas and R is the maximum resistance during contact with the gas. Ni/f-MWCNTs sensors indicated the highest sensitivity to NH_3 compared to ethanol, methanol and acetone, and was observed a rapid increase resistance when the sensor contacts with molecules of ammonia. A similar situation was observed with the f-MWCNTs based sensor element. Theoretical and experimental studies are related it with the transfer of electron from the ammonia gas to the CNTs. The obtained results show that the sensitivity to ammonia is increased two times as a result of deposition of nickel nanoparticles on f-MWCNTs. Achieving this effect allows the preparing of a new type of ammonia sensor device with a simple operating principle that can operate at room temperature.

Ab INITIO STUDY OF STRUCTURAL AND ELECTRONIC PROPERTIES OF ZnSe

Jafarova V.N., Mamedov N.T.
Institute of Physics, Azerbaijan
vcafarova@beu.edu.az

DMSs have attracted much interest in recent years because of both semiconducting and magnetic properties within the same compound. These compounds are expected have promising potentiality in new spin-based technology as in spintronic. However, ZnSe is ideally suited for fabrication of photo detectors, blue-LED, short wavelength lasers, solar cells, infrared windows, night vision applications, quantum-well and photovoltaic devices.

Present work based on the DFT-LSDA+U method, a detailed theoretical study on the structural and electronic properties of pure ZnSe wurtzite structures are provided. *Ab initio* calculations were performed by implemented DFT-LSDA using ATK program software. The electron-ion interactions are taken into account through the FHI pseudopotential. The single-particle Kohn-Sham wave functions were expanded in a linear combination of numerical real-space atomic orbitals as DZP basis set with a kinetic energy cutoff of 75 Ha. The atomic coordinates are fully optimized until the force and stress on each atom converges to less than 0.001 *eV/Å* and 0.001 $eV/Å^3$, respectively. The reciprocal space integration was performed with the 7×7×7 MP k-point sampling.

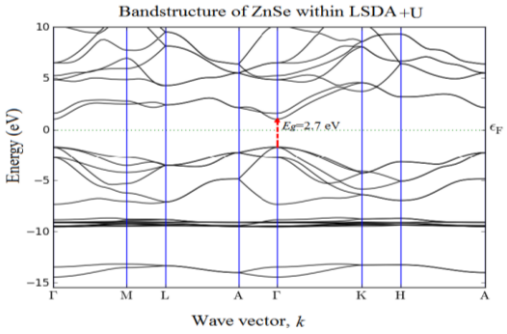

Fig. DFT-LSDA+U calculated energy band structure of ZnSe.

In this work, have been able to reproduce the experimental value of the energy gap for bulk system only using additionally Hubbard *U* parameters in DFT-LSDA calculations. The value of Hubbard *U* semi-empirical correction was taken 4.5 eV for Zn 4d states and 3.5 *eV* for Se 4p states. Ab initio calculated values of structural parameters of bulk ZnSe structure equal to *a*=3.918 *Å* (exp. 3.996 *Å*), *c*=6.394 *Å* (exp. 6.55 *Å*). The calculated energy band gap (2.7 *eV*, exp. [1] 2.7 eV (T=295K)) of ZnSe is in excellent agreement with experimental results. It is obtained that the valence band maximum and conduction band minimum are occurs at the Gamma point, indicating that the ZnSe is a direct semiconductor.

THE THERMOELECTRIC POWER OF SUPERCONDUCTING $Bi_2Sr_2Ca_{0.8}Zn_{0.2}Cu_2O_{8+X}$

Ragimov S.S.[1,2], Agayeva G.I.[2], Babayeva A.[2]
[1] Institute for Physical Problems, Baku State University, Baku, Azerbaijan
[2]Institute of Physics of ANAS, Baku, Azerbaijan
sadiyar.raqimov@bsu.edu.az

The study of transport properties is important for understanding the mechanism of superconductivity and the nature of charge carriers in high-temperature superconductors (HTSC). Thermoelectric power (S) is a sensitive transport property for understanding the mechanism of conduction and the nature of charge carriers.

It is known, that between Bi-O layers in Bi-based high temperature superconductors there are a weak bond. To improve the superconducting properties of Bi-based HTSC, the main content elements may be replaced by various other ones. In this case, the structural properties do not change significantly, however, a change in the concentration of charge carriers affects the critical temperature.

It was investigated the temperature dependence of the specific resistivity and thermoelectric power of polycrystalline sample $Bi_2Sr_2Ca_{0,8}Zn_{0,2}Cu_2O_{8+X}$ with a partial replacement of Ca by the Zn element of the Bi-2:2:1:2 system in the 75-300K temperature interval.

The phase purity of $Bi_2Sr_2Ca_{0.8}Zn_{0,2}Cu_2O_{8+X}$ was investigated by using a Brucker -D8 advance diffractometer. According to the intensities of the diffraction peaks, the main phase is tetragonal phase. The additional diffraction peaks do not correspond to $Bi_2Sr_2CaCu_2O_x$ is observed in $Bi_2Sr_2Ca_{0.8}Zn_{0.2}Cu_2O_{8+X}$.

It was observed, that the temperature dependence of thermal power pass through a maximum before the superconducting phase transition and sharply decreases to zero with decreasing temperature. At temperatures above the maximum, the thermoelectric power has a negative slope, with dS/dT= -0,021μV/K^2 ($Bi_2Sr_2Ca_{0.8}Zn_{0.2}Cu_2O_{8+X}$) value. The thermal power sign is positive, which is indicated that, the positive carriers are dominant. Above the T_{max} the thermal power decreases linearly with increasing temperature. This behavior indicates to fact that, the electrons are also involved in conductivity. The obtained experimental results on the thermal power were analyzed on the framework of the Xin's two band model. The concentration of holes per copper atom and the band gap of the semiconductor type Bi-O layers are determined. It was shown that the partial replacement of the calcium element with zinc in $Bi_2Sr_2Ca_{0.8}Zn_{0.2}Cu_2O_{8+X}$ does not change the structure of Bi-O layers.

MAGNETIC PROPERTIES IN BIOLOGICAL SYSTEMS

Khalilov Rovshan[1,2], Nasibova Aygun[1,2]
[1] Baku State University, Baku, Azerbaijan
[2] Azerbaijan National Academy of Sciences, Institute of Radiation Problems, Baku, Azerbaijan.
hrovshan@hotmail.com

Magnetic nanoparticles - magnetite (Fe3O4) and magemite (γ-Fe2O3) play an important role in the functioning of living systems. These nanoparticles cause the formation of magnetic properties in natural systems and the formation of a broad EPR signal.

In our previous works, we studied the EPR spectra of leaves and seeds of various trees and shrubs growing in ecologically polluted areas of the Absheron Peninsula, and the EPR spectra of seedlings of different

types of plant seeds exposed to ionizing gamma radiation, and finally, we found the formation of iron oxide magnetic nanoparticles - magnetite (Fe3O4) and magemites (γ-Fe2O3) in plants during stress, and the formation of anomalous magnetic properties in them. We have shown that these nanoparticles lead to the formation of magnetic properties in biological systems and the formation of a broad EPR signal, which was first detected in plants by us.

Research of one of the valuable plants of Absheron peninsula of Azerbaijan Republic (Mardakan and Nardaran territories), fig leaves, showed that as a result of biomineralization under stress conditions, they form magnetic iron oxide nanoparticles. In addition, the high intensity of the broad EPR signal characteristic of nanophase magnetic particles found on fig leaves in Mardakan indicates that the plant system in this area is more exposed to pollutants and that this area is more environmentally polluted than Nardaran.

Experiments have shown once again that stress factors cause the formation of nanophase particles of biogenic origin in living systems. These nanoparticles lead to the formation of magnetic properties in biological systems and the formation of the broad EPR signal that we first discovered in plants.

ON THE EXACT SOLUTION OF THE QUANTUM HARMONIC OSCILLATOR MODEL EXHIBITING SEMICONFINEMENT EFFECT

Jafarov E.I.[1], Van der Jeugt J.[2]
[1]Institute of Physics, ANAS, Baku, Azerbaijan
[2]Department of Applied Mathematics, Computer Science and Statistics, Faculty of Sciences, Ghent University, Krijgslaan 281-S9, 9000 Gent, Belgium
ejafarov@physics.science.az

The talk will be based in our recently published papers, where we developed a new model of a one-dimensional nonrelativistic canonical quantum harmonic oscillator exhibiting semiconfinement effect. This effect is achieved thanks to application of the the method of the replacement of the constant effective mass by the position-dependent one. We were able to solve the problem exactly and discovered that its energy

spectrum completely overlaps with the energy spectrum of the so-called Hermite oscillator, whereas the wavefunctions of the stationary states are expressed via the generalized Laguerre polynomials. We also solved exactly same problem for case when it is under the suddenly applied external homogeneous field. Additionally, transition probabilities from ground to arbitrary excited states of a one-dimensional nonrelativistic canonical quantum harmonic oscillator exhibiting semiconfinement effect are computed exactly in case of the suddenly applied external homogeneous field.

IONIC CONDUCTIVITY IN SOLID SOLUTIONS OF $TlSe_{1-x}S_x$

Salmanov F.T., Aliyeva N.A., Mammadov R.A.
Institute of Radiation Problems of ANAS, Baku, Azerbaijan
ramil.m.azadoglu@gmail.com

The temperature dependence of the conductivity and switching effects in solid solutions of $TlSe_{1-x}S_x$ (x=0; 0,1) has been investigated. Above 400K phase transition to the superionic conductivity are discovery. It is suggested that the ion conductivity is caused by the diffusion of Tl^+ ions over vacancies in the thallium sublattice between ($Tl^{3+}Se^{2-}{}_2$) nanorods. In this crystals S-type switching effect are revealed. It is suggested that the switching effect is related to the transition of crystals to the superionic state, which is accompanied by diffusion of Tl^{1+} ions. $TlSe_{1-x}S_x$ (x=0; 0,1) are materials in which the features of one-dimensional system manifest itself under certain condition, due to which these compounds are widely investigated. In this work, we report about an experimental study of the conductivity and switching effect in solid solutions of $TlSe_{1-x}S_x$ (x=0; 0,1) in wide temperature range.

The conductivity was measured by the four-contact method in two directions: parallel (σ_{II} (T)) and perpendicular (($\sigma_{\perp}$(T)) to tetragonal axis c of the crystal. The experimental samples were prepared in the form of rectangular plates 0.4–0.6 mm thick. Contacts with the samples were formed by a silver conducting paste on the plate surface. The permittivity and conductivity were measured by E7-25, digital immittance meters at frequencies of 25–10^6 Hz in a temperature range of 100–450 K. The measuring field amplitude didn't exceed 1 V cm^{-1}.

The experimental points of the temperature dependence ln ($\sigma \cdot T$) in the range of the sharp jump of conductivity are described by a straight line, which is given by the following equation for ionic conductivity:

$$\sigma \cdot T = \sigma_0 \exp(-\Delta E/kT)$$

where ΔE is the conductivity activation energy and k is the Boltzmann constant. The activation energies for the TlSe crystal the corresponding values are $\Delta E_{\perp}$=0,07 eV and $\Delta E_{//}$=0,1 eV.

The linear character of the dependence ln($\sigma \cdot T$) on1/T above the conductivity jump in the dependence of σ on 1/T indicates dominance of ionic conductivity, which is mainly due to the diffusion of Tl^+ ions over vacancies in the thallium sublattice of solid solutions of $TlSe_{1-x}S_x$. This change occurs as a result of the phase transition, which is accompanied by disordering of the Tl sublattice in these solid solutions. This conduction mechanism is typical of superionic conductors.

The dependences of the conductivity of solid solutions of $TlSe_{1-x}S_x$ on the electric field strength E are measured at different temperatures. A further increase in E led to a linear increase in σ, which is explained by the increase in the ionic component of conductivity as a result of gradual disordering of the cationic Tl sublattice in the electric field; in this range, the ionic conductivity begins to dominate over the electronic component and, when reaching the critical temperature, the conductivity sharply rises by a factor of 1000.

ANTI-STOCKS COMPONENT OF LASER IMPULS IN THE OPTICAL FIBER AT CARS

Kasumova R.J.[1], Safarova G.A.[1], Kerimli N.V.[2]
[1]Baku State University, Baku, Azerbaijan
[2]Azerbaijan Medical University, Baku, Azerbaijan
nazaket_kerimli@mail.ru

It has been analyzed nonstationary interaction of waves in optical fibers. Based on dispersion theory in the first approach it has been analyzed the nonlinear interaction between long impulse of strong pumping

wave and super short impulse of Stocks wave with quadratic phase modulation. It has been examined the influence of different parameters of regime (coefficient of phase modulation, phase miss-match of group velocities) on spectrum of anti-Stocks wave within optical fiber. It has been shown that the phase modulation of excitatory laser impulse leads to widening of central maximum of anti-Stokes component.

PHOTOCONDUCTIVITY OF ZnO THIN FILMS

Jabiyeva A.A.
Baku State University, Baku, Azerbaijan
aynurchobanova98@gmail.com

The ZnO thin films were deposited by Chemical Bath Deposition Technique and by SILAR method on glass and Si substrate. The reagents used in this experiment were zinc chloride, aqueous ammonia. 0.1 M of zinc chloride was prepared and small drops of ammonia were added and stirred continuously using a magnetic stirrer to obtain optimum pH of 9.4 for this deposition. 70 ml solution of zinc chloride and aqueous ammonia were put in 100 ml beaker and the substrates whose surface had been prepared under standard conditions were vertically suspended in the beaker and the solution was constantly stirred using magnetic stirrer in a water bath of constant temperature of 80°C. After 60 minutes, the substrate with deposited thin films were removed, rinsed with distilled water and left to dry. The as-deposited ZnO thin films were also annealed at 200°C and 300°C in a furnace.

ZnO thin films have been deposited onto the glass substrates by SILAR method. Aqueous zinc sulphate solution was used as source of zinc ion. First, the cleaned glass substrate was immersed in zinc sulphate solution, so to get zinc complex adsorbed onto the substrate, and in the hot distilled water. The second bath served the additional purpose of removal of loosely bound particles from the substrate, and formation of ZnO particles. The rinsing period was varied in such manner that ZnO films of different grain sizes could be deposited. We fixed adsorption period at 30 s, and we varied rinsing period 20 s, 30 s, and 40 s.

In the present study the structural and optical properties of various films are compared and analyzed. The XRD patterns were recorded for all annealed ZnO thin films. The absorbance of the film was also measured using UV mini Schmadzu UV-VIS spectrophotometer in the wavelength range 300-1100 nm. The obtained ZnO thin films show variation in structural, optical and optoelectronic properties on deposition parameters and conditions.

The photocurrent varies linearly with the increase in the bias voltage. While all films show more or less similar responses, the photocurrent efficiencies measured under similar conditions are different.

ELECTRICAL AND OPTICAL PROPERTIES OF ZnSTe THIN FILMS PREPARED BY CHEMICAL BATH DEPOSITION

Khanmammadova E.A.
Azerbaijan State Oil and Industry University, Baku, Azerbaijan
dadashovaelmira@mail.ru

ZnSTe thin films are deposited by chemical bath deposition (CBD) on a glass substrate. Prior to the deposition, the glass substrate with dimensions of 75×25×1 mm^3 is cleaned in a systematical order. The substrate is kept in diluted chromic acid for 5 min, and rinsed in tap water after wards. Subsequently, the cleaning is further carried out with detergent only to be rinsed again in deionized water. In the last step of the cleaning process, the substrate is kept in ethyl alcohol (99.9% purity) for 10 min and rinsed with deionized water. The drying of the glass substrate is completed in an oven set at 100 °C for 2 h. The chemical constituents and materials for the ZnSTe thin film processing are selected with great care considering their function in the solutions. The ZnSTe thin film process solution consists of 1 M $ZnSO_4$, 2.5 mL NH_3/NH_4Cl buffer solution (pH=10.7), 0.8 mL 0.66 M K_2TeO_3, 2.5 mL 1 M N_2H_4CS (thiourea), and 0.5 mL 3.75 M $N(CH_2CH2OH)3$ (TEA) mixed with 12 mL of deionized water. The deposition time is kept at 0,5, 1,0, and 1,5 h for one immersing. The temperature is kept at 80 °C at all times during the process of the thin film production.

The thickness measurements of the thin films are performed gravimetrical analysis tool that has a sensitivity of 0.1 mg, and capable of weighing loads up to 210 g. Specific resistivity measurements of thin films are obtained with Hall measurements at room temperature. The specific equipment utilized for these measurements is an Ecopia Hall effect measurement system HS-3000.The optical properties of the thin films are then determined by the Perkin Elmer UV-Vis Lamda 2S spectrophotometer in the region of h =300– 1100 nm wavelength. It should also be mentioned that the UV-Vis analysis is carried out at room temperature to obtain the absorbance (*A*) and optical transmittance *T*) values. With those room temperature optical transmittance values, they are let free of their dependency on the absorbance of substrate material.

The thickness values of the thin films deposited in 0,5, 1,0, and 1,5 h, are measured as 210, 775 and 1375 nm, respectively. The optical transmittance (*T*%) and absorbance (*A*) values for the ZnSTe thin films between λ = 300–1100 nm region is given.

The examination of the transmittance and absorbance values yields a correlation between the film thickness and optical transmittance. The results reveal that an increase in the film thickness leads to a decline in the optical transmittance by 50% to 90%. The absorbance band edge is initialized at ~ 310, 320, and 330 nm, for 0,5, 1,0, and 1,5 h deposition intervals, respectively.

The thin films produced at 80°C in different deposition time are adequate candidates for photovoltaic solar panel windows and light emitting diode (LED) applications due to their optical and electrical properties. They can also be utilized in optical applications as such reflectors, as films possess a high refractive index.

ELECTRONIC PROPERTIES OF A-15 TYPE SUPERCONDUCTOR Ti_3Sb

Mammadova S.O.
Institute of Physics, Azerbaijan National Academy of Sciences, Azerbaijan
seide.memmedova@physics.science.az

The standard crystal structure symmetry of A15 type superconductors, with spin-orbit coupling, creates gapped crossing near the Fermi level. The topological surface states near the Fermi surface of A15 superconductors Ta_3Sb, Ta_3Pb, and Ta_3Sn was revealed in the recent theoretical investigation, point out to host a topological superconductor candidate [1, 2]. In [3] work classifies Ti_3Ir, Ti_3Sb as a time-reversal preserved topological superconductor.

The electronic properties of the Ti_3Sb compound were calculated using the density-functional theory within the *spin*-polarized generalized gradient approximation. The kinetic cut-off energy was 150 Ry. The primitive cell of Ti_3Sb was relaxed and optimized with force and stress tolerances of 0.01eV/Å and 0.01eV/Å^3, respectively. The initial parameters of Ti_3Sb were derived from the basic arrangement of the Cr_3Si–type structure, with Pm-3n (no.223), cubic space group symmetry.

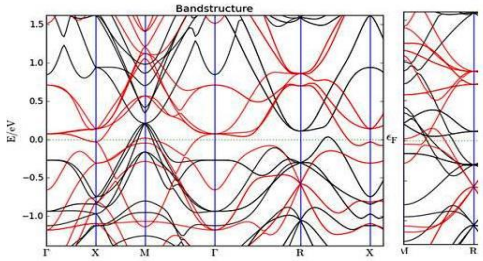

Figure 1. Electronic band structure of Ti_3Sb.

The electronic band structure of the Ti_3Sb presents metallic feature with separate band manifolds, i.e., separation of the valence and the conduction bands in the whole Brillouin zone as introduced in Fig. 1.

ANALYTICAL SOLUTION OF SCHRÖDINGER EQUATION FOR LINEAR COMBINATION OF THE MANNING-ROSEN AND YUKAWA CLASS POTENTIALS

Bayramova G. A.
Baku State University, Azerbaijan
gunel.bayramova2016@yandex.ru

In the present work, an analytical solution for bound states of the modified Schrödinger equation is found for the new supposed combined Manning-Rosen potential plus the Yukawa class. To overcome the difficulties arising in the case $l \neq 0$ in the centrifugal part of the Manning-Rosen potential plus the Yukawa class for bound states, we applied the developed approximation. Analytical expressions for the energy eigenvalue and the corresponding radial wave functions for an arbitrary value $l \neq 0$ of the orbital quantum number are obtained. And also obtained eigenfunctions expressed in terms of hypergeometric functions. It is shown that energy levels and eigenfunctions are very sensitive to the choice of potential parameters.

WEYL POINTS IN ACOUSTIC METAMATERIALS: THEORY AND APPLICATIONS

Amirullah M. Mamedov, Ekmel Ozbay
NANOTAM, Bilkent University, Ankara 06800 Turkey
mamedov@bilkent.edu.tr

Weyl semimetals are materials in which the electrons have linear dispersions in all directions while being doubly degenerate at a single point, called Weyl point, near the Fermi surface in 3D momentum space. Since the Weyl point or Weyl cone in Weyl semimetals represents a special dispersion of electrons moving in periodic potentials, the question naturally arises as to whether a similar dispersion or the Weyl point for classical wave propagating in artificial periodic structures exists.

Following the developments of Weyl phononic crystals with Weyl points for acoustic waves we report the theoretical investigation of Weyl points in 3D acoustic metamaterials. This study presented a fully continuous, load-bearing, elastic metamaterial capable of indirectionally-propagating and topologically-protected surface states. The design of the 3D unit cell, inspired to sandwich composites, consisted in a layered prismatic lattice with different cross-sections in which the layers were spaced by solid cylindrical elements and by slanted circular beams connecting consecutive faces of prismatic unit cell. The analysis of the lattice dynamics highlighted the existence of Weyl points following the breaking of the z-mirror-symmetry and the P-symmetry of the lattice. To gain insight into the mechanism leading to the formation of these degenerate points, we evaluated the topological invariants using ab-initio calculations.

This study may serve as a basis to develop composite-like structures having advanced elastic waveguiding capabilities for applications.

OVERVIEW OF THE ATLAS EXPERIMENT RESULTS

Cheplakov Alexander
Joint Institute for Nuclear Research, Dubna, Russia
alexander.cheplakov@jinr.ru

The Run 3 at the Large Hadron Collider will start at CERN in Spring 2022. By that time a rich and comprehensive program of the LHC detectors upgrade will be completed. Precision tests of the Standard Model and searches for New Physics phenomena using the full 2015−2018 (Run 2) dataset corresponding to 139 fb^{-1} are continuing. Selected results of the ATLAS experiment will be presented as well as the prospects towards the high luminosity era of the LHC operation.

DYNAMICS OF AC SQUID ON JOSEPHSON JUNCTION WITH UNHARMONİC CURRENT-PHASE RELATION

Askerzade Iman
Department of Computer Engineering and Center of Excellence of Superconductivity Research, Ankara University, Ankara, Turkey
Institute of Physics ANAS, Baku, Azerbaijan
imasker@eng.ankara.edu.tr

It is well known that ac SQUID consists of one Josephson junctions, including to superconducting loop. Suppose that a magnetic flux Φe passes through the interior of the superconducting ring. The flux on the JJ is not equal external magnetic flux Φe. Their difference is due to the screening current circulating in the ring. Such rings with JJ deserve as sensitive elements in SQUIDs. In all early studies of the dynamical properties of ac SQUID on JJ with unharmonic current-phase relation (see [1,2]), it was considered that CPR has a harmonic character

$$I = I_{c0} \sin \phi \tag{1}$$

Relationship (1) is fulfilled with a high accuracy for JJs on low temperature superconductors. In the case of JJs on high temperature superconductors, the CPR becomes unharmonic,

$$I = I_c f_\alpha(\phi) = I_{c0}(\sin\phi + \alpha \sin 2\phi) \tag{2}$$

where unharmonicity parameter α depends on the junction preparation technology. In general, anharmonicity in the CPR for high temperature and Fe-based superconductors-based JJ is associated with the d-wave behavior of the order parameter and many band characters of superconducting state in new superconducting compounds. Some dynamical properties of single JJs with an uanharmonic CPR (2) were studied in papers.

In this study we carried out the analysis of the dynamics of ac SQUID on Josephson junction with unharmonic current-phase relation. It was obtained expression for the effective critical current in this system. It is shown that, the dynamical properties of ac SQUID on JJ with unconventional CPR is determined by the renormalized critical current of JJ. Delay time and escape rate analyzed for different cases.

PRIMORDIAL BLACK HOLES AND SOME OF THE OBSERVATIONAL CONSEQUENCES

Rahvar S.
Sharif University of Technology, Iran
rahvar@sharif.edu

Primordial Black Holes (PBHs) as a result of large fluctuations of matter and energy in the early universe are one of the candidates for dark matter. Recent observations of gravitational wave (GW) signals indicate that the mass of black holes is tens time of the solar masses, much larger than the astrophysical black holes. In this talk, we will investigate the possibility of PBHs as the candidates for the source of GWs in the binary system where through merging in the binary systems produces the gravitational waves. Also, we study the probability that PBHs can collide with the earth. We will discuss the likelihood of this collision and at the end, constrain the PBHs that can compose the matter content of the Universe.

FUNDAMENTALS OF QUANTUM COMPUTING

Sajid Qamar
COMSATS University Islamabad, Pakistan
sajid_qamar@hotmail.com

In principle, Quantum Computers, which are based on quantum mechanics, can be exponentially fast than any fast-classical computers. Reason being, these can have inherent parallelism due to entanglement and superposition of states during operation. Quantum computing has attracted many companies like Google, IBM, Microsoft, Intel, etc. The research on quantum computers started in early 1980s when Richard Feynman pointed out that quantum physics cannot be simulated with classical computer therefore a quantum computer is needed to simulate quantum physics. Later, David Deutsch suggested a model for universal quantum computer. The interest in quantum computing has increased exponentially after Peter Shor and Lov Grover put forwarded their algorithms. A

standard model of quantum computer may consist of an array of qubits which are used as a framework for the quantum computation.

Quantum computing has had a tremendous impact in the field of cryptography. Peter Shor's algorithm has proved that classical cryptography is not safe against quantum computers and hence classical cryptographic systems are at risk. In this realm, new cryptographic systems and schemes based on quantum mechanics principles have been explored and presented. To add this, quantum entanglement is an important ingredient of quantum computing and is a pure quantum mechanical phenomenon which describes the correlation between two subsystems. Classical computers can only simulate non-entangled systems while quantum computers are needed for simulation of multi-entanglement. Recently, IBM has released a series of quantum devices that consist of five to twenty superconducting qubits. In this talk, basic understanding of quantum computing is presented along with some highlights on the past, present and future of quantum computing.

HIGH ANGULAR RESOLUTION AND TIME DELAY OF UNIQUE DOUBLE GRAVITATIONALLY LENSED QUASARS SDSS J1721+8842 FROM MAIDANAK OBSERVATORY

Asfandiyarov I.M.[1], Ehgamberdiev Sh.A.[1,2]
[1]Ulugh Beg Astronomical Institute of the Uzbekistan Academy of Sciences, Astronomicheskaya 33, 100052 Tashkent, Uzbekistan
[2]Department of Astronomy and Astrophysics, Physics Faculty, National University of Uzbekistan, 4 University str., Tashkent 100174, Uzbekistan
ildar@astrin.uz

We present the results of the detection of active variability and optical oscillations of the intrinsic light curves and of gravitationally lensed quasars SDSS J1721+8842, for the period 2018-2020 based on observations from the Maidanak observatory. Based on the best observations from the AZT-22 telescope with a quality of seeing=0.6-0.7”, followed by digital processing of MCS deconvolution, high angular resolution images

with a value of FWHM=0.26” of individual lensed point components, their light curves and lensing elliptical galaxy were obtained [2]. Precision astrometry of individual lensed components was obtained, which made it possible to estimate the measurement accuracy of ±0.015”. The intrinsic active optical variability of the components of lensed quasars that characterize nonstationary processes and oscillations resulting from variable energy release in active nuclei and accretion disks around supermassive black holes is determined. The sequence of variables of the lensed components A-C-B-D of SDSS J1721+8842 with a time delay is determined: AC=-8.5±1.7 days, AB=-10.3±1.7 days, and AD=-18.7±2.8 days.

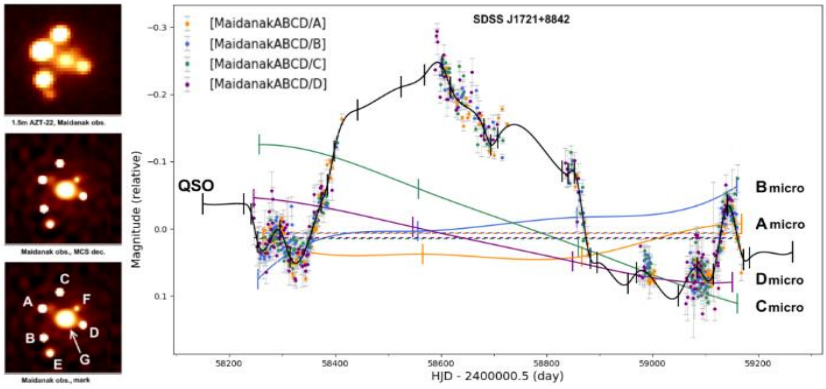

Fig.1. Results of MCS deconvolution of SDSS J1721+8842 from Maidanak observatory and intrinsic light curve of lensed quasars and extrinsic microlensing for the 2018-2020y.

DISPERSION OF THE INCOHERENT NEUTRON WAVES WHEN PASSING THROUGH THE MATTER

Abdulvahabova S.G., Bayramova T.O.
Baku State University, Baku, Azerbaijan
Sacidaabdulvahabova@bsu.edu.az; Tunzalabayramova@bsu.edu.az

On the basis of the density inhomogeneity of the crystal, we have studied the distribution of incoherent neutron wave. Fluctuations in the density of the matter cause scattering neutron wave. The starting point of

the calculation was the well-known formulas of the diffraction theory and the theory of multiple scattering. These formulas have been obtained under the assumption that the imaginary part of the optical potential is a local operator. The imaginary part of this potential models' inelastic processes and determines the amplification of an incoherent wave in the input channel. The resulting formulas are applied to the calculation of the dispersion properties of the incoherent neutron wave. According to the results, the frequency of the scattered nucleon wave decreases with increasing density fluctuations. The results show, that the effective cross section for scattering from all nuclei of matter is not the additive sum of the effective cross section of the scattering from one nucleus. This is due to the interference of neutron waves.

DEUTERON IN THE FRAMEWORK OF SOFT-WALL MODEL ADS/QCD

Huseynova N.J., Mamedov Sh.A., Badalov V.
Institute for Physical Problems, Baku State University Baku, Azerbaijan
nerminh236@gmail.com

Deuterium is used in heavy water moderated fission reactors, usually as liquid D_2O, to slow neutrons without the high neutron absorption of ordinary hydrogen. In research reactors, liquid D_2 is used in cold sources to moderate neutrons to very low energies and wavelengths appropriate for scattering experiments. Experimentally, deuterium is the most common nuclide used in nuclear fusion reactor designs, especially in combination with tritium, because of the large reaction rate (or nuclear cross section) and high energy yield of the D–T reaction.

In present work, the profile function of deuteron is described in the framework of soft-wall model of the Anti-de Sitter (AdS)/Quantum Chromodynamics (QCD), where the nonpertur-bative aspects (such as confinement and chiral symmetry breaking) of QCD and finiteness condition of the 5D action is provided by multiplying an extra exponential factor (called Dilaton field) to the Lagrangian in the action.

We introduce deuteron field as a twist 6 vector field in the bulk of AdS space and write action for this field in this bulk. We consider Dilaton

wave function in the 4D as a boundary value of the 5D field. Using this action, we write Lagrange-Euler equation for the deuteron field and obtain an equation over the *z* coordinate. Solving this equation, we find profile function for the deuteron in the framework soft-wall model AdS/QCD.

POLARIZATION OF NUCLEON IN THE LOCAL POTENTIAL WITH SPIN-ORBITAL INTERACTION

Afandiyeva I.G., Ahmedov R.A.
Azerbaijan State University of Oil and Industry, Baku, Azerbaijan
afandiyeva.irada@asoiu.edu.az; ahmedov.rasim@asoiu.edu.az

A study of the calculations of polarization effects associated with the scattering of hadrons on the nucleus in the pulse approximation. The local interaction potential includes the spin-orbit interaction. In this case, the transition occurs directly from the initial to the final state of the cluster transfer without changing the internal states of the nucleons. The scattering amplitude contains a term that depends on the spin orientation and a term that does not depend on the spin orientation, and the polarization occurs due to interference between these two parts of the scattering. The degree of polarization is proportional to the probability that the cluster "aimed" at the initial nucleus with the corresponding values of momentum and angular momentum are captured to form a composite nucleus. The polarization sign depends on the value of the incident particle energy. Depending on the energy, there is interference from positive and negative scattering angles and this affects the sign of polarization. It is of interest to study polarization for individual energy regions. This can monitor the change in the polarization sign.

THE BOLTZMAN'S "COMPLEXIONS" IN PLANK'S BLACK-BODY RADIATION

Isayeva E.A.
Institute of Physics, ANAS, Baku, Azerbaijan
elmira@physics.ab.az

It is known the energy depends on temperature as E=kT. However, this law doesn't explain black body radiation (ultraviolet catastrophe). Therefore, Plank has taken another law of dependence energy on entropy: dU=TdS. Boltzmann has expressed S from chaos conception S=klogW, where W is thermodynamic probability of system. The probability itself connected with combinatory theory. Here Boltzmann has considered set of states of system P (P is large) which can be theoretically observed by our experiment and atoms which are not perceived by us (N is small). N are thrown on P. The number of combinations of this arrangement ξ is the "complexions", as them called by Boltzmann himself.

$$\xi = \frac{(N+P-1)!}{(N-1)!\,P!} = \frac{(N+P)^{N+P}}{N^N\,P^P}$$

Plank has used these "complexions" to get his formula of black body radiation. The thermodynamic probability W is proportional on this ξ. By using $S_N = klog\xi$, $S = \frac{S_N}{N}$ and $\frac{dS}{dU} = \frac{1}{T}$ Plank has got his formula $U = \frac{\varepsilon}{e^{\frac{\varepsilon}{kT}}-1}$. He can do it with account degenerate state of energy.

In our proposal we will get this formula for case without degeneration by using new scheme, where P= 2 , ξ=N+1. The Gibbs Canonical distribution connecting number of atoms with energy: $N_n = Af_n e^{\frac{-E_n}{kT}}$, where f_n is the stutistical weight or level of degeneration. To get rid of degeneration and go over our cheme it is necessary N_n devide on f_n. Then

$$n = \frac{N_n}{f_n} = Ae^{\frac{-E_n}{kT}},$$

Where n is number of atoms on one level of energy E_n . In case $n = n$+1 we obtain:

$$n+1 = Ae^{\frac{-E_{n+1}}{kT}}$$

where E_{n+1} is next energy level. When in system of n+1 atom remain n atoms then it is radiation. This radiation is the portion of energy ε : $E_n - E_{n+1} = \varepsilon$. Let's devide $n+1$ on n .$\frac{n+1}{n} = 1 + \frac{1}{n} = e^{\frac{E_n - E_{n+1}}{kT}}$, then $n = \frac{1}{e^{\frac{\varepsilon}{kT}} - 1}$. If all atoms will radiate the quant energy of ε , then we will get finding energy of radiation of black-body $U = \frac{\varepsilon}{e^{\frac{\varepsilon}{kT}} - 1}$. It is formula of Plank.

The question may arise, what to do with degenerate states, since we are considering the nondegenerate case. Do they not radiate energy? The fact of the matter is that they do not emit, because one of the degenerate states with the energy E_n is realized in life, in our experiment.

PYGMY DIPOLE RESONANCE IN ^{164}DY

Guliyev E.[1], Quliyev H.[2], Kuliev A.A.[2]
[1]State Agency on Nuclear and Radiological Activity Regulation, Ministry *of Emergency Situations, Baku, Azerbaijan*
[2]The National Aviation Academy of Azerbaijan, Baku, Azerbaijan
akbar.guliyev@fhn.gov.az

In this study the excitation of the pygmy dipole resonance (PDR) in even-even ^{156}Dy is investigated through quasiparticle random-phase approximation (QRPA), where an electric response emerges by showing ample distribution at energies below 10 MeV. We, therefore, study the transition cross sections and probabilities, photon strength functions, transition strengths, isospin character, and collectivity of the predicted E1 responses.

The computed transition probabilities for E1 spread over energy region of $6 \leq E \leq 10$ MeV with a structure similar to resonance, where the strength tends to be distributed over many different peaks of the K=0 and K=±1 component, with either of them dominating the response. The results extracted from our calculations agree well with those nuclei that having PDR in the neighborhood of ^{156}Dy nucleus of interest [1,2]. Despite in general to the PDR attributed the excitation below 8 MeV the calculations

for ^{156}Dy nucleus have shown the summed strength taken up to the threshold energy (~ 9.6 MeV) in good agreement with well-known systematics. Therefore, for the nuclei with threshold energy around 10 MeV, it's possible to observe PDR in these energies.

Recently, the structure and collectivity of E1 excitations under the particle threshold energy has become the subject of theoretical studies [3]. The calculation realized that for both K=0 and K=±1 component of E1 excitations below the particle threshold energy the electric dipole excitations are mainly formed by only-neutron-neutron or only-proton-proton configurations, the minor contribution of the other does not exceed 10% of the total in any of the cases. The results reveal that the E1 transition strengths in ^{156}Dy nucleus below the particle threshold, microscopic interpretations of states show structural differences than macroscopic interpretations.

From analyzing the results obtained here, we can say PDR mode mainly is weakly collective in nature than that for the Giant Dipole Resonance and the small B(E1)$\leq$ 0.15e^2fm^2 values are characteristic of them around near the neutron binding energy (6-8 MeV).

It is well known that spin-flip resonance (SFR) shares almost the same energy interval with PDR and may overlap with it. To investigate the role of SFR in formation of excitations below 10 MeV, here we studied the contribution of M1 excitations in the $^{154\text{-}164}$Dy spectrum below 10 MeV. The comparison of the calculated results of the E1 and M1 dipole transition indicates a dominant role of E1 contribution, with there being no considerable predicted spin-flip contribution to the dipole strength in the PDR region.

INVESTIGATION OF THE MAGNETIC DIPOLE MOMENTS OF THE $I^{\pi}K=1^{+}1$ STATES WITH EXTREMELY SHORT LIFETIMES ($\leq 10^{-15}$ SECOND)

Kuliev A.A.
The National Aviation Academy of Azerbaijan, Baku, Azerbaijan
akuliev80@yahoo.com

Magnetic moments are one of the attractive features of atomic nuclei that play an important role in nuclear structure and are used to test the validity of nuclear models. In this study for even-even $^{144\text{-}154}$Sm nuclei, the axially symmetric basis has been used to describe the magnetic moments of $I^{\pi}K=1^{+}1$ states in the framework of the random-phase approximation.

The first time we obtain the formula for magnetic dipole moments of $1^{+}1$ excitations. The measured magnitude of the magnetic moment μ_{1^+} is associated with the intrinsic internal magnetic moment $\overline{\mu}'_{1^+}$ in relation

$$\mu_{1^+} = \frac{1}{2}\left(g_R + \bar{\mu}'_{1^+}\right) \quad ; \quad \bar{\mu}'_{1^+} = \sum_{\tau=n,p}\left(s_{ss'}\psi^i_{qs}\psi^i_{qs'}\right)_\tau + \sum_{\tau=p}\left(l_{ss'}\psi^i_{qs}\psi^i_{qs'}\right)_\tau$$

Where g_R and ψ^i_{qs} correspond to rotational gyromagnetic factor and the phonon two-quasiparticle amplitudes of even-even nuclei. The $s_{ss'}$ and $l_{ss'}$ are spin and orbital matrix elements, respectively.

Until today, there are no experimental data for magnetic moments of the excited states with extremely short lifetimes (femto seconds). Therefore, to gain a deeper understanding of the deformation dependence of the summed magnetic moments, in figure 1 we show δ_2 and δ_2^2 dependence of the magnetic moments of $1^{+}1$excitations.

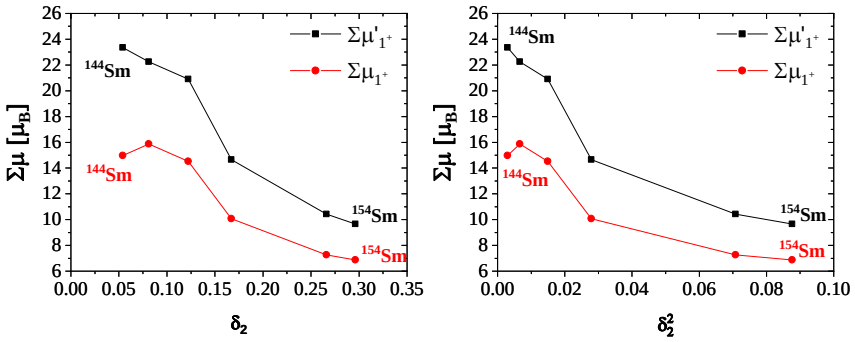

Fig. 1. The summed magnetic moments of 1^+1 excitations below 4 MeV as functions of δ_2 and δ_2^2 deformation parameters for $^{144\text{-}154}$Sm. Here $\mu_B = E\hbar/2mc$.

As can be seen from the figure with increasing deformation parameters the summed values of the magnetic moments decrease almost inversely. The magnetic moments of spheroidal light $^{144\text{-}148}$Sm nuclei are about two times greater than the magnetic moments of well-deformed heavy $^{150\text{-}154}$Sm nuclei. It should be noted the remarkable features of 1^+1 states obtained from experimental results are the quadratic dependence of the summed B(M1) values on the ground-state deformation parameter δ_2.

EXPERIMENTAL STUDY OF INFLUENCE OF DIFFERENT LEVELS OF HELIOGEOPHYSICAL ACTIVITY FLUCTUATIONS ON THE FUNCTIONAL STATE OF THE ADULT FEMALE BRAIN

Allahverdiyeva Aysel[1,2], Allahverdiyev Ali[1], Babayev Elchin[3]
[1]Institute of Physiology named after A.I.Garayev, Azerbaijan National Academy of Sciences
[2]Institute of Physical Problems, Baku State University
[3]Baku State University

Heliogeophysical activity changes not only affects the functioning and reliability of technical systems in space and on the ground, but may also endanger the biosphere, particularly, human beings. A number of works dedicated to investigation of these kinds of influences reveals that

not only central, but also the vegetative nervous system of human beings is very sensitive to geomagnetic disturbances.

We continued our studies on the influence of geomagnetic field disturbances on the functional state and adaptive capabilities of the human brain of healthy individuals.

Here we present the results of a personalized study of the bioelectrical activity of the human brain of female aged between 30-35 in a state of relaxed wakefulness on magnetically quiet days (when planetary geomagnetic index Kp = 1-2) and on days with weak geomagnetic disturbances (Kp = 4). Registration of bioelectric activity of the human brain was carried out on a computerized encephalograph "Neuron-Spectrum-5", which is a versatile and expandable 32-channel digital electroencephalograph (EEG) system with a large number of high-quality polygraphic channels to record any physiological signals.

Using "Neuron-Spectrum.NET" software for EEG recording and analysis, we have studied artifact-free 10 second EEG segments of both hemispheres with the temporal areas. Geomagnetic Kp index is used in analysis which is more reliable index for study of changes in EEG characteristics.

The conducted electrophysiological studies indicate that on days with a weak geomagnetic disturbance, in comparison with calm days, there was a diffuse increase in the index and in the right temporal region of the amplitude of the theta-rhythm, on the background of a decrease in its frequency, a diffuse increase in the index, frequency and amplitude of delta-rhythm and an increase in the index, frequency and amplitude of the fast-frequency beta-rhythm (beta-2), mainly in the right hemisphere.

Considering that the theta-rhythm is generated by the structures of the hippocampal formation, a diffuse increase in the severity of the theta rhythm on days of geomagnetic disturbance indicates the activation of the septo-hypocampal system and an increase in its contribution to the formation of the bioelectric activity of the cortical regions. It is known that the subcortical structures and the hippocampal formation are a sensitive screen that reacts to electromagnetic oscillations of the external environment.

Obtained in the structural organization of the electroencephalogram, on days of geomagnetic disturbance, the ratio of slow-fast rhythms, indicate an imbalance in the activity of the activating and deactivating links of nonspecific systems. There is an increase in ascending synchronizing influences and a weakening of activation messages.

The increase in the severity of the beta-2 rhythm with a right hemispheric accent observed on the days of geomagnetic disturbance on the background of a decrease in the representation of the beta-1 rhythm and an increase in the values of the delta rhythm characteristics is associated with a compensatory reaction of the brain regulatory formations in response to the imbalance in the links of nonspecific systems and the prevalence of in the structure of the EEG of slow activity.

The right hemisphere emphasis of increase of beta-2 rhythm, in response to increased geomagnetic activity, is probably associated with greater activation of the right hemisphere, which is responsible for emotional responses. On days of geomagnetic disturbances, in EEG in some women in the frontal-parietal regions of both hemispheres, bilaterally-synchronously there were registered the pointed and sharp waves exceeding the background by amplitude.

The area of registration of flashes, their frequency range and bilateral synchronization indicate the diencephalic genesis of paroxysmal activity provoked by the reaction of these cerebral regions to the geomagnetic disturbances.

Paroxysmality on the EEG, provoked by an increase in the geomagnetic situation, suggests the need to develop a number of preventive and therapeutic measures in the so called “risk” group.

SPECIFIC CYCLIC PATTERNS OF INFLUENZA INCIDENCE IN AZERBAIJAN ON LONG TIME-SERIES OF DATA AND POSSIBLE RELATION WITH SOLAR AND GEOPHYSICAL ACTIVITY

Babayev Elchin, Asgarov Abbas, Pirguliyev Mahir
Baku State University
mahir@bsu.edu.az

The spread of epidemics and pandemics of infectious diseases, including influenza, depend mainly on individual, physiological or immunological factors as well as on population/social and specific healthcare system phenomena but their appearance might be also related to various

meteorological or heliogeophysical factors as part of the natural physical environment. The aims of this study were to investigate the temporal dynamics of monthly influenza incidence in Azerbaijan by using relatively long time-series of monthly data (considered period 1976-2000 covers more than two 11-year solar cycles, namely full cycles 22 and 23, and partially 24 with ascending and descending phases of the considered solar cycles), to estimate any seasonal and multicomponent cycles and to consider influenza incidence cyclicity for similarities to and associations with main heliogeophysical cycles. The data were divided in 3 main intervals: Interval 1 (time period: 1976-1990, number of months: n=180), Interval 2 (1991-1995, n=60) and Interval 3 (1996-2000, n=60). It was done to reflect eventual underlying demographic, social and other changes occurring during this period and possible influencing the population and their health state, particularly, influenza incidences.

Results of Scargle's periodogram analysis based on the performance of the program for calculating the discrete Fourier spectrum and statistically significant periods are discussed.

A number of multiannual cycles with different periods were observed and most of these cycles correspond to similar cyclic parameters of heliogeophysical activity. It is revealed that influenza incidence/occurrence (morbidity) is correlated with solar activity (SA) accompanied by decreased cosmic ray activity (CRA) and gradually changing (background, having maxima just before and after 11-year SA maximum) geomagnetic activity (GMA) meanwhile severe geomagnetic disturbances (which are intense at solar maximum year(s)) and proton flux does not show significant correlations with influenza morbidity.

Investigations reveal that influenza epidemic usually begins 2 - 3 years before and/or 2 - 3 years after the 11-year sunspot cycle maximum. SA might indirectly influence influenza outbreaks by means of (through) GMA influence on biological organism. Virological-morphological study shows that majority of pandemics takes place at the ascending phase of solar cycle, just before SA maximum. Some strains of influenza virus show periodicity of appearance approximately every 30-35 years, which is close to three solar cycle length or so called ~ 35-year Bruckner (climatic) cycle.

Distribution of an influenza epidemic in the minimum and maximum of SA could be explained by quantity of UV-radiation, received by an or-

ganism during different phases of solar activity cycle; an alternative hypothesis to explain variations in influenza infections could be an effect of vitamin D when increased solar activity decreases (through ozone and UV-regime) the global vitamin D status in humans, decreasing their immunity to the influenza virus.

Influenza shows seasonal dependence being maximum in February in middle-latitude Northern country; the seasonal factor can move nearer or remove a flash of influenza outbreaks.

GLOBAL AND REGIONAL BIOEFFICIENCY OF HELIOGEOPHYSICAL FACTORS IN SUBARCTIC AND MIDDLE LATITUDES

Samsonov S.
Federal State Budgetary Scientific Institution, Yu.G. Shafer Institute of Cosmophysical Research and Aeronomy of Siberian Branch of the RA of Sciences, Yakutsk, Russia
s_samsonov@ikfia.ysn.ru

The connection between geomagnetic disturbances and cardiovascular events has been actively studied both in the past and at the present time. It is known that the same geomagnetic disturbances cause different responses of the cardiovascular system of volunteers, depending on the region of residence. Based on the results of synchronous multi-latitude monitoring in subarctic (Yakutsk) and middle (Saratov) latitudes, the myocardium response to changes in space weather was estimated according to the T-wave coefficient in the ECG phase portrait. Measurements had been carried out daily for 2 months. The groups of volunteers in different regions were comparable in age and gender. The synchronization of the dynamics of the T-wave coefficient with the dynamics of the Kp-index of geomagnetic disturbance was analyzed. Two groups of geomagnetic disturbances were distinguished: Group 1 - disturbances to which the reaction of the myocardium was of the same type in subarctic and middle latitudes; Group 2 - disturbances that did not cause the same type of myo-

cardial reaction in the surveyed volunteers from different regions. The differences in geomagnetic disturbances in groups 1 and 2 are analyzed for a set of indicators, including the values of the solar wind parameters, the Bz-component of the interplanetary magnetic field, the Kp-index of geomagnetic disturbance, and middle latitudes.

BIOEFFECTIVENESS OF GEOMAGNETIC VARIATIONS IN THE PERIOD AND OUT OF THE PERIOD OF CORONAVIRUS INFECTION

Parshina S.[1], Samsonov S.[2]

[1] Saratov State Medical University n.a. V.I. Razumovsky of the Ministry of Health of Russia,
Saratov, Russia

[2] Federal State Budgetary Scientific Institution, Yu.G. Shafer Institute of Cosmophysical Research and Aeronomy of Siberian Branch of the RA of Sciences, Yakutsk Scientific Center of the Siberian Branch of the Russian Academy of Sciences, Yakutsk, Russia

parshinasvetlana@mail.ru

The impact of space weather factors on human health is being studied by many research teams, and in the context of the ongoing epidemic of coronavirus infection, it attracts special attention of modern researchers. The bioeffectiveness of geomagnetic variations in the minimum of the 11-year solar cycle was studied in a long-term 2-month monitoring of the cardiac sensitivity of healthy volunteers during the coronavirus pandemic (2020) and outside the pandemic (2019). Observation groups in 2019 and in 2020 consisted of the same volunteers. The conditions for the occurrence of direct and delayed (by 1-2 days) myocardial reactions were established, taking into account certain values of the Kp-index of geomagnetic disturbance, the dynamic pressure of the solar wind and the Bz-component of the interplanetary magnetic field both during the period of the coronavirus infection pandemic and outside this period.

BIOTROPIC EFFECTS OF THE AURORAL ELECTROJET DURING THE PERIOD OF MINIMAL ACTIVITY OF THE 11-YEAR SOLAR CYCLE

Kodochigova A.[1], Samsonov S.[2], Polidanov M.[1]

[1]Saratov State Medical University n.a. V.I. Razumovsky of the Ministry of Health of Russia, 410012, Saratov, Russia

[2]Federal State Budgetary Scientific Institution, Yu.G. Shafer Institute of Cosmophysical Research and Aeronomy of Siberian Branch of the RA of Sciences, Yakutsk, Russia

kodochigovaai@yandex.ru

In recent decades, the scientific community has been actively increasing its interest in the problem of solar-biosphere relations, namely, the influence of space weather factors on the Earth's biosphere and, in particular, human health: both physical and psychological. Space weather has a multifaceted effect on the human body, however, in some cases, its influence remains a mystery. This is especially true for high latitudes, where the impact of space weather is greatest. The report examines the influence of the auroral electrojet during the period of minimal activity of the 11-year solar cycle on the psychological characteristics of the personality of the inhabitants of the polar latitudes, through the prism of their anxiety, to identify the risk of developing psychosomatic pathology in them. In a number of papers, it was shown that the most pronounced biotropic effects of space weather were detected at high latitudes (using the example of the influence of geomagnetic disturbance on the cardiovascular system) precisely at minimal solar activity. To achieve this goal, an integrative indicator of heliogeomagnetic disturbance was established – the Kr index (daily during March and April 2019); in addition, a special AE index was used, including measurements of high-latitude stations in the polar oval area, allowing detailed investigation of geomagnetic disturbances; to study the psycho–emotional state - the author's approach based on a combination of a number of psychological techniques. It was shown that the influence of the auroral electrojet varies depending on the presence of psychological sensitivity to changes in geomagnetic disturbance and anxiety levels of the observed persons.

PROPERTIES OF ERYTHROCYTES IN PATIENTS WITH ANGINA IN DIFFERENT PERIODS OF THE 11-YEAR SOLAR CYCLE

Parshina S., Tokaeva L.
Saratov State Medical University n.a. V.I. Razumovsky of the Ministry of Health of Russia, Saratov, Russia
624494@mail.ru

It is known that the short-term and long-term reactions of the human body to fluctuations in solar and geomagnetic activity may differ. For example, on the days of a geomagnetic storm, an increase in the daily frequency of acute myocardial infarction is observed, however, the analysis of the relationships between the daily amount of myocardial infarction and geomagnetic activity over longer periods sometimes yields conflicting results. In the well-known works of Yu.I.Gurfinkel, the phenomenon of erythrocyte sludge (gluing) is noted during geomagnetic disturbances in patients with coronary heart disease. The aim of this work was to assess the functional properties of erythrocytes (aggregation activity and deformability) in a longer period - in different phases of the 11-year solar cycle.

In the 23rd 11-year cycle of solar activity, two periods were distinguished. The first half of the 11-year cycle (the period of increased solar activity) was characterized by high values of Wolf numbers (112.0 ± 2.9). The second half of the 11-year cycle (the period of decline in solar activity) was characterized by lower values of the Wolf numbers (62.4 ± 3.9). To estimate solar activity from Wolf numbers, we used data from the Institute for Space Research, Russian Academy of Sciences. We examined 115 patients with secondary unstable angina pectoris: during the period of increased solar activity - 64 people, and in the recession phase - 51 people. The growth phase of solar activity in patients with secondary unstable angina pectoris is characterized by a decrease in the aggregation activity of erythrocytes and an increase in their deformability, which indicates the activation of protective and adaptive mechanisms aimed at maintaining oxygen delivery to tissues. In the phase of decline in solar activity in the

11-year cycle, in comparison with the growth phase, the aggregation capacity of erythrocytes increases and their deformability decreases. Thus, the phase of the decline in solar activity in the 11-year cycle is characterized by a lower activation of the compensatory mechanisms of the blood rheology system. The results obtained indicate that fluctuations in solar activity act not only as activators of the pathogenetic mechanisms of cardiovascular pathology, but also as factors that activate the protective and adaptive reactions of the human body. Probably, evolutionarily, it is these features that ensure the existence of the human body as a component of the biosphere.

SOLAR-EARTH COMMUNICATIONS, REACTIVE OXYGEN SPECIES AND STRUCTURAL DNA DAMAGE

Tekutskaya E.
Kuban State University of the Ministry Science and Education of the Russian Federation, Russia
tekytska@mail.ru

Reactive oxygen species play a significant role in the regulation of the basic functions of the cell both under normal conditions and when the cell is exposed to exogenous and endogenous factors under conditions of variations in electromagnetic and radiation at different levels of solar activity. The effect of a low-intensity alternating magnetic field, comparable in intensity to the geomagnetic field, on the degree of oxidative damage to DNA in blood serum of healthy donors, was studied by determining the content of 8-hydroxy-2-deoxyguanosine and single-strand breaks in DNA. There was an increase in the level of 8-OHdG in DNA by a factor of 1.5-2 in comparison with non-irradiated samples, as well as a nonlinear change in the content of lipid peroxide in blood serum. The obtained effects can be associated with the generation of reactive oxygen species in aquatic environments with changes in solar activity, which can affect the adaptive capabilities of the human body as a whole.

ELECTRON MOTION IN A CONTINUOUS MEDIA WITH EXTERNAL MAGNETIC FIELD

Abbaszade J.M., Abdullazade Ch.V., Agayeva U.F., Ahmadova G.T., Aliyeva, A.Y., Aliyeva N.E., Ali R.R., Aslanova R.K., Davudova K.L., Ismayilova G.E., Jafarli Kh.D., Maharramova L.G., Muradova S.M., Pir-Mahammad Abdullahi Sh.Sh., Suleymanli A.M., Zeynalova Ch.A. Jafarov R.G.

[1] Baku State University, Baku, Azerbaijan

fizing08@mail.ru , r.g.jafarov@gmail.com

An electromagnetic process has a fundamental sense for a number of natural phenomena. The combination of the classical electrodynamics with hydrodynamics has resulted in magnetic hydrodynamics, which is directly related to plasma physics. When solving magnetic hydrodynamics equations in the form of a plane wave for electron precessions propagating in the continuous media located in the external uniform magnetic field, according to the dispersion law, the electron precession frequency ω substantially depends on the direction of the wave vector $\vec{k}$ as $\omega = (4\pi\rho)^{-1/2}\vec{H}\vec{k}$. I.e., the electron motion in the ideal-like continuous media which located in the constant magnetic field is an electron spontaneous moving and precession in the Alfven wave propagating in the constant magnetic field, in principle.

In this paper, we study the propagation of small perturbations of an electron in a continuous media (with neglect of all dissipation processes in it), i.e. in an ideal liquid (or gas), located in a uniform constant magnetic field B. The wave function of an electron is found in states in which it has certain values of momentum and angular momentum along the direction of the field. The energy spectrum and wave function are calculated. To study this problem, we determine the energy levels of the electron in the constant magnetic field as following by L.D.Landau with alternative method for solution of Schrödinger equation. Firstly, and then we calculate the energy levels and wave function of electron moving and precession and then the lifetime of the electron residence at the corresponding quantum levels during precession.

SPECTRAL ACTIVITY OF THE HERBIG Ae STAR HD 31648

Rustamov B.N.[1,2], Mikailov Kh.M.[1], Alisheva K.I.[1,2], Mammadova S.O.[2], Aliyeva V.I.[2]

[1] Baku State University, Baku, Azerbaijan

[2] Shamakhy Astrophysical Observatory named after N. Tusi ANAS, Azerbaijan

bayram_rustam@yahoo.com

The physics of the observed peculiarities of young stars type Ae/Be Herbig is mainly determined by the results of the interaction between the young star and the surrounding circumstellar medium. In this regard, for the analysis are chosen the following features in the spectrum of the star HD31648: lines of the Balmer series of hydrogen (Hα - Hδ), HeI 5876 Å, resonance sodium doublet DNaI and FeII 42 ($\lambda\lambda$ 4924 Å, 5018 Å, 5169 Å).

Spectral observations of the star HD31648 were carried out at the Cassegrain focus of the 2-meter telescope of the Shamakhy Astrophysical Observatory named after N.Tusi, on the fiber echelle spectrograph ShaFES, with a spectral resolution R = 28000, in the wavelength region λλ3900–7500 ÅÅ. The processing of echelle spectra was carried out by standard method using the new version of the DECH 30 program.

The observed lines Hα and Hβ in the spectrum of the star HD31648 show profiles type P Cyg, which are direct indicators of mass ejection. The Hα line profile can be classified as P Cyg III, with a secondary blue emission peak. The greatest variability is observed in the blue part of the Hα profile. January 25, 2019, a classic P Cyg profile was observed. The two-component profile, with the ratio V/R << 1, was observed on two dates (12.14.19 and 01.17.20), and at 01.17.20 the intensity of the blue emission component increased, while the intensity of the red emission component decreased. On 12.21.19, a secondary emission component was found on the blue wing of the Hα line.

In the central part of the profile of the Hβ line, the structure type P Cyg with a variable emission component and broad photospheric wings is observed. Except January 25, 2019, a weak emission component was simultaneously observed in the blue side of absorption of P Cyg. On the night of 12.21.19, a weak absorption circumstellar component appeared on the blue absorption wing, synchronously with the appearance of a similar

structure in the Hα line. On 01.17.20, in the intensities of the blue and red emission components in the absorption P Cyg, in the Hβ profile occurred a similar change, as in the Hα line.

The resonance doublet DNaI in the spectrum of the star HD31648 consists of two components - a narrow interstellar component (IS) and strong variable circumstellar component (CS) with a P Cyg structure. The radial velocities of the IS component on average is 13.3 km/s at both lines D1 and D2 NaI. A weak absorption circumstellar component is noticeably released in the red part, at 01.25.2019, but at 12.21.2019 and 01.17.2020, in the blue part of the CS absorption.

SPECTRAL STUDY OF THE NOVA ASASSN-17HX (SCT2017)

Mikailov Kh.M.[1], Alisheva K.I.[1,2], Rustamov B.N.[1,2], Alakbarov I.A.[1], Alili A.H.[1]
[1]Baku State University, Baku, Azerbaijan
[2]N.Tusi Shamakhy astrophysical Observatory of ANAS, Shamakhy, Azerbaijan
kamalaalisheva@bsu.edu.az

The outbreak of the Nova ASASSN-17hx for the first time was detected by the All Sky Automated Survey for Super Novae (ASASSN) and announced in Astronome's Telegram on June 23, 24, 2017. We have carried out spectral observations of this star. The observations were carried out on the fiber optic echelle spectrograph ShaFES, at the Cassegrain focus of the 2-m telescope of the Shamakhy Astrophysical Observatory during August-November for 15 nights with different intervals. The obtained spectra, with a resolution of R = 28000 (in the wavelength range λλ3900-8000ÅÅ), cover the moments of minimum and maximum on the light curve, as well as the moment of the secondary outburst of the Nova ASASSN-17hx. Also, for building a complete picture of the processes occurring at the Novaya ASASSN-17hx, we used the ESO (R =110000) and ARAS (R =9000-11000) spectra obtained in July, August and October.

All spectra were processed using the DECH 30 program. Measured the profiles of the spectral lines were constructed, the radial velocities of the stellar and interstellar spectral lines. It was found that the Balmer

lines are more intense, the HeI lines are noticeable, the lines of ionized metals make up the majority. With the exception of HeI, all absorption lines show a two-component structure. The first narrow component arises during the outburst of 1 maximum, and the second broad component of absorption during the second outburst. This proves that there were 2 powerful ejections of matter on the star. The velocity of the first was -450 km/s (FWH=30 km/s), and the second -685 km/s (FWHM=130 km/s). At the maximum, the lines show mainly P-Cyg profiles. The absorption of the Hα line shows a five-component structure with the corresponding radial velocities RV_1 =-1146 km/s, RV_2 =-1054 km/s, RV_3 =-972 km/s, RV_4 =-798 km/s, RV_5 =-508 km/s. This is due to layers, with different velocities (it is assumed that this may be due to the presence of different velocity layers in the upper atmosphere). The profiles of the absorption lines of the interstellar medium NaI and CaII show an eight-component structure with, respectively, radial velocities of -13.2 km/s, +8.3 km/s, +25.4 km/s, +48.5 km/s, +57.9 km/s, +63.6 km/s , +73.8 km/s, +102.3 km/s. This indicates that the interstellar medium in the direction of the star has a multilayer structure.

Also, a light curve was plotted during the observation period, the data of which were taken from the AAVSO (photometric base). This was done for carrying out a comparative analysis of the spectrum and light curve of the star.

THE FUNDAMENTAL PARAMETERS OF THE STAR HD164613(F2II)

Samedov Z.A.[1,2], Aliyeva Z.F. [1], Hajiyeva G.M.[2], Rustam U.R.[2]
[1]Bakı State University, Azerbaijan
[2]Shamakhi Astrophysical Observatory of ANAS, Azerbaijan
zahir.01@mail.ru

In this work the fundamental parameters of HD164613(F2II) star: the effective temperatures T_{eff} and the acceleration of gravity g, the microturbulent velocity ξ_t and the metallicity [Fe/H] are determined. The

spectrum of the star was obtained with the spectrograph of the CCD-matrix of the 2-meter telescope of the Shamakhi Astrophysical Observatory of ANAS (R=56000, S/N=150-400). The spectra were developed by DECH program, the equivalent widths of spectral lines were measured. The effective temperature T_{eff} and the acceleration of gravity g of the stars were determined by the model and the parallax method [2,3]. The model method is based on a comparison of the observed and theoretically calculated values of the photometric quantities [c1], Q, and the equivalent widths of the spectral lines of the hydrogen Balmer series. The parallax method does not depend on models. We determined the T_{eff}=6800K, logg=2.6 for the star HD164613(F2II). In [1] is determined Teff=6874K for the star HD164613, which corresponds to the value obtained by us.

On the base of the Kurucz ATLAS 9 program the basic parametric model T_{eff}=6800K, logg=2.6 was calculated and giving various values to the microturbulent velocity ξ_t in the stellar atmosphere the abundance of iron $log\varepsilon(FeII)$ was determined on the basis of this model. The atomic data of spectral lines are taken from the VALD 3 database [vald.astro.uu.se]. According to the graph, where the abundance of the element does not depend on the equivalent widths of the spectral lines, ξ_t determined the microturbulent velocity in the atmosphere of the studied star. The microturbulent velocity $\xi_t = 3$ km/sec, the abundance of iron element $log\varepsilon(Fe)$=7.36±0.12 was obtained according to *FeII* lines. The metallicity of the star is [Fe/H]=-0.11. As is shown the metallicity is practically the same in the studied star and Sun [4], so, they are formed from the same metallicity matter. This result is important from the point of view of the theory of the chemical evolution of stars.

THE CONTRAST OF CORONAL HOLES AND RELATION WITH PARAMETERS OF THE SOLAR WIND AT 1AU

Asgarov Abbas
Baku State University, Azerbaijan
asgarov@gmail.com

We analyzed more than 400 images obtained in the λ284˚A channel. It is shown that the contrast of coronal holes (CH) determines the speed of the solar wind streams to the same extent as their area does. The time interval under examination covers about 1500 days in the declining phase of cycle 23 (from2002 to 2006). We considered all coronal holes recorded during that interval in the absence of coronal mass ejections (CME). The comparison was also made with some other parameters of the solar wind (e.g., density, temperature, and magnetic field). A fairly high correlation (0.70–0.89) was obtained with the velocity, especially during the periods of moderate activity, which makes this method useful for everyday forecasts. The ratio of CH brightness to the mean brightness of the disk in the λ284˚A channel is about 25%.

ESFFECTS OF GEOMAGNETIC STORMS ON THE MID-LATITUDE D-REGION IONOSPHERE

Bayramova E.V., Mustafa F.R.
Shamakhy Astrophysical Observatory named after Nasraddin Tusi, ANAS, Shamakhy, Azerbaijan
famil.mustafa@gmail.com

The response of D Layer Preparation Time (DLPT) depth to geomagnetic storms during 2008-2011 is studied to investigate the effect of geomagnetic storms on the D layer of the Ionosphere. The Very Low Frequency (VLF) signal at 19.6 kHz transmitted from the GBZ transmitter station Anthorn, UK (54^{o}N, 3^{o}W) and recorded by the AWESOME receiver at the Shamakhy Astrophysical Observatory named after N.Tusi, Shamakhy, Azerbaijan (40^{o}N, 48^{o}E) is used for analysis. 5 geomagnetically disturbed

days (Ap>26) are studied. A decrease in DLPT depth is observed for the storm day on October 11, 2008, while an increase is observed for all other storms.

NON-LINEAR DAMPING OF SURFACE ALFVEN WAVES DUE TO UNITURBULENCE

Ismayilli Rajab
KU Leuven, Belgium
rajab.ismayilli@kuleuven.be

We investigate MHD plasma turbulence in the theoretical model at the interface where a unidirectionally propagating surface Alfven wave creates turbulence, named “uniturbulence.” In particular, we study the non-linear damping of the surface Alfven wave. We consider an inhomogeneity across the background magnetic field in a Cartesian coordinate system. We calculate explicit expressions for the wave energy density and energy cascade rate for propagating waves using the Elsasser formalism. We perform a series of 3D ideal MHD simulations for a numerical demonstration of the non-linearly self-cascading model of unidirectional surface Alfven waves using the code MPI-AMRVAC. We show that surface Alfven wave damping in the numerical simulation models follows the analytically derived theoretical damping time scale formula. The formula and the simulations show that the damping time is inversely proportional to the wave’s amplitude and density contrast. This nature of the unidirectional cascade might play a role in heating the coronal plasma.

ACTIVE PERSONAL PROTECTIVE EQUIPMENT USING HEPA FILTERS WITH IMPREGNATED NANOPARTICLES

Chicua T., Chirakadze A., Mitagvaria N.,
Jishiashvili D., Jishiashvili A., Buachidze Z.
Georgian Technical University, Tbilisi, Georgia
ajishiashvili@gmail.com

For a long period of time reducing direct contact, cleaning surfaces, physical barriers, physical distancing, respiratory hygiene and use of masks within the droplet distance was the main and exclusive protection strategy, while wearing of high-grade protection was carried out only for the so-called aerosol-generating health-care procedures. This has largely contributed to the rapid spread of a new viral infection, primarily among medical personnel, patients and other specific groups of the population. However, in April 2020 the researchers of the Institute for problems of Engineering Physics of the Georgian Technical University started a project on developing the high-grade active personal protective equipment based on HEPA filters with impregnated nanoparticles of zinc and copper oxides, which not only filtered the air, but also deactivated viruses that entered the filter. Presently it was found that in fact the infectious virus is mainly airborne, and people can be infected when they inhale aerosols produced by other persons who are at a considerable distance[1,2]. Hence, reducing transmission of SARS-CoV-2 requires measures to avoid inhalation of infectious aerosols, including ventilation, air filtration and disinfection, and higher-grade protection for health-care staff and front-line workers. Portable HEPA purifiers were recognized as the most suitable remedy for eliminating airborne SARS-CoV-2 from indoor environments [3]. The presented research reports microwave enhanced synthesis of quasi-spherical CuO nanoparticles [4] and ZnO nano-sized tetrapods [5], the ultrasound enhanced impregnation and acute toxicity testing of the synthesized nanoparticles to white rats and bird embryos and the preliminary testing of the antibacterial and antiviral efficacy of the developed filters.

DESIGNING NEW TYPE ESM FOR THE SYNTHESIS OF INNOVATED STRUCTURAL NANOFIBERS: BASED ON ESM

Nasibov I., Mirsultanova R., Gahramanli L., Ali R., Gurbanova F.
Baku State University, Azerbaijan
ilyasnesibov18@gmail.com

The diameter of nanofibers is generally less than 1000 nm. Nanofibers are one of three main types of nanomaterials, beside nanoparticles and nanosurfaces. Polymer nanofibers are a consequential class of nanomaterials. Various production techniques are used for synthesis of nanofibers at laboratory and industry (electrospinning, phase separation, melt-blown, template synthesis, drawing, etc. Electrospinning has been recognized as an efficient technique for the fabrication of polymer nanofibers. Electrospinning is a spinning technique using electrostatic forces to produce nanofibers from polymer solutions or melts. The typical setup of basic ESM is: 1. High voltage power supply (5 – 50 kV), 2. Syringe pump for polymer solution, 3. Collecting drum or plate (Cooper, Aluminum, Glass, polymer sheet and foil, and many more materials can be used as plate collector with designed holder). In the electrospinning process, a high voltage power supply is used to create an electrically charged jet of a polymer solution or melt out of the pipette. The electrospinning process is usually conducted at room temperature. Our Electrospinning Machine has a new modular system for synthesis different structural nanofibers. This ESM has 3-channel pump for different polymer solutions (different sources for nanofibers). Each channel can be controlled independently for individual syringe. It is designed for continual infusion for electrospinning. In addition to the, new type ESM has single nozzle and multi nozzle systems: 1 inlet, 10 outlet; 1 inlet 5 outlet; multi inlet-multi outlet. Hence, new type ESM has multi-channel pump too for this setup. Also, ESM has side by side nozzle system for synthesis innovated structural nanofibers from different solution sources. The nozzle has 2 type internal structure for synthesis new nanofibers from two different solution sources: 1. Side by side nozzle 2. Spiral nozzle. Etc: we have two different solution sources for synthesis one nanofiber. If we use a new type nozzle (side by side nozzle), the structure of the nanofiber will be side by side. In Fig.1. shown the schematic diagram

of ESM.

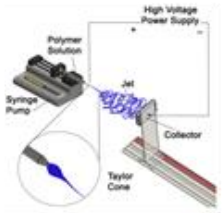

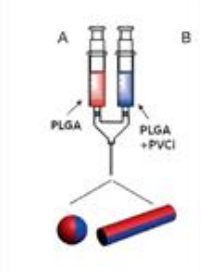

1 2

3

Fig.1. Schematic diagram: 1- Electrospinning proccess; 2-Side by side nozzle; 3-Polymer jet.

SYNTHESIS OF AG-DOPED CO_3O_4 NANOPARTICLES BY SONO-CHEMICAL METHOD

Muradov M.B., Mammadyarova S.J., Eyvazova G.M., Balayeva O.O.
[1]*Baku State University, Baku, Azerbaijan*
Sevinc.memmedyarova@inbox.ru

Among transition metal oxides, Co_3O_4 nanoparticles (NPs) is of great importance due to its unique properties and remarkable applications such as gas sensor, supercapacitor, anode material in Li-ion rechargeable battery catalyst and etc. It is possible to enhance physicochemical properties of nanostructures by doping process. In the present work, we have synthesized pure Co_3O_4 and silver doped Co_3O_4 NPs (10% Ag:Co_3O_4) by sono-chemical method and subsequent calcination at 500^{o}C for4h. For the synthesis, cobalt nitrate [$Co(NO_3)_2 \cdot 7H_2O$], silver nitrate ($AgNO_3$) and sodium hydroxide (NaOH) were used as precursors. Polyvinyl alcohol was used as stabilizing agent. X-ray diffraction (XRD) was used to determine the phase structure and composition of prepared samples. In the XRD pattern of pure Co_3O_4, the diffraction peaks were appeared at 2θ=18.91^o, 31.25^o,

36.84^o, 38.56^o, 59.37^o and 65.19^o corresponding to (111), (220), (311), (222) (511) and (440) crystal planes of Co_3O_4. These observed peaks are well assigned to the cubic structure, which matches well with the standard data (JCPDS card no.89-0598). A gradual shift towards higher angles was observed for the Ag-doped Co_3O_4 NPs and this XRD data clearly shows no peaks corresponding to Ag or Ag_2O. XRD patterns of two samples retain the same structure of pure Co_3O_4, it indicates that silver doping has not changed the crystal structure of cobalt oxide. The average crystallite size of pure and Ag-doped Co_3O_4 NPs, determined by the Debye Scherrer's formula were 22.5 nm and 17.5 nm, respectively. The reduction in particle size for the doped nanoparticles can be attributed to the internal microstructural strain and local distortion in the Co_3O_4 lattice due to incorporation of the Ag^+ ions. Because, the ionic radii of Ag^+ (1.26 A) is higher than the ionic radii of Co^{2+}(0.72 A). The Ultraviolet-visible (UV-vis) absorption spectra for the Co_3O_4 and Ag:Co_3O_4 samples was recorded in the wavelength range of 200 nm to 900 nm. Pure Co_3O_4 exhibited two absorption peaks at 469.2 nm and 773.8 nm. The first absorption band can be attributed to the $O^{2-} \rightarrow Co^{2+}$ charge transfer process, while the second band assigned to the $O^{2-} \rightarrow Co^{3+}$ charge transfer. Ag-doped Co_3O_4 NPs showed absorption peaks at 448.2 nm and 773.2 nm. This lower wavelength shift or blue shift is attributed to the quantum confinement effect. Energy dispersive X-ray spectroscopy (EDX) was used to determine the elemental composition of obtained nanoparticles. EDX pattern of Ag-doped Co_3O_4 NPs shows the presence of silver, cobalt and oxygen elements. The atomic percentage of these elements is 2.12%, 48.41% and 49.47%, respectively. The Ag/Co atomic ratio is near to the theoretical ratio of $Ag_{0.1}Co_{2.9}O_4$.

SYNTHESIS AND TESTING OF METAL MAGNETIC AND ISOTOPIC ENRICHED BORON NITRIDE NANOPARTICLES

Mitagvaria N., Chirakadze A., Jishiashvili D., Dvali N., Gigineishvili A., Buachidze Z., Chigogidze K., Khuskivadze N., Gulashvili M.
Georgian Technical University, Tbilisi, Georgia
nanakhuskivadze53@gmail.com

Boron nitride nanoparticles and nanosheets (BNNPs), in combination with the Curie temperature-controlled metal magnetic nanoparticles are highly promising materials for biomedical application due to their excellent biocompatibility and extremely low toxicity. They also attract particular attention due to the prospect of their application in localized combined radiotherapy of cancer using isotopic enriched boron nitride nanomaterials.

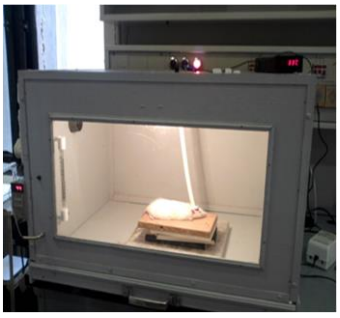

The conducted research deals with the microwave enhanced low-temperature synthesis from gaseous phase mixture and acute toxicity testing of the isotopic enriched hexagonal boron nitride nanosheets with the only difference that the nanosheets were synthesized from the isotopic ^{10}B and ^{11}B enriched precursor. Taking into account the growing activity of wildlife and laboratory animal defenders causing a sharp and rapid tightening of the relevant regulations an improved method of general toxicity testing of the synthesized nanomaterials using a continuous observation of behavioral effects in white rats during passing the branched maze, in combination with the whole body hyperthermia and the continuous monitoring of blood oxygen saturation, systolic blood pressure, body temperature and oxidative stress indicators. The results obtained confirmed the

higher crystallinity of the microwave synthesized and annealed boron nitride nanosheets in comparison with boron nitride nanoparticles processed under conventional heating (see Figure 1.). Boron nitride encapsulated Ni-Cu and Ag:$LaMnO_3$ nanoparticles showed a neglectable acute toxicity, slightly higher than the toxicity of saline solution.

The tested rat in a hyperthermia chamber: the temperature is automatically maintained in the range of 39–45^{O}C.

ELECTRICAL AND OPTICAL PROPERTIES OF CdS THIN FILMS

Jafarov M.A., Kazımzadə A.H., Nasirov E.F.
Baku State University, Baku, Azerbaijan
maarif.jafarov@ mail.ru

In this study, influence of ammonia concentration and temperature of the mixer was maintained at 90°C, the deposition time was 2 h and the pH of the solution was maintained at 11.0 to deposit CdS thin films by chemical bath deposition method and to understand the growth mechanism and its impact of structural, optical and electrical properties. For deposition of the films 30 ml of 0.004 M $CdCl_2$ solution is used as cationic precursor, 20 ml of 0.005 M $SC(NH_2)_2$ solution is used as anionic precursor, 30 ml of 0.3 M NH_4Cl serves as a buffer and 26 ml of (0.5, 1.0, 1.5 and 2.0 N) NH_3 is the complexing agent.

The structural, optical and electrical properties of the CdS film were characterized. The crystalline structure of CdS thin films has been investigated by the X-ray diffraction measurements. All films deposited on glass substrate are no sharp peak which indicates the samples are in amorphous nature as illustrated by the X-ray scattering curves.

The XRD spectra are obtained by scanning of intensity versus 2θ. The broad hump in the wide-angle region from 10-80°. The presence of small peaks in the X- ray diffractogram reveals the formation of nanocrystalline CdS thin films. The peaks are not sharp indicating that the average crystallite size is small. Data obtained from the optical characterization of the CdS thin films in the wavelength range 300-1200 nm.

The electrical resistivity of the CdS thin film deposited on the glass substrate plotted between the variations of logarithm of resistivity (ln ρ) with reciprocal of temperature (1000/T). The resistivity observes that decreases with increases in temperature. The measurement shows that the as deposited CdS films have the resistivity at 32°C. It observed that resistivity decreases with increase in temperature suggesting the semiconductor behavior of CdS. The activation energy for the as deposited CdS film is calculated and is found out from 1.3797-2.5800 eV

The optical absorption and transmission spectrum were recorded at room temperature. The The absorption peaks were centered at 351 nm for the samples of 0.5, 1.0, 1.5 and 2.0 N of NH_3. The spectrum also showed that absorbance was high in the UV and low in VIS-NIR region. Hence, absorbance of the film decreases with increasing wavelength and decreasing the photon energy. Absorption edge of CdS thin films shows a clear shift to the lower wavelength as compared to its bulk counterpart.

From the plot, the variation of $(\alpha h\gamma)^2$ versus photon energy for different concentration of ammonia, CdS thin films itis observed that a slight variation in the band gap values as the concentration of ammonia increases. This variation in the band gap is depends upon the grain size and lattice parameters. The band gap energy for the films prepared in different concentration ammonia varies from 2.51 to 2.62 eV.

A ZINC-OXIDE NANOPARTICLE-BASED FORMULATTION WITH LOW DOSE HYDROCHLOROQUINE AND AZYTHROMICINE

Mitagvaria N., Chirakadze A., Dvali N., Petriashvili G., Chichua T., Chigogidze K. Khuskivadze N., Gulashvili M.
Georgian Technical University, Tbilisi, Georgia
nanakhuskivadze53@gmail.com

Surprisingly, despite that primary care physicians should see COVID-19 patients first, only one study has described characteristics and key outcomes of COVID-19 diagnosed patients in an outpatient setting. Unfortunately, until today the early clinical phase of COVID-19 has not been the focus of research, although it is well known, that timing of antiviral treatment is often crucially critical. Based on the general experience of the clinical application principles of antiviral therapies, as (e. g., in case of influenza A, antiviral treatments should be used as early as possible in the course of infection, before it spreads from upper to lower respiratory tract causing severe inflammatory reactions. In our opinion, due to the lack of vaccines as well as SARS-CoV-2 specific therapies, the proposed use of repurposed antiviral drugs remains a vitally valid practical consideration. The first retrospective case series study with COVID-19 outpatients was done to clarify if the outpatient risk stratification might allow for rapid treatment decision shortly after onset of symptoms and the triple 5-day therapy with zinc plus low dose HCQ, and azithromycin might significantly reduce the hospitalization and fatality rate compared with the relevant public reference data of untreated patients [5]. The results of the study were statistically representative [6]: treatment of COVID-19 outpatients started as early as possible using the combination of zinc with low dose of hydroxychloroquine and azythromicine, brought to significantly less hospitalizations and 5 times less all-cause deaths. No cardiac effects were indicated. The proposed research presents the results of an independent study carried out in 2021 with the aim to develop a zinc oxide nanoparticle-based formulation for antiviral use and test their acute toxicity to the chick embryos using visible and visible spectrum ovoscopy and to white rats using a long-term monitoring of behavioral and physiological characteristics.

PHOTOCATALYSTS FOR WATER SPLITTING BASED ON THE *p*-Ge/*n*-$CuIu_5S_8$/Ag(NP) STRUCTURE

Huseynov A., Salmanov V., Mammadov R.,
Bairamova A., Mirsultanova R.
Baku State University, Baku, Azerbaijan
aguseinov@bsu.edu.az

The ecological state of our environment requires an urgent rejection of the use of all types of fossil fuels. These energy sources can be replaced by alternative renewable energies and hydrogen produced by electrolysis using renewable and nuclear electricity. However, now the efficiency of existing technological units producing hydrogen by electrolysis with the splitting of water, which is the cheapest raw material, is at a very low level and their use is unprofitable. Photocatalytic systems for producing hydrogen from various reagents are relatively efficient. In these systems, photocatalysts, in which electron-hole pairs are generated under the action of light, play an important role. Therefore, the search for photocatalysts that are sensitive to sunlight and chemically stable in electrocatalytic reactions and capable of generating proton ions is an urgent task of photocatalyst.

This work presents the results of the manufacture and use of a photocatalyst based on *p*-Ge/*n*-$CuIn_5S_8$/Ag (NP). This multilayer structure is formed on a glass substrate. A thin layer of p-type germanium ~10 μm thick was deposited on the cleaned glass surface heated to a temperature of 150°C (this temperature ensures good adhesion of the sprayed film to the glass surface) by thermal evaporation in vacuum. The germanium layer on the glass played the role of a current-supplying electrode and injected electrons into the light-sensitive layer of the defective *n*-$CuIn_5S_8$ semiconductor.

Thin films of the $CuIn_5S_8$ compound were obtained by explosive evaporation of the substance in a vacuum. In this method, crushed to an average size of ~100 μm, dust grains of the $CuIn_5S_8$ crystal are fed in a vacuum chamber by a special device in portions into a graphite crucible heated to 1080 °C. The dust particles instantly evaporate and in the molecular state are deposited on the surface of a thin *p*-Ge layer.

At the next stage of manufacturing the photocatalyst, a colloidal solution of silver nanoparticles in ethanol, in an amount of 0.3 mg, was applied uniformly on the surface of a CuIn5S8 thin film with an area of 6 cm2 and dried in the open air. Further, the multilayer structure *p*-Ge/*n*-$CuIn_5S_8$/Ag (NPs) on a glass substrate was subjected to thermal annealing at a temperature of 250°C in a vacuum chamber to enhance the adhesion of silver nanoparticles to the surface of the $CuIn_5S_8$ film.
The photocatalyst produced by the above method was used as the anode, and the platinum plate was used as the cathode. The photovoltaic cell was filled with distilled water, in which, when a voltage of 24V was applied to the electrodes, a current of 60 μA flowed. The photocatalyst was illuminated by focused radiation from an incandescent lamp. According to calculations, in one and a half hours of time, the volume of hydrogen released on the cell was 120 cm^{-3} and the efficiency of the photovoltaic cell was 4,2%.

$Cu_2ZnSnSe_4$ THIN FILM BASED SOLAR CELLS OBTINED BU MAGNETRON SPUTTERING METHOD

Mursakulov N.N., Nuriyeva S.G., Abdulzade N.N., Sabzaliyeva CH.E., Abdullayev G. M.
Institute of Physics, ANAS, Baku, Azerbaijan
nmursakulov@physics.ab.az

In this work thin $Cu_2ZnSnSe_4$ (CZTSe) films were obtained by the magnetron sputtering method. The material was sputtered from a target obtained by pressing crystalline CZTSe powder, which, in turn, were obtained by us by the method described in [1] for CZTS. The crystallinity of CZTSe was checked by X-ray diffraction and X-ray phase analysis, and the composition was determined by elemental analysis on the scanning electron microscope (SEM). Thin CZTSe films were obtained on sodium glass substrates and on thin-film molybdenum deposited on glass substrates. The morphological features of the surface of the films were investigated under a metallurgical optical microscope and under an atomic force microscope (AFM). The AFM was used to determine the film roughness and grain size on films of Mo, CZTSe on

a glass substrate, CZTSe on Mo, and CdS on CZTSe / Mo, depending on the modes and conditions of magnetron sputtering. The result was obtained a thin CZTSe film with an ideal composition, with a mirror-like surface, for use in solar cells. Ellipsometric and Raman studies of these films have been carried out. X-ray studies of CZTSe thin films have shown that on glass substrates are obtained thin amorphous layers but they tend to crystallize. Studies of the absorption spectrum at the intrinsic absorption edge have shown that the intrinsic absorption edge is shifted towards short waves. This is due to the fact that films with a thickness of about 100-120 nm were used. A solar cell with a glass/Mo/CZTSe/CdS/ Mo / structure, thus obtained a CZTSe film, without any temperature treatments (annealing) and without applying antireflection coatings, showed a conversion efficiency of ~ 2.1%, while the structure still had significant leakage current and high series resistance. It is expected that the conversion efficiency will be improved by further optimizing the obtaining technology, increasing the thickness of the absorbing layer to the optimal value, choosing and applying buffer and antireflection coatings. Various technological modes of the magnetron sputtering method have been investigated to obtain high-quality thin layers of $Cu_2ZnSnSe_4$ for solar cells. It is shown that this method can be used to obtain homogeneous thin films with a mirror-like morphology of their surface.

SYNTHESIZE OF COPPER CADMIUM SULPHIDE (CuCdS2) NANOPARTICLES ON THE BASIS OF FUNCTIONALIZED NITRILE BUTADIENE RUBBER BY SILAR METHOD

Balayeva O.O., İmamaliyeva N.N., Azizov A.A.,
Muradov M.B., Alosmanov R.M., Gahramanli L.R., Eyvazova G.M.
Baku State University, Baku, Azerbaijan
ofeliyabalayeva@bsu.edu.az

Binary and ternary metal sulfide nano-materials are very useful for optoelectronic applications due to their optical, electrical and magnetic properties in various fields. It is found that the optical band gaps of the synthesized ternary alloy nanorods are influenced by the metallic compositions, suggesting their possible applications in photocatalysis. $CuCdS_2$

nanocrystals with high luminescence properties are very important semiconductor material for various optical applications.

In the present study, copper cadmium sulfide ($CuCdS_2$) semiconductor nanoparticles were synthesized by SILAR method. Oxidative-phosphorylated nitrile butadiene rubber (PhNBR) has been used as a polymer matrix for the stabilization of nanoparticles. For the formation of $CuCdS_2$ nanoparticles 0.1M solutions of $CuCl_2 \times 2H_2O$, $CdCl_2 \times 2.5H_2O$ and $Na_2S \times 9H_2O$ crystal hydrates were used in the experiment. After adsorption of Cu^{2+} and Cd^{2+} cations from $CuCl_2 \times 2H_2O$ and $CdCl_2 \times 2.5H_2O$ mixed solution onto 0.2 g of PhNBR, the sorbent was washed with distilled water and sulfidation was carried out to complete the reaction. According to the results obtained from the X-ray diffractometer (XRD), the average size of the nanoparticles after cycles 5 and 15 was estimated as 1.13 and 3.57 nm, respectively. The intensive diffraction peaks observed at diffraction angles $2\theta = 26.77^o$ (002) and 46.93^o (103) correspond to $CuCdS_2$ nanoparticles. The optical bang gap energy of obtained $CuCdS_2$ /PhNBR is 2.7 eV.

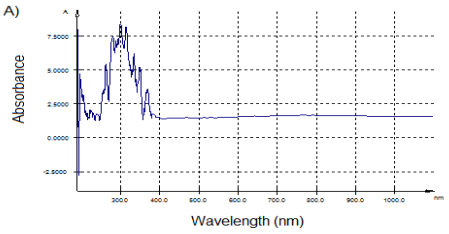

STRUCTURE AND OPTICAL PROPERTIES OF Ag NANOWIRES

Nuriyeva S., Hasanov K.
Baku State University, Baku, Azerbaijan
snuriyeva@bsu.edu.az

Silver nanowires are widely used in catalysis, nanoelectronics, solar cells, and biosensors due to their electrical and thermal conductivity, low surface resistance, photoluminescence, high transparency, and good biocompatibility. In this research proposed a halide-mediated polyol method

with significantly reduced reaction time for the synthesis of AgNW. Reaction parameters also have different effects on the morphology of the obtained products. Also, the influence of Cl- and Br- ion concentrations on the formation of nanowires were investigated.

The crystal structure and phase composition of AgNW were identified by comparing them with X-ray diffractograms of known structures. X-ray diffraction diagrams of the studied nanowires show 2θ~38.67°, 44.73°, 64.79°, 77.77°, 81.89° angles. This diffraction pattern is compatible with ICDD (PDF-2 / Release 2011 RDB) database file 00-004-0783. The diffraction peaks of the existing faces allow us to say that the silver corresponds to the face-centered cubic structure of silver.

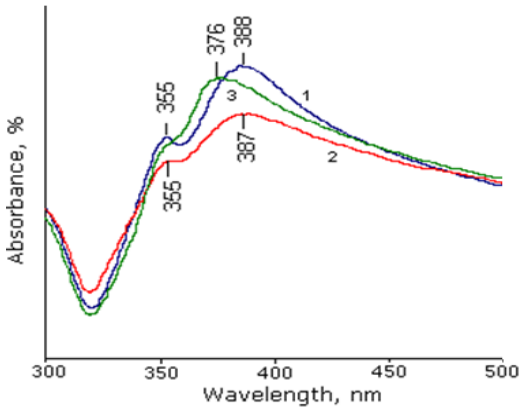

Fig. 1. UV-vis spectra of AgNW synthesized at different concentrations of halide compounds NaCl/KBr: 1- 0.01M/0.005M; 2- 0.01M/0.01M; 3- 0.005M/0.01M

Fig. 1 shows the UV-Vis absorption spectrum of Ag nanowires at three different concentrations of NaCl and KBr. The two characteristic absorption peaks of silver nanowires around 355 nm and 380 nm correspond to surface plasmon absorption. The characteristic blueshift of the peak at low concentrations of Cl- ion is due to changes in the size (diameter and length) of the formed nanowires. Thus, it is assumed that thinner and longer nanowires are formed.

ENHANCEMENT OF THE PL INTENSITY OF PVDF+PbS/CdS NANOCOMPOSITES AFTER ELECTRO-THERMO-POLARIZATION

Ramazanov M.A. [1], **Jafarov M.A.** [1], **Angelo Chianese**[2], **Hajiyeva F.V.**[1], **Novruzova, A.A.**[1]
[1]*Baku State University, Azerbaijan*
[2]*Sapienza University, Italy*
n.a_physicist@yahoo.com

Polymer nanocomposites have potentially enhanced properties. It has been observed that the implementation of different surface modification methods successfully can be improved properties of nanocomposites. This article discusses the influence of electro-thermo-polarization (ETP) on photoluminescence (PL) properties of polymer nanocomposites based on PVDF and PbS/CdS nanoparticles. A detailed description of electro-thermal polarization treatment, polarization mechanism, and role of surface charge and its polarity on surface properties are discussed. It was investigated that after ETP of nanocomposites PL intensity is increasing. By comparing the results of the intensity of the PL spectra of nanocomposites, it was determined that polarized composites with a 5% mass content of nanoparticles have relatively high luminescence. This leads to the activation of the luminescence centers, which is the cause of the increase in the PL emission intensity in this nanocomposite after the ETP. Scanning electron microscopy clearly revealed that PbS and CdS nanoparticles were successfully formed in the polymer matrix. Structure of nanocomposites also were investigated by XRD analysis.

RESEARCH OF X-RAY STRUCTURE SPECTRUM OF MAGNETITE NANOPARTICLES-CHRYSIN SYSTEM

Qurbanova N., Karimova A., Nuriyeva S., Shirinova H.
Baku State University, Baku, Azerbaijan
qurbanli.nergiz@mail.ru

In this research work, X-ray structure analysis of PEG (polyethylene glycol) coated Fe_3O_4nanoparticles (NPs) and chrysin drug system was taken in 3 different concentrations was performed. The co-precipitation method with modified parameters was used for the synthesis of magnetite NPs. The loading of the drug onto magnetite NPs was carried out by the non-covalent method.

Initially, the ratio of Fe_3O_4NPs and drug was taken as 1:1. In this case, 12.90°, 15.00°, 17.84°, 27.78° 2θ observed in the X-ray diffractogram of Fe_3O_4 and chrysin system conformed tothe diffraction peaks of chrysin, 30.30°, 35.66° 43.29°, 57.17°, 62.81° 2θ accommodated to magnetite NPs. 17.78°, 27.57° 2θ observed in the X-ray diffractogram of the sample taken at a concentration which the drug selected twice less than NPs reconciled with diffraction peaks of chrysin, 30.24°, 35.48°, 43.21°, 57.18°, 62.71° 2θ conformed to Fe_3O_4NPs. 12.86°, 14.96°, 17.81°, 22.48°, 24.84° 2θ observed in the X-ray spectral analysis for samples which chrysin doubled compared to NPs accommodated to the diffraction peaks of the drug, 35.58°, 43.31°, 62.78°, 57.37° 2θ harmonized to magnetite NPs. Effective loading of the drug on Fe_3O_4NPs became known in the result of the analyzes.

In this research work, it was determined that by varying the concentration of the drug, it is possible to vary the loading degree of its on the NPs. Synthesized samples can be applied successfully on the magnetite drug delivery systems for cancer therapy.

GAP-DEPENDENT COUPLING OF WEDGE-CHANNEL NANOPARTICLE HETERODIMERS

Illyashenko-Raguin L.N.
Kharkiv Natinal University of Radio Electronics, Kharkiv, Ukraine
mila.illyashenko@gmail.com

The current intense interest in the properties of metal nanoparticles (NPs) for their applications in all branches of science and technology for economic grows and prosperity of humans, including Life Sciences & Health, Design & Manufacturing of Components & Systems, Agriculture & Food, Emerging Lighting & Electronics & Displays, Information & Communication, Industrial Manufacturing & Quality, Security & Metrology & Sensors, Automotive & Transport, Photonics Research & Education & Training is mostly due to their Plasmon Resonances (PRs), which result in resonantly enhanced scattering and absorption. These effects depend strongly on size, shape, material of NP and on properties of that matter, in which NP is situated [1].

When two NPs are close to each other, forming a dimer of NPs, it results in novel, coupling induced, resonantly enhanced scattering and absorption properties, which depend on:

- orientation of NPs with respect to each other;
- orientation of NPs with respect to direction of the light source illumination.

It is not possible to investigate these properties with strategies, developed for the investigation of single NP. The problem becomes even more difficult, when two coupled NPs form a heretodimer, namely dimer of NPs of different size, different shape, different materials.

While the shape of each individual NP may be the reason for appearance of special kinds of PR, such as *Wedge Plasmon Polariton* (WPP) and *Channel Plasmon Polariton* (CPP), the electromagnetic interactions of NPs in dimmers and heterodimers may lead to appearance of so-called *Gap Plasmon Polariton* (GPP). PR effects in NPs, when only one kind of resonance from specified WPP, CPP or GPP exists in structure, are rather well understood. However, to understand PR effects, when combination of

several kinds of PRs appear in dimers and heterodimers remains a challenging problem. This work is devoted to investigation of the PR coupling effects in dimer and heterodimer of such NPs, one of those may have WPP, while another may have CPP, when GPP also appear due to the NP coupling. The dependence of such effects on distance between NP in heterodimer is investigated and optimal distance to obtain the best possible resonantly enhanced scattering and absorption properties is found by means of novel numerical simulation algorithm, made due to the development of Conformal Mapping Enhanced Spectral Fourier-Galerkin Boundary Integral Equation method with Analytical Regularization based on Singularity Subtraction improved by Fast Fourier Transform (FFT) [1], that is known to be a very useful and versatile tool to solve Electromagnetic Transmission Problems, which appear in Photonics and Plasmonic research. The set of numerical experiments lead to development of mathematical relations used as design rules, which qualitatively describe the coupling effects in heterodimers as a function on interparticle distance.

MOLECULAR MECHANICS SIMULATION OF CONFORMATIONAL BEHAVIOR OF ANTICANCER AAP-H PEPTIDE

Agaeva G.A., Agaeva U. T., Godjaev N.M.
Institute for Physical Problems, Baku State University, Azerbaijan
gulshen@mail.ru

It is known that some marine organisms possess antithrombotic, antitumor, and antibacterial activities. The bioactive substances of these marine organisms have played important roles in the development of innovative medicines. Prostate cancer (PCa) is one of the most common malignancies of the male urinary system and is also the leading cause of cancer-related death in men. The anticancer peptide *AAP-H* is a pentapeptide from the sea anemone *Anthopleura anjunae* with an amino acid sequence *Tyr-Val-Pro-Gly-Pro. The results of numerous* studies indicated that AAP-H peptide was nontoxic and exhibited antitumor activities in

prostate cancer DU-145 cells in vitro and in vivo. For determination a mechanism of action of this pentapeptide and to investigate its structure-function relations is required the knowledge of the conformational specificity and flexibility of backbone and side chains of molecule allowing a rational design of functional groups acting selectively at their receptor level. The conformational behavior of AAP-H peptide and conformational dynamics of its side chains at the present article have been investigated by molecular mechanics method, which allow to determine a whole set of energetically preferred conformers of peptide molecule. The sequential method was used, combining all low-energy conformations of constitutive residues. The conformational potential energy of a molecule is given as the sum of the independent contributions of dispersion, electrostatic, torsional interactions and hydrogen bonds energies. The detailed analysis of the conformational flexibility of AAP-H peptide was founded the limited quantity of stable conformers. The obtained results have shown that the stable conformers of pentapeptide have tendency adopt a beta-turn structure. The obtained results and discussion lead to the following conclusions: (I). molecular mechanics simulation in polar condition confirm the small flexibility of the sequence of AAP-H peptide; (II). the β-turn conformation on C-terminal tetrapeptide segment of peptide was more stabilized by dispersion interactions between residues. The conformational analysis helped reveal a number of special features of spatial arrangement of these drug-based pentapeptide. The determined stable structures of AAP-H peptide may be used as the basis for the design of further selective agonists.

CONFORMATIONAL AND MOLECULAR DOCKING ANALYSIS OF CAPECITABINE THAT HAS ANTICANCER ACTIVITY

Sefa Celik[1], Sevim Akyuz[2], Aysen E. Ozel[1]
[1]Physics Department, Science Faculty, Istanbul University, Vezneciler, Istanbul, Turkey
[2]Physics Department, Science and Letters Faculty, Istanbul Kultur University, Atakoy Campus, Bakirkoy, Istanbul, Turkey
scelik@istanbul.edu.tr

The most stable molecular structure of the Capecitabine ($C_{15}H_{22}FN_3O_6$) molecule, which is extensively used as an antineoplastic drug to treat metastatic and advanced types of breast and colon cancer, was investigated in gas phase using the Spartan06 software utilizing the PM3 technique (see Figure 1). From the hundred conformers discovered by the conformation research, the most stable and possible conformations were determined. These conformation's dihedral angle, total, and relative energy values were all compared and tabulated. For molecular docking studies, the most stable conformation achieved by the PM3 technique was used. A molecular docking studies was conducted to determine the probable binding modes between the title compound and DNA and, as well as the target protein α5β1 and αIIbβ3 integrins. The investigated molecule's 3D docked structures, as well as the interacting groups of ligand receptor complexes, were computed and shown in figures.

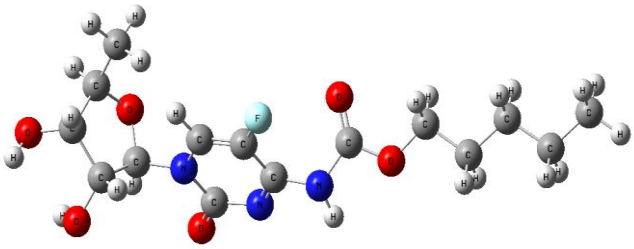

Figure 1. The most stable conformer of Capecitabine

MAGNETIC PROPERTIES OF Si DOPED AND ADSORBED MONOLAYER GRAPHENE WITH VACANCY

Huseynova S.S., Mammadova S.O.
Institute of Physics, Azerbaijan National Academy of Sciences, Azerbaijan
s.huseynova@physics.science.az

Ab initio calculations of the vacancy magnetic moments formed in defective graphene supercells have been carried out. It was found that Si-doped or Si-adsorbed graphene supercell consisting of 50 carbon atoms with vacancies exhibit ferromagnetic spin ordering. The density of states of supercells and local magnetic moments formed in the vicinity of vacancy carbon atoms are calculated. The calculated energy characteristics and magnetic moments of Si containing defect graphene supercells agree with the literature data.

According to the obtained results Si-doped and adsorbed graphene supercell consisting of 50 carbon atoms with vacancies differ from each other.

- the total magnetic moment Si doped graphene with vacancy: 5×5 graphene 1.011μ_B, Si adsorbed on 5×5 graphene -0.997 μ_B.

- acquired magnetic moments are: Si doped 5×5 graphene 0.489μ_B (C_{22},C_{33}), Si adsorbed on 5×5 graphene 0.807μ_B(C_{27}).

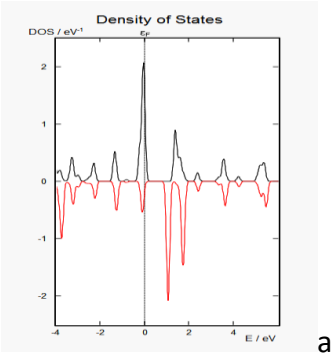

a)

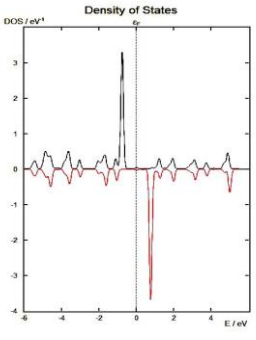

b)

Figure 1: DOS of Si a) doped (C_{22}) and b) adsorbed (C_{27}) monovacancy graphene consisting of 50 atoms

The silicon-based microelectronics are developed different methods for determining the characteristics and behavior control of doping and defects. These methods, taking into account modern computational methods, for example, density functional theory calculations also make it possible to modify the properties of graphene.

HYDRATION NUMBERS OF IONS IN AQUEOUS SOLUTIONS OF KCL, KCL+PEG, KCL+SODIUM CITRATE

Masimov E.A., Shahbazova G.M., Suleymanzade A.A.
Baku State University, Baku, Azerbaijan
Shahbazova.gunel@mail.ru

Hydration is the process where ions become surrounded with water molecules. The degree of hydration is characterized by the hydration number (h) and the thickness of the hydration shell of the solute particles.

Hydration numbers obtained in principle by various methods, are significantly different from each other. Some methods result in quite an incredible number of hydrations. Naturally, experimental methods, setting the number of water molecules around the ions to different distances from the center of the ion cannot produce identical results. In addition, when calculating the number of water molecules, ions are not captured near changing its parameters, density, dielectric constant, and others., which also leads to erroneous values.

In this work, refraction properties of diluted aqueous solutions of potassium chloride are studied. The hydration numbers of ions have been determined by the refractometric method.

We measured the concentration dependence of the refractive index of dilute aqueous solutions of potassium chloride. The obtained data in the coordinates $\frac{n^2-1}{n^2+2} \rightarrow$c% are represented in Fig. 1

An analytical formula was obtained that relates the slope of the linear portion of the concentration dependence of the refractive index with the number of ion hydration.

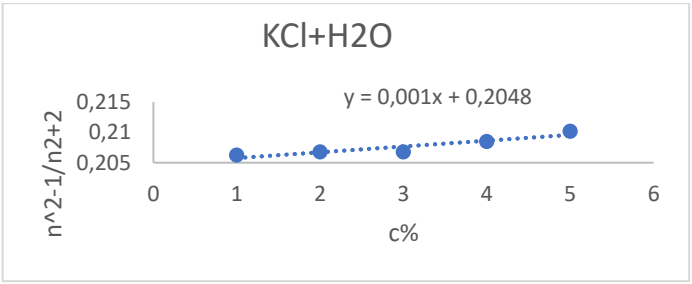

Fig.1. Dependence n^2-1/n^2+2 →c in the aqueous solution KCl

As follows from the figures, these dependencies are linear. From the slope of this dependence, the sum of the hydration numbers of K^+ and Cl^- ions was calculated using the formula given it turned out to be equal to h_{K^+}+ h_{Cl^-} = 23,7. We also determined the sum of hydration numbers of ions K^+ and CL^- in an aqueous solution of KCl +PEG-6000 and KCl+ sodium citrate. With the influence of PEG and sodium citrate to the aqueous solution of KCl the sum of hydration numbers of ions K^+ and CL^- are decreases.

PROTON THERAPY OF CANCER USING METAL AND ISOTOPE ENRICHED BORON NITRIDE NANOPARTICLES

Chirakadze A., Mitagvaria N., Jishiashvili D., Dvali N., Sapojnikova N., Gigineishvili A., Buachidze Z., Chigogidze K., Khuskivadze N., Gorgadze K.
Georgian Technical University, Tbilisi, Georgia
achirakadze@gtu.ge

Cancer therapy using high energy charged particles (primary, proton beams) is the most adavanced modality for the treatment of several kinds of cancer successfully used in more than 110 medical centers around the world. Increasing of the biological efficacy and safety of proton (hadron) therapy is a crucially emerging problem of modern medicine and space astrobiology. One of the most productive approaches is the so - called localized combined therapy using various kinds of nano-based fluids and involving nuclear reactions. An optimal "ensemble" of the adjuvant therapeutic modalities must consist of Curie temperature controlled magnetic (in our case, boron nitride encapsulated Ni-Cu and Ag:$LaMnO_3$ nanoparticles) and isotopic enriched boron nitride (^{10}B, ^{11}B) nanoparticles, which

can provide the treatment synergistic to radiotherapy. Moreover, due to the boron-proton and boron-neutron capture reactions, isotopic enriched ^{10} B and ^{11} B nanoparticles with the appropriate optimal spatial distribution inside and at the tumor boundaries, as a result of nuclear reactions, can generate a sufficient concentration of alpha particles and bring to a drastical reduce of the number of protons and thermal/epithermal secondary neutrons affecting healthy cells. An optimized distribution of the isotopic enriched ^{10} B, ^{11} B nanoparticles and Li atoms can also improve the spatial distribution of the proton beam in body tissues. Mathematical simulation also showed that the enhanced proton therapy coud move close to ^{12}C ion hadron therapy, but without its complications.

NANOPARTICLES ENHANCING RADIOTHRAPY OF CANCER AND THEIR ACUTE TOXICITY TO BIRD EMBRYOS

Chirakadze A., Dvali N., Petriashvili G., Chichua T., Ambokadze M., Chigogidze K., Gorgadze K.,
Georgian Technical University, Tbilisi, Georgia
achirakadze@gtu.ge

Photon therapy is widely used in more than 110 medical centers around the world. The localized combined therapy using radiotherapy, mild hyperthermia, chemotherapy, photodynamic therapy ROS therapy a prospective tool to increase the biological effectiveness and safety of cancer therapy while the most advanced kind of the hyperthermia is the Curie temperature controlled localized hyperthermia (CTCLH) A principally new approach is the usage of the isotopic enriched ^{10}B and ^{11}B containing nanomaterials (both in the form of pure boron and boron nitride) nanoparticles and boron-neutron and boron-proton capture nuclear reaction products Novel microwave enhanced methods of synthesis magnetic metal nanoparticles, isotopic enriched hexagonal boron nitride (hBN) nanosheets and boron nitride encapsulated magnetic metal nanoparticles for the (CTCLH) and localized boron-neutron and boron-proton capture therapy were developed and their magnetic properties were tested. A novel ovoscopy method of testing the acute toxicity of the synthesized

nanomaterials to avian embryos excluding the use of mammals and other living animals for drug testing was examined.

INTERACTION NANOPARTICLES WITH PLANTS TOWARDS TO THE INCREASE THE TOLERANCE TO SALINITY AND DROUGHT

Ahmadov I., Hasanova F., Babanli (Aliyeva) S.
Baku State University, Azerbaijan
ismatahmadov@mail.ru

The application of nanotechnology for an intensive and sustainable agricultural strategy is already underway, which makes the use of nanoparticles important in this strategy. The use of nanoparticles requires clarification of the nature of their interaction with plants. In recent years, the accumulation of nanoparticles in plants, migration from the soil to its organs, the effect on important morphophysiological parameters, photosynthetic activity, biochemical and mineral nutrition processes have been well studied. Significant progress has also been made in the study of salinity and drought, the main abiotic stressors that seriously affect plant growth and productivity. The main task is to increase the plant's tolerance to these factors. The use of nanoparticles holds important promise in increasing plant resistance to salt and drought. Thus, from nanoparticles based on metals, CuO increases the amount of antisan, proline in plants (Liang X et al., 2013), which leads to an increase in drought resistance. ZnO nanoparticles affect the root system of plants, reducing their need for water (Prakash & Chung, 2016). Quenching of reactive oxygen species (ROS) is a universal mechanism for increasing plant resistance to abiotic stressors. It is known that stressors cause an increase in ROS in plants, while the activity of catalase and other enzymes rapidly increases. The role of nanoparticles in the regulation of this process is widely studied in the presented article. It was found that nanoparticles of Al, Fe, Zn, Cu, along with morphophysiological changes in plants, increase resistance to salt and drought by changing the activity of enzymes.

DEVELOPMENT, LABORATORY STUDY AND FIELD TESTING OF NEW NANOPARTICLE BASED COMBINED INSECTICIDES

Chirakadze A., Mitagvaria N., Dvali N., Gigineishvili A., Petriashvili G., Ambokadze M., Chigogidze K., Khuskivadze N., Buachidze Z., Gulashvili M.
Georgian Technical University, Tbilisi, Georgia
achirakadze@gtu.ge

The Brown Marmorated Stink Bug (BMSB) is among the most serious pests for agriculture. It also can cause a significant social nuisance. Development and laboratory testing of new synergistic insecticidal mixtures highly effective against this invasive pest and less toxic to the living environment is an extremely urgent challenge for the modern applied entomology. Development and study of a wide range of new highly effective pesticides having low toxicity against the living environment (primarily - humans, mammalians, bees and other beneficial insects, aquatic organisms' reptiles, etc.) is of a paramount importance for agriculture and environmental safety. In recent years, special attention has been paid to the development and testing of synergistic combinations of active substances of different chemical types of action which should be highly toxic against pests and provide effective inhibition of the development of pest resistance to insecticides. Use of nano-materials as synergistic components of pesticides can provide a novel approach for coming closer to a more sustainable balance between the sharp increase in agricultural production and conservation of nature, although they can pose a considerable threat to environment. The presented study reports the results of laboratory and field testing of the insecticidal combinations containing pyrethroid, synthetic substances, essential oils, mineral), a 100% biodegradable emulsifier, hydroxyethylcelluslose (HEC) and environmentally compatible solvents. The laboratory tests, field trials and acute toxicity testing on white rats clearly showed that all the tested combinations are characterized with the high synergy of components, sharply increased biological effectiveness of synergystic and reduced acute toxicity in comparison with the widely used highly effective insecticidal pyrethroid/organophodphorus combination "Prostore 420 EC". The biological effectivity, synergy rate of

the alumina nano-powder based combinations were for about 12-15 % higher than of the diatomite and kaolin based micro-powers, while the environmental safety was within the experimental accuracy of testing.

ELECTRONIC AND STRUCTURAL PROPERTIES OF FE-DOPED BOROPHENE SHEETS: IN-SILICO STUDY

Jafarova V.[1], Yavar T. Azar[2]
[1] Institute of Physics of Azerbaijan National Academy of Sciences, Baku, Azerbaijan
[2] Physics and accelerators school, NSTRI, Tehran, Iran
vcafarova@beu.edu.az

The outstanding achievements of low-dimensional materials such as graphene, boron-nitrides, phosphorene, and transition metal dichalcogenides in electronic and optoelectronics devices motivated the scientific community to examine the feasibility of employing other 2D layers. One of the stunning achievements of the search for new 2D-systems was the introduction of the single-layer borophene sheet. Among several synthesized structural phases of borophene, χ_3 and β_{12} are the most stable ones.

This work explores the structural, electronic and magnetic properties of borophene sheets after doping with a single Fe-atom. All calculations were done employing density functional theory using both pure and hybrid exchange-correlation functional.

In order to eliminate the unwanted interaction effects between neighbor images, 2x4 and 3x4 supercells were used for χ_3 and β_{12} respectively, also iron was absorbed at the hexagon center.

Our findings show that Fe adsorption causes a small out-of-plane distortion for both χ_3 and β_{12}brphene structure. On the other hand, exploring spin polarization of Fe-doped structures implies a relatively different response of χ_3 and β_{12}layers to Fe-atom doping. These apparent differences can be explained as a result of nonequivalent boron neighbors in two structures. Tunable spin-polarization of Iron-doped borophene sheets is of interest to potential spintronic and catalyst applications.

SPATIAL AND ELECTRONIC STRUCTURE OF SOME AZO-DERIVATIVES OF β-DIKETONES ACCORDING TO QUANTUM CHEMICAL CALCULATIONS BY SEMI-EMPIRICAL PM3 METHOD

Demukhamedova S.D.[1], Alieva I.N.[2]
[1]Baku State University, Baku, Azerbaijan
svetlanabest@mail.ru

Azo derivatives of β-diketones continue to be relevant scientific objects due to their potentially wide range of applications. In particular, materials based on them have found wide application in organic, coordination, and supramolecular chemistry and in medicine. It is known that azo-derivatives of β-diketones can exist in several tautomeric forms and can rapidly transform into each other with proton transfer. The selection of various substituents can significantly change the physical and chemical properties, as well as the biological activity of compounds created on their basis.

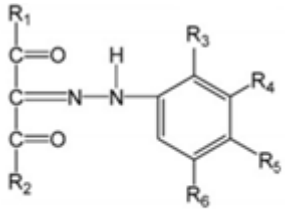

Fig.1. Azo derivatives of β-diketones

Arylhydrazones of β-diketones- (E)-3-(2-(2-(1-(dimethylamino)-1,3-dioxobutane-2-ylidene)hydrazinyl)-2-hydroxy-5-nitrobenzol sulfonic acid (H_3L^1) were synthesized in the Structural Chemistry Laboratory of the Higher Technical Institute of the University of Lisbon. To answer the questions whether the studied tautomers are planar structures, which of them are most stable in the gas phase, how the formation of an intramolecular hydrogen bond affects their structure, and also to understand the process of proton transfer, accompanied by a rearrangement of the electron density, and therefore, leading to significant changes in the structure and physical properties of tautomers, quantum-chemical calculations were carried out. The spatial and electronic structure of eight tautomers Z-enol-

azo-I, Z-enol-azo-II, E-enol-azo-I, E-enol-azo-II, keto-azo, hydrazo-I, hydrazo- II and hydrazo-III were studied by the molecular mechanics method MM + and further calculations by the semiempirical method of quantum chemistry PM3 using the HyperChem software package. In this work, the following radicals were considered for the H_3L^1 tautomers (Fig. 1): R_3 = OH; R_4 =SO_3H; R_5 = H; R_6 = NO_2; R_1 and R_2 are alternately $N(CH_3)_2$ and CH_3 radicals. As a result of the calculation, geometric (bond lengths, bond and dihedral angles), energy and electronic parameters (total energies, energies of HOMO and LUMO orbitals, dipole moments, Mulliken charges on atoms) were obtained for all tautomers. All optimized tautomers have a quasi-flat structure. The stability of the tautomeric forms is largely due to the ability of these compounds to establish intramolecular hydrogen bonds. For all tautomers, the sites of formation and the lengths of the formed hydrogen bonds were determined, varying from 1.77 to 2.51 Å. The most stable and compact was the hydrazo-III structure with minimal value of enrgyand a dipole moment of 5.92 D, stabilized by strong intramolecular resonance binding (RAHB) between the hydrazone N-NH fragment and the carbonyl group, forming a six-membered ring. Analysis of the results obtained allowed us to theoretically characterize the structures of stable tautomers.

ACTIVATION PARAMETERS OF BASIC FLOW IN AQUEOUS SOLUTIONS OF LiCl, NaCl, and KCl SALTS AND PARTIAL MOLAR VOLUME OF SALTS IN SOLUTION

Masimov E.A., Pashayev B.G., Surkhayli A.E.
Baku State University, Faculty of Physics
p.q.bakhtiyar@gmail.com

Thus, the existing structure of water collapses, and a new structure of the solution is formed. Ions cause two opposite changes in the structure of water. On the one hand, the electric field of ions disrupts the order of the molecules inherent in pure water, and this effect leads to an increase in the entropy of the system. On the other hand, the electric field of ions directs water molecules and leads to their regular arrangement around

the ion which leads to a decrease in entropy. In the end, the change in the entropy of the system is positive (ions have a destructive effect on the structure of water) or negative (ions have a structural effect on the structure of water), depending on which of these two effects prevails.

It is known that LiCl, NaCl, and KCl salts dissociate when dissolved in water and, as a result, break down into Li^+ and Cl^-, Na^+ and Cl^-, K^+ and Cl^-, respectively. Since Li^+, Na^+, K^+, and Cl^- ions are present in living organisms, these ions play an important role in the biological processes that take place here. For this purpose, the dynamic viscosity and density of aqueous solutions of LiCl, NaCl, and KCl salts were measured at 10^0 – 60^0C temperature and 0 - 0.07 molar fraction. Using the experimental results, viscous flow activation of Gibbs energy ($\Delta G_\eta^{\neq}$), viscous flow activation enthalpy ($\Delta H_\eta^{\neq}$), viscous flow activation entropy ($\Delta S_\eta^{\neq}$) of an investigated solution, KCl, KBr, KI partial molar volumes ($\tilde{V}$) in solution dependence of concentration was analyzed. It was found that in the considered temperature and concentration range increases with increasing concentration for an aqueous solution of all three salts (LiCl, NaCl, KCl), the parameter is almost unchanged for an aqueous solution of LiCl salt, up to x ≈ 0.04 of concentration for an aqueous solution of NaCl salt decreases, and then almost does not change, and for an aqueous solution of KCl salt decreases, the parameter decreases, and $\tilde{V}$ increases. Also for a given temperature and concentration $\Delta G_\eta^{\neq}$ (water-LiCl)> $\Delta G_\eta^{\neq}$ (water-NaCl)> $\Delta G_\eta^{\neq}$ (water-KCl), $\Delta H_\eta^{\neq}$ (water-LiCl)> $\Delta H_\eta^{\neq}$ (water-NaCl)> $\Delta H_\eta^{\neq}$ (water-KCl), $\Delta S_\eta^{\neq}$ (water-LiCl)> $\Delta S_\eta^{\neq}$ (water -NaCl)> $\Delta S_\eta^{\neq}$ (su-KCl), $\tilde{V}$ (su-LiCl) <$\tilde{V}$ (su-NaCl) <$\tilde{V}$ (su-KCl) in equality are obtained. Thus, based on the analysis of the viscous flow and volume properties of the water-LiCl, water-NaCl, and water-KCl systems in the considered temperature and concentration range, we can say that as the concentration of LiCl, NaCl, and KCl in solution increases, the structure of water collapses. Also, the KCl salt has a stronger destructive effect on the structure of water than NaCl, and NaCl salt has a stronger destructive effect than LiCl. That is, the destructive effect of salts on the structure of water increases in the order of LiCl, NaCl, KCl.

EXPOSURE OF CELLS AND CANCER TISSUES TO RADIOMIMETICS, LOCALIZED AND WHB HYPERTHERMIA

Chirakadze A., Mitagvaria N., Jishiashvili A., Phichkhaia G., Buachidze Z., Gigineishvili A., Jishiashvili D., Khuskivadze N., Chigogidze K., Khomeriki I.
Georgian Technical University, Tbilisi, Georgia
ajishiashvili@gmail.com

Chemotherapeutic agents and radiomimetics are used to directly or indirectly inhibit the uncontrolled growth and proliferation of cancer cells. They are classified according to their mechanism of action and include Antimetabolites, Alkylating agents, Topoisomerase inhibitors, Mitotic inhibitors, Antitumor antibiotics, Protein kinase inhibitors. It is known that the combined use of proton therapy and traditional hyperthermia (WHB) can cause a noticeable clinical effect (especially in the case of radioresistant cells), which significantly depends on temperature, duration and localization of heating, as well as concentration and radiation penetrating ability. Before the commissioning of high-energy proton sources in Georgia in 2024, we used Antitumor antibiotics Bleomycin, Actinomycin D, Doxorubicin and Mitomycin in doses that cause DNA damage similar to the effects of therapeutic proton beams, to simulate processes and qualitatively evaluate the effectiveness of combination therapy, in combination with WHB hyperthermia or without it. Evaluation of the combined effect was carried out on cell cultures and a line of white rats with modeling of Ehrlich's tumor, as well as squamous cell carcinoma of the tongue. To simulate Ehrlich's tumor, a suspension containing a solution of (NaCl) 2 and tumor cells is injected subcutaneously in the back. To model tongue squamous cell carcinoma in rats, 4-Nitroquinoline N-oxide, which is a water-soluble synthetic carcinogen of the quinoline group, is used. On the 40-45th day, in 98% of cases, a histologically and immuno-histologically confirmed tumor with a diameter of 0.3 cm (carcinoma in situ) developed on the root of the tongue. Superparamagnetic CuNi, AgxLa1-xMnO3, Fe3O4 nanoparticles were used as sources of local heating and to increase the penetrating power of the radiomimetic, and TiO2 nanoparticles were used to change the penetrating power of the radiomimetic. In all studied cases, hyper-

thermia significantly enhanced the chemotherapeutic effect, and local hyperthermia and the addition of TiO2 nanoparticles enhanced the observed effect by about 50-100%.In the future, the study will be continued with the use of reactive oxygen species (ROS). It is also envisaged to test the combined toxicity of all the above agents by a novel method using fixation of indicators (transit time, time spent in the illuminated and dark areas, the number of erroneous and correct decisions, relative changes in blood oxygen saturation, relative changes in blood pressure, relative changes in body temperature, blood viscosity, plasma viscosity, hematocrit, aggregation and deformability of erythrocytes) when the test animals (white rats) pass a multibranched maze, and estimate the highest allowable doses to guarantee the safety of treatment.

USING THE GROUND AND SPACE BASED REMOTE SENSING OBSERVATIONS IN AIR QUALITY FORECASTING

Ravan Ahmadov
CIRES, University of Colorado, Boulder, CO 80309, USA,
NOAA Global Systems Laboratory, Boulder, CO 80305, USA
ravan.ahmadov@noaa.gov

Air pollution impacts human health, visibility, and climate. High concentrations of particulate matter and ozone in the air can result in stroke, heart disease, cancer, and other diseases among population. According to the World Health Organization air pollution kills millions of people every year worldwide [www.who.int/health-topics/air-pollution].

I will present the air quality modeling development and applications ongoing in our laboratory to forecast air pollution over the United States. These air quality forecast models are designed to simulate chemical emissions from anthropogenic and biogenic sources, wildfires, and dust. We ingest the satellite detections of fire radiative power (FRP) into the air quality forecast models to estimate the biomass burning emissions and fire heat flux. The high spatial resolution FRP retrievals from the Visible Infrared Imaging Radiometer Suite (VIIRS) provide fine scale information

about the location and intensity of the wildfires across the globe. Currently there are two VIIRS instruments on the polar orbiting NOAA-20 and Suomi-NPP satellites, which provide us with the real-time FRP detections. Additionally, these satellites provide us with the aerosol optical depth (AOD) retrievals. The high-resolution satellite AOD data can be ingested to the air quality models to improve forecasting the air pollution.

In addition to the satellite platforms, there are ground based remote sensing observations. These ground-based measurements provide valuable datasets for air quality research and forecasting applications. The AERONET (AErosol RObotic NETwork) project is a federation of ground-based remote sensing aerosol networks established by NASA [Aerosol Robotic Network (AERONET) Homepage (nasa.gov)]. There are more than hundred AERONET sites in the US alone. We use the AERONET provided hourly (daytime only) AOD at 550nm to evaluate the smoke (particulate matter from biomass burning) forecasts during the 2020 and 2021 fire seasons in the US.

Finally, I will show some examples of the global air quality model applications to forecast the long-range transport of dust and smoke.

MHD WAVES AND INSTABILITIES IN THE COLLISION LESS SPACE PLASMA

Dzhalilov Namig
Shamakhy Astrophysical Observatory named after N. Tusi, Azerbaijan National Academy of Sciences, Azerbaijan
dnamig@gmail.com

Using the 16-moment equations that take into account heat fluxes in anisotropic collisionless bi-Maxwellian plasma, the properties of magnetohydrodynamic (MHD) instabilities are investigated. For all instabilities occurring in the MHD approach (the usual incompressible firehose instability, the second type of compressible almost longitudinal firehose instability, and the almost transverse mirror instability of slow magnetosonic modes, as well as thermal instability caused by the heat flux directed along the magnetic field), their kinetic analogs are considered. We obtained also

general MHD dispersion equation taking into account two components of plasma (electrons and protons) and heat fluxes along the magnetic field. The thresholds and instability growth rates obtained in the MHD and kinetic approaches are found to be in good agreement. The results prove that, in contrast to the familiar CGL (Chew–Goldberger–Low) approximate model, the anisotropic MHD approach provides a correct description of the large-scale dynamics of collisionless anisotropic plasmas, such as solar corona, solar wind, and ionospheric and magnetospheric plasmas on the basis of the developed theory the MHD instabilities of temperature-anisotropic coronal plasma are considered. We show that aperiodic mirror instabilities of slow MHD waves can develop under solar coronal conditions for weak magnetic fields (B < 1 G) and periodic ion-acoustic instabilities can develop for strong magnetic fields (B > 10 G). We have found the instability growth rates and estimated the temporal and spatial scales of development and decay of the periodic instability. We show that the instabilities under consideration can play a prominent role in the energy balance of the corona and may be considered as a large-scale energy source of the wave coronal heating mechanism.

We considered supersonic flows of two semi-infinite anisotropic and homogeneous plasma layers with different physical parameters and velocities. For the general case, i.e., when the interface between these two flows is a transition layer with a finite thickness, we derived a general linear differential equation framework for determining the eigenmodes in the system.

Furthermore, we considered thoroughly the limiting case of a zero thickness transition zone (contact discontinuity). It is shown that the shear flow excites the KH instability and “couples” the various branches of the free-plasma oscillations to each other. It is found that the region of mode interaction is determined by the resonance regions when the longitudinal phase velocities of the waves match. In the resonance flows with an average speed, the KH instability occurs. The growth rates of the KH instability are calculated as a function of the parameters, including the degree of plasma anisotropy. The obtained results are applied to the plasma conditions in the bimodal solar wind in the vicinity of the contact discontinuity between different flow patterns (fast and slow wind).

SPECIFICS OF ENHANCING SAFETY OF CANCER TREATMENT DURING PANDEMICS USING NANOPARTICLE MIXTURES

Chubinidze G., Chirakadze A., Phichkhaia G., Buachidze Z., Chigogidze K. Gigineishvili A., Khuskivadze N., Gulashvili M.
Caucasus University, Tbilisi, Georgia
ketevan_chigogidze@yahoo.com

Certain forms of cancer and its treatments, along with the many other special conditions, chronic illnesses and addictions, significantly increase the risk of Covid-19 and the severity of the disease. Despite the expected success of mass vaccination, the problem will still remain relevant, since in the foreseeable future there will be a fairly large category of especially vulnerable groups of the population, such as elderly people, pregnant women, hypersensitive, patients with many chronic diseases, cancer patients, patients with psychological problems, etc. In this regard, our group has chosen several priority areas for the purpose of development, testing and implementation of the active complex combinations based on nanoparticles and nanocomposites, photosensitizers, liquid crystals and dyes with high antiviral activity (including the new coronavirus infection COVID-19).To date, laboratory work on the development and testing of a UV generator of reactive oxygen species (ROS) based on titanium dioxide nanoparticles and various photosensitizers has been completed. Biological effectiveness of combination of the generated ROS in combination with zinc nanoparticles and low dose hydrochloroquine against the following strains of microorganisms American Type Culture Collection (ATCC) S. aureus, P. aeruginosa, E. coli, B. cereus, B. Subtilis was studied. Testing was carried out according to EN 13727 (Quantitative suspension test for the evaluation of bactericidal activity in the medical area) and EN 14476 (Quantitative suspension test for evaluation of virucidal activity in the medical area) standards, with nanoparticle concentrations in the aqueous solution of 10-50 μg /ml and exposure times of 5 min, 15 min and 30 min. It was found that the strains of S. aureus, P. aeruginosa, E. coli, B. subtilis. were completely deactivated, and the number of active B. cereus spores decreased by 10-12 times. Upon direct addition and homog-

enization of the synthesized nanoparticles in a nutrient medium at a concentration of 80-100 μg/ml and further incubation, complete deactivation of B. cereus spores was observed. A new generator utilizing various nanoparticle mixtures and visible light has been designed and manufactured, and laboratory testing will start in the nearest future.

SENSORS BASED ON NANOMATERİALS

Bellucci S.
INFN-Laboratori Nazionali di Frascati, Via E. Fermi 54, 00044 Frascati, Italy
bellucci@lnf.infn.it

Advanced two-dimensional materials and artificial intelligence for chemical and biological sensing devices will be described. We will review results in electrochemical sensing methods, as well se the fabrication and uses of two-dimensional materials such as graphene as well as transition metal dichalcogenides. I will also outline an intelligent system for the detection of viruses, in the context of Risk Prevention, developing solutions to counter and contain the effects of any future pandemic. It is a microplatform equipped with an innovative technology for real-time detection of the presence of viruses in human breath and aerosol, such as human coronavirus (using for experimentation low pathogenicity strains such as 229E - Alphacoronavirus - or OC43, Betacoronavirus). Such an achievement will be an unprecedented breakthrough, as no technology capable of such monitoring is currently available. The proposed sensing system will be applicable to both face masks (indoor and outdoor use) and air conditioning systems. The proposed sensing will be bound to membranes of conductive nanomaterials, on which selective antibodies to the target viruses have been immobilized, and then deposited on screen printed electrodes (SPE). The determination of the presence of the virus in the aerosol will take place in real time in a label-free manner, i.e. without the addition of reagents, through the measurement of the electrical pulse or the variation of the current of current (at potential applied at the ends of the membrane) following the formation of the virus/antibody-membrane

complex. Signal processing will also rely on artificial intelligence (AI) paradigms to mitigate uncertainty related to changes in environmental and operational conditions.

SOLAR – TERRESTRIAL RELATIONS AND BIOSPHERE: FROM EARLY EARTH TO PRESENT

Ragulskaya M.
Department of Solar Physics and Solar-Earth Relations, Institute of Terrestrial Magnetism and Radio Wave Propagation, RA of Sciences, Moscow, Russia
ra_mary@mail.ru

The report considers the influence of space weather factors and the solar dynamics on the biosphere of the early and modern Earth. The verification of the available theoretical models of the formation of the Solar system and physical conditions on the early Earth is carried out from the point of view of the possibility of the modern form life development. The emergence of the biosphere and the geomagnetic field was determined not only by the conditions on the Earth itself, but also by the dynamics of the early Sun, the migration of giant planets and the formation of the Earth-Moon system. Prospects for expanding the search for bacterial life on Mars, on satellites of outer planets and exoplanets are being considered. The development of flu pandemics 1880-2020 and Geno geographic features of the pandemic COVID-19 in conditions of low solar activity are being discussed.

DELAMINATION AND REDOX BEHAVIOR OF BLACK PHOSPHOROUS

Gomez-Perez J.F., Deák C., Kukovecz Á.
Interdisciplinary Excellence Center, University of Szeged, Department of Applied and Environmental Chemistry, H-6720 Szeged, Rerrich Béla tér 1. kakos@chem.u-szeged.hu

Black phosphorus is a stable allotope of phosphorus with a layered structure. It can be delaminated into 2D nanosheets of phosphorene very similarly to the process of obtaining graphene from graphite. As the materials science community has become interested in this material because of its interesting electronic properties, the number of related publications has ramped up from less than 10 in 2013 to over 1200 in 2018. In this talk I will first review the most important characteristics of phosphorene, then discuss its exfoliation behavior. The second talk of the talk will introduce the redox behavior of few-layer black phosphorus based on a combined UV-Vis, XPS, and Raman spectrometric study.

MOLECULAR MODELING APPLIED TO THE BIOLOGICALLY ACTIVE SUBSTANCES

Akverdieva G.A, Demukhmedova S.D., Akhmedov N.A.
Institute for Physical Problems, Baku State University, Baku, Azerbaijan gulnaraakverdieva@bsu.edu.az

In the represented work the role and possibilities of molecular modeling methods in modern research on the development of new drugs are discussed. The search for new substances with specific biological activity is a problem that requires the use of modern molecular modeling techniques. Numerical calculations of the structure using computers is an effective tool for studying the molecular mechanisms of biochemical processes and the reactivity of physiologically active compounds.

The development of the representations on the interaction mechanism of pharmaceutical substance with the receptor and the understanding its electoral ability are possible owing to the structure-functional investigations. Many experimental works are devoted to the structure-functional investigations of the biologically active molecules. Note that none of these used methods led to a sufficient clarity, and even more so to a reasonable quantitative representation of the structure of such molecules. At present, the use of various theoretical calculation methods, the recent achievements of the computer technology, including programs with a graphic representation of spatial structures, allows researchers to construct all possible models of the peptide molecules under study. The research work conducted on the basis of molecular modeling within the framework of the pharmacophore concept is most relevant. Pharmacophore-based designs can be used to control chemical modifications of molecules to improve receptor recognition and increase biological activity. This can be useful to provide some insight into the nature of the functional groups in the receptor responsible for binding to established drugs.

The possibilities of a theoretical study of the spatial molecular structure are demonstrated on the example of biologically active substances - neuropeptides, melanotropins, cardiopeptides, opioid and anticancer peptides, antiviral, antiinflammatory, immunomodulatory and antihypertensive drugs studied in Biophysics Department of Institute for Physical Problems of Baku State University. By molecular mechanics, molecular dynamics, quantum chemistry, molecular docking methods with application of modern programs the conformational profiles, geometry, structural, electronic and spectral parameters, molecular and physical properties of the mentioned molecules have been established. Using received results and data of SAR studies the bioactive conformations for some of the investigated molecules were assessed and the pharmacophore models for their interaction with the specific receptors were constructed. An estimation of the arrangement of pharmacophore elements of the investigated molecules can be used for design of the peptidomimetics. The results of research create the prospects for the purposeful synthesis of steady medical products.

THE STUDY OF THE OPTICAL CHARACTERISTICS OF p-CuAgTe

Jalilova Kh.D., Gadjiyeva G.S.
Institute of Physics, ANAS, Baku, Azerbaijan
jalilova1951@gmail.com

In this paper with the purpose to investigation of energy band structure of p-CuAgTe in the range of own absorption the fundamental optical functions: refractive index – n(ω), absorption index-k(ω), dielectric constants $\varepsilon_1(\omega)$, $\varepsilon_1(\omega)$, ε_x, the function of the characteristic volume energy losses-Imε^{-1} (ω), the effective mass of charge carriers is estimated. The treatment of obtained data by means of Kramers-Kronings relations allowed to estimate the complete of fundamental optical constants:$\varepsilon_1(\omega)$, $\varepsilon_2(\omega)$,-Imε^{-1},n,k in the energy range 0.05-0.5 and 1.0-6.2 eV and make supposition about the electron's transmission from low-lying level to conduction zone. Also, the effective mass of charge carries, the lifetime of the plasma oscillation, the plasma energy and direct transition energy in between the zones was estimated. It has been shown that lifetime of plasma oscillations is calculated from peak-Im$\varepsilon^{-1}(\omega)$ on the half width level by relation $\Delta\omega/\omega = 2/\omega_\rho\tau$and equal to $\tau = 4.7 * 10^{-13} sec.$, also plasma resonance energy $\hbar\omega\rho = 0.05$ eV. Maximal of main volume plasmons: 0.21(0.1 eV) and 0.22(0.144eV) indicates that in excitation of volume plasmons besides valent electrons also deeper level`s electrons are taken place. The shift of main peak-Im$\varepsilon^{-1}(\omega)$ about maximum of ε_2 on 0.07eV and in visible region on 0.75eV determines energy of longitudinalcross splitting of transitions.

RELAXATION PROPERTIES OF PP AND PE – BASED NANOCOMPOSITES

Huseynova A.S.[1], Hajiyeva F.V.[2]
[1] Institute of Physics ANAS, Baku, Azerbaijan
[2] Baku State University, Baku, Azerbaijan
aem05@rambler.ru

The dependences of the relaxation time on temperature are investigated for a number of polymers. At the intersection of the continued straight lines with the dashed vertical, corresponding to the storage temperature of the electret (room temperature), the expected lifetimes of the electret

charge during storage under these conditions were obtained. The developed new electret polymer nanocomposites based on PP, PE and nanoparticles 1% MnO_2 (PP/1% MnO_2), 0.5%MnO_2(PP/0.5%MnO_2), 7%ZrO_2 (PP/7%ZrO_2), 2%TiO_2 (PP/2%TiO_2), 1%$PbCrO_4$(PE/1%$PbCrO_4$), showed an electret effect, which significantly surpasses the known traditional analogs in its characteristics, which makes it is possible to use these nanocomposites to obtain highly efficient electret microphones, electroacoustic devices, etc.

The stability of the electret charges of nanocompositions has been investigated at relatively high temperatures [3]. This was due to the fact that it took a long time to determine the lifetime of electret charges at room temperature. Therefore, in order to establish the real lifetime of electrets by extrapolation, the lifetime at room temperature was determined using the following relationship:

$$\tau = \tau_0 \cdot \exp\left(-\frac{E}{kT}\right)$$

where τ is the lifetime at a given temperature; τ_0 - lifetime at room temperature; E-activation energy of electret charges; Boltzmann's k-constant. It was found that the lifetime of polymer nanocomposites based on PP/1%MnO_2 is 575 days, for nanocomposites based on PP/0.5%MnO_2 - 487 days, for PP/ZrO_2 - 225 days, for PP/TiO_2 - 321 days, and for nanocomposites based on PE/$PbCrO_4$ - 134 days.

The dependences of E and τ_0 on time are highlighted taking into account their independence from each other. In fact, they are connected in a complex way due to the presence of the process of displacement of charge carriers and polarization in the internal field of the electret.

FEATURES OF THE OPTICAL ABSORPTION SPECTRUM IN THE Sb-Se CHALCOGENIDE GLASS SYSTEM

Mekhtiyeva S.I.[1], Isayev A.I.[1], Alekberov R.I.[1,2], Sadikhli R.F.[1], Mammadova H.I.[1], Garibova S.N.[1,3]
[1] Institute of Physics, ANAS, Baku, Azerbaijan
[2] Azerbaijan State University of Economics (UNEC), Azerbaijan
[3] Khazar University, Baku, Azerbaijan
ramida_sadikhli@mail.ru

Chalcogenide glasses are promising for use in optoelectronics, fiber optics, nonlinear optical systems and in memory devices. In the presented work, the optical absorption spectra were measured of $Se_{33}Sb_{67}$, $Se_{50}Sb_{50}$, $Se_{60}Sb_{40}$, $Se_{70}Sb_{30}$, $Se_{80}Sb_{20}$ chalcogenide glass compositions. It was found that the optical absorption spectrum of the studied materials consists of three parts; The weak absorption region (α <1cm^{-1}), which absorption coefficient is very weak dependence on the energy of the photon, the region of exponential absorption obeying the Urbach rule (α=1÷10^3 cm^{-1}) and region dependence obeying to Taus' law ($\alpha \geq 10^4$ см$^{-1}$) [3]. The dependence of the absorption coefficient (α) on the energy photon(hν) in the region obeying Taus' law.

$$\alpha h\nu = A\left(h\nu - E_g\right)^2 \quad (1)$$

which A -constant is weakly dependent on temperature.

The dependence of $(\alpha h\nu)^{1/2}$ on hν was defined and by extrapolating the linear part of the graph to the zero value of the absorption coefficient was determined optical band gap (E_g) for studied compositions. The presence of a linear dependence on a sufficiently wide range of photon energy indicates that the electronic transitions correspond to allowed indirect transitions. In order to determine relationship between the optical absorption coefficient and the near order parameters characterizing the amorphous matrix and other physical quantities was calculated the mean coordination number (Z), cohesive energy (CE) according to the following formula.

$$Z = 3X_{Sb} + 2X_{Se} \quad (2)$$

$$CE = \sum_i c_i E_i \quad (3)$$

Which, X is molar fraction of chemical elements in matter, c_i is the relative amount of chemical bonds determined according to the chemical bond approach (CBA), E_i is the energy of the chemical bonds. The relative amount of chemical bonds in compositions with different chemical compositions is determined by the ratio R - the ratio of the number of possible covalent bonds between chalcogen atoms to the number of covalent bonds between non-chalcogen atoms. The value of R = 1 corresponds only to the stoichiometric composition of heterepolar bonds ($Se_{60}Sb_{40}$). In compositions rich with chalcogen atoms ($Se_{70}Sb_{30}$, $Se_{80}Sb_{20}$), the value of R is greater than 1, but in compositions with chalcogen deficiency ($Se_{33}Sb_{67}$, $Se_{50}Sb_{50}$) is less than 1.

INFLUENCE OF INTERLAYER INTERACTION CHANGES ON *Bi_2Te_3* LAYERED CRYSTALS INTRALAYER BONDS

Gahramanov S.Sh., Gahramanov K.Sh., Abdullayev, N.A.
Institute of Physics, ANAS, Baku, Azerbaijan
samir.gahramanov@gmail.com

It is shown that the anomalies observed in the temperature dependence of the crystal lattice parameters and kinetic parameters of bismuth telluride doped with copper and indium *Bi_2Te_3<In,Cu>* are explained by changes in the chemical bond and the effect of defect centers. The redistribution of the electron density between the metal and the central chalcogen layer in the quintet-layer of the crystal framework, in a certain temperature range, leads to a negative thermal coefficient of linear expansion (TCLE). The polarity of the covalent bond and the decrease in the *$Bi\text{-}Te^{(2)}$* interatomic distances are directly affected by the magnitude of the interlayer interaction. The energy of thermal motion, when approaching the value of the energy of interlayer interaction, leads to deviation of bonds and to fluctuations in the distribution of electron density in the volume of the crystal.

The polarity of the covalent bond changes, leading to a conformational transition, which is expressed in a decrease in the *$Bi\text{-}Te^{(2)}$* interatomic distances; experimental confirmation of this process was observed in negative TCLE values at temperatures energetically correlating with the

value of the interlayer interaction. The resonance of hybrid bonds undergoes transitions along the extrema, changing bond angles and interatomic distances, a conformational transition occurs, the most pronounced was observed at a negative TCLE of about 270K. The change in interatomic distances through the next cycle of the corresponding energy is not so pronounced due to temperature smearing.

The transition temperature depends on the magnitude of the interlayer interaction: covalent bridges formed by interlayer inclusions enhance the interaction between opposite layers of quintet packets, therefore the temperatures at which negative TCLE are observed for pure and doped materials have different values. The energy of thermal motion corresponding to the ambient temperature, when approaching the value of the energy of interlayer interaction, leads to a deviation of the bond and to fluctuations in the distribution of the electron density. The stronger the interlayer interaction, the higher the temperature, i.e. the more energy is required to "soften" it.

Interlayer bonds are more sensitive to changes in the parameters of the external environment, therefore, it can be concluded that the above processes are influenced by fluctuations in interlayer bonds, which affect the hybridization of the orbitals of atoms inside the quintet and lead to a change in the covalent radius. A change in the interlayer interaction, leading to a redistribution of the electron density from the edges of the quintet to the inside of the layer, to a bond with the central chalcogen, changes the bond from a long-range resonant to a covalent form with a fraction of ionicity, and then to an ionic-covalent one, bringing the interatomic distances closer together as the nature of the bond changes.

This work was supported by the Science Development Foundation under the President of the Republic of Azerbaijan (Grant No. EIF/MQM/Elm-Tehsil-1-2016-1(26)-71/16/1-M-01).

SPATIAL STRUCTURE OF OCTAPEPTIDE MOLECULE

Ismailova L.I., Abbasli R.M., Akhmedov N.A.
Baku State University, Institute for Physical Problems, Baku, Azerbaijan
lara.ismailova.52@mail.ru

One of the basic problems for molecular biophysics is investigating of the spatial organization of the peptide molecules. It is known that peptides regulate all functions of a living organism. Using the regulatory peptides of the human body, you can create new drugs. This scientific work is devoted to study the spatial organization, conformational possibilities of the octapeptide molecules Pro-Pro-Gly-Leu-Gly-Pro-Leu-Arg.

The calculations were carried out by the method of theoretical conformational analysis with regard to nonvalent, electrostatic and torsional interactions and energy of the hydrogen bonds.and a special computer program. The low-energy conformations of this molecule and the values of the dihedral angles of the main chain and side chains are found and the energy of the intra- and inter-residue interactions was estimated. The conformational mobility of the amino acid side chains is investigated and the amino acids with specific interplays with different receptors are founded.

The conformational possibilities of the octapeptide molecule Pro-Pro-Gly-Leu-Gly-Pro-Leu-Arg. were studied in fragments. First, the conformational properties of the tetrapeptide Pro-Pro-Gly-Leu were determined based on the stable conformations of the monopeptides N-acetyl-L-proline, L-glycine and. N-acetyl-L-leysine. Then the spatial structure of the hexapeptide Pro-Pro-Gly-Leu-Gly-Pro was studied. And finally, the addition of the hexapeptide Pro-Pro-Gly-Leu-Gly-Pro and dipeptide Leu-Arg allowed us to calculate the spatial structure of the all octapeptide molecule Pro-Pro-Gly-Leu-Gly-Pro-Leu-Arg.

The low-energy conformations of this molecule, the values of the dihedral angles of the main chain and side chains of amino acid residues were found, the energy of intra-and inter-residual interactions was estimated. The relative energy of the conformations of the octapeptide molecule varied within the range 0– 10 kcal/mol. Study of the spatial structure of the octapeptide molecule have almost 11 low-energy conformations. The global conformation of this molecule (E_{rel}=0 kcal/mol) is $BBBB_{3222}PRR_{2122}B_{3222}$. It is revealed that low energy conformations of

these molecules have the folded and half folded types of backbone. These forms bring part of the backbone and the side chains of the amino acids together, and they result in convenient interactions.

The results can be used to study the spatial structure of octapeptide molecule as well as to study the conformational capabilities of side chains when interacting with receptor molecules. The side chain of Arg8 have sufficient conformational freedom in the low-energy structures of the octapeptide molecule under study and it can be assumed that they can participate in interaction with receptors and with other conformations. Thus, the theoretical conformational analysis of the octapeptide molecule led to such structural organizations of molecules that do not exclude the realization by the molecules of a number of various functions that require strictly specific interactions with various receptors.

It is revealed that low energy conformations of this molecule have the folded and half-folded type of backbone. These folded forms bring parts of the backbone and the side chains of the amino acids together, and they result in convenient interactions.

SMALL–SİZED STRUCTURES DEPOSİTED FROM A SHARP EMITTER ON A NEARBY SURFACE

Gasanov I.S. , Eminov Sh.O., Aliyev S.A., Mammedova G.H., Gurbanov I.I., Akberov E.M., Mamedov F.E.
Institute of Physics, ANAS, Baku, Azerbaijan
sabir.eliyev.1950@mail.ru

The processes of applying the nanodroplet phase from a sharp emitter to a nearby moving surface by means of a finely dispersed phase of a liquid metal ion source (LMIS) are considered. In order to deposit narrow strips, the emitting needle was located at a close distance from the moving surface. At a needle-surface distance of the order of 80 μm, massive continuous paths of several microns wide were obtained on the axis of a wide and thin trace of ions (In^+, Sn^+). The structure of the deposited strips with a length of more than 10 mm is granular. To deposit narrower structures, efficient cooling of the conductive movable substrate is necessary.

MAGNETIC PROPERTIES of $Zn_{1-x}Fe_xSe$ COMPOUND

Ismayilova N.A. [1], Abbasov I.I.[2]
[1]Institute of Physics, ANAS, Baku, Azerbaijan
[2]Azerbaijan State Oil and Industry University, Baku, Azerbaijan
ismayilova_narmin_84@mail.ru

Magnetic properties of ZnSe compound investigated in references [1, 2]. The authors of these works report that $Zn_{1-x}Fe_xSe$ solid solutions show paramagnetic properties at low temperatures and in low magnetic fields. [3] A simple explanation of the systematic behavior of the magnetic states, doped compounds III–V and II–VI is also given. Shown that V or Cr-doped ZnS, ZnSe, and ZnTe are ferromagnetic without p- or n-type doping treatment. However, Mn-, Fe-, Co- or Ni-doped ZnS, ZnSe and ZnTe are spin-glass states.

Magnetic properties of doped with Fe:ZnSe investigated by implementing the Density Functional Theory (DFT) [4] method using the Atomistix Tool Kit program software (ATK, http://quantumwise.com/) [5].

Given that the d orbitals of iron atoms contain unpaired electrons, these electrons cause additional magnetization in the matter. Thus, the study of the magnetization of the compound is of great interest. For this reason, in the presented work we investigate magnetic properties doped with Fe atoms ZnSe supercell structure containing 16, 32, 64, 128 atoms. We calculated the energy difference (ΔE) between FM and AFM states for ZnSe, which is defined as ΔE = E(AFM) - E(FM) (Table). A negative value of ΔE means that AFM is favored over FM and vice versa. Our calculation result show that the AFM arrangement of this compound is more favorable than Ferromagnetic and Paramagnetic configurations.

Table. Calculated total energy in antiferromagnetic and ferromagnetic states for supercell containing 16, 32, 64, 128 atoms

Supercell	Atom number	E(AFM)-E(FM) meV/atom
$Zn_6Fe_2Se_8$	16	-0.12717
$Zn_{14}Fe_2Se_{16}$	32	-0.06126
$Zn_{30}Fe_2Se_{32}$	64	-0.04351
$Zn_{62}Fe_2Se_{64}$	128	-0.01846

THERMALLY STIMULATED CURRENTS IN BISMUTH SILICATE

Bagiev V.E., Rustamov F.A., Darvishov N.H., Mamedov M.Z.
Institute for Physical Problems, Baku State University, Baku, Azerbaijan
v_bagiev@mail.ru

Photorefractive crystals of the sillenite type ($Bi_{12}XO_{20}$, where X=Ge, Si, Ti), one of which is bismuth silicate, are effective materials for holographic recording and storage of information. In the process of recording and storing information in these crystals, impurity centers in their band gap play an essential role. In this work we investigated the adhesion levels in bismuth silicate by the thermally stimulated conductivity (TSC) method. Research was carried out in the Me - $Bi_{12}SiO_{20}$ – Me (Me = Ag, Al) system. The electrodes were applied in a sandwich configuration. Sample thickness 0.1 ÷ 1mm, applied external voltage 1 ÷ 300 V, temperature range 70 ÷ 400 K. The precooled samples were exposed to illumination of 1 ÷ 3 eV energy, covering intrinsic and impurity range of photosensitivity. Studies have shown that in single crystals of bismuth silicate, in temperature range 90 ÷ 350 K, there is a complex spectrum with seven maxima. Previously, when analyzing the TST curves in $Bi_{12}SiO_{20}$, in order to determine the parameters of the adhesion levels, method we used, that took into account the shape and location of the maxima. However, the presence of many closely spaced TST peaks leads to distortion of their shape and location.

In this work, to analyze the TSC peaks, the temperature dependences of the TSC currents were calculated using analytical formulas for various types of adhesion levels, and also fitted to experimental curves with a variation of three independent adjustable parameters. For low – temperature maximum (T_{max} = 145K), the best agreement with experiment in achieved when applying the formula for the adhesion level with a bimolecular type of recombination. Consequently, the adhesion levels that determine this maximum are centers with a bimolecular type of recombination.

Using the fitting parameters within the framework of this model, the depth of the adhesion level E_{t1} = 0.23 eV, the electron captures cross section $S_t = 1.1 \cdot 10^{-20} sm^2$ and the electron density at the initial moment at the adhesion level $n_0 = 1.4 \cdot 10^{18}\ sm^{-3}$ are determined.

Thus, the calculation and fitting to experimental data using analytical formulas for various capture and recombination mechanisms makes it possible to more correctly determine the type of adhesion levels in $Bi_{12}SiO_{20}$ and its microscopic parameters, such as depth of occurrence, the capture cross section for electrons and their concentration.

PLASMA MODIFICATION OF ELECTROPHYSICAL PROPERTIES OF COMPOSITE MATERIALS

Dadashov Z.A., Guseynova G. KH., Ramazanova I.S., Tatardar F.N
Institute of Physics of ANAS, Baku, Azerbaijan
dadashov.zamir@mail.ru

Existing piezo-, pyroelectric converters and control measuring devices based on them are extensive used in medical diagnostics, optical communication systems as well as in various fields of technique. The main exponents of these systems and devices are identified by the macroscopic parameters of piezoelectric, pyroelectric converters (piezo sensitivity, piezo coefficient etc.). Therefore, it is necessary to develop novel types of piezoelectric converters as well as more effective technologies to improve the properties of existing piezoelectric materials. For this purpose, we use electric gas discharge plasma which is the most effective technology to change the surface heterogeneity of the polymer matrix of the composite (polymer matrix: HDPE and piezo phase: PZT-5A, PZT-8). The plasma was created in the air gap of 2.5 mm by the sinusoidal voltage of 7 kV. Under the influence of electric gas discharge plasma, oxygen-derived functional groups (C = O, C-O-C, COH, OP) are formed or changed in the polymer chain. Experimental results show that the HDPE macromolecule of non-polar polymer oxidizes at a short time and decreases its non- polarity. The resulting polar groups are very greedy for electrons and can localize them. The formation of different oxygen-containing groups in the polymer chain increases the electronegativity of the polymer. Thus, the modification of the polymer phase of composites under the influence of pre-electric gas discharge plasma is the effective technological method to improve the

electro- physical (piezo coefficient, piezo-sensitivity, etc.) characteristics of the polymer- based composites.

THREE-DIMENSIONAL STRUCTURE OF THE GLUTEOMORPHIN MOLECULE

Akhmedov N.A., Agayeva L.N., Abbasli R.M., Ismailova L.I.
Institute for Physical Problems, Baku State University, Baku, Azerbaijan
Namiq.49@bk.ru

Gluteomorphin is an opioid peptide that is formed when the gliadin component of the gluten protein is digested. It is usually broken down into amino acids by digestive enzymes.

We have investigated the structural and functional organizations of the opioid peptides. This work is a continuation of our previous research. The molecule was calculated using the method of theoretical conformational analysis. The potential function of the system is chosen as the sum of non-bonded, electrostatic and torsion interactions and the energy of hydrogen bonds. Nonvalent interactions were assessed by Lennard-Jones potential. Electrostatic interactions were calculated in a monopole approximation according to the Coulomb's law using partial charges on atoms. The conformational possibilities of the gluteomorphin molecule were studied under the conditions of the water environment. The energy of hydrogen bonds was estimated using the Morse potential.

The three-dimensional structure of the gluteomorphin molecule (Tyr1-Pro2-Gln3-Pro4-Gln5-Pro6-Phe7-OH) was investigated based on the low-energy conformations of the corresponding amino acid residues. The calculation results show that the conformations of eight shapes efeeee, efefef, efefee, eeefef, efeeef, eeefee, eeeeee and eeeeef fall into the energy range 0–3 kcal/mol. The energy of non-valence interactions in low-energy conformations changes in the energy range (-29.3) - (- 27.1) kcal/mol, electrostatic interactions (-3.8) - (- 2.5) kcal/mol, torsion interactions (5.2) - (3.2) kcal/mol. The relative energy range 0 - 3.0 kcal/mol includes 8 efeeee shape conformations, 9 efefef shape conformations, 5 efefee shape conformations, 7 eeefef shape conformations, 2 efeeef

shape conformations, 2 eeefee shape conformations, 1 eeeeee shape conformation, and 3 eeeeef shape conformation. The global conformation of the gluteomorphin molecule is the $B_1RB_{12}BB_{12}BB_3$ conformation of the efeeee shape. The conformation is advantageous for non-bonded and electrostatic interactions. In this conformation effective di-, tri, and tetrapeptide interactions arise: Tyr1 effectively interacts with the Pro2-Gln3-Pro4 fragment, Gln3 with Pro4-Gln5, Gln5 with Pro6-Phe7.

Thus, the spatial structure of the molecule of gluteomorphin can be represented by eight structural types, and it can be suggested that the molecule performs its physiological functions in these structures. On the basis of these structures, one can propose its synthetic analogs and calculate the spatial structure of the gluteomorphin molecule. The theoretical conformational analysis of the heptapeptide molecule of gluteomorphin has led to such a structural organization of the molecule that does not exclude the implementation of a whole range of functions by the molecule, requiring strictly specific interactions with various receptors.

INFLUENCE OF A COMPLEX PROFILE QUANTUM WELL PARAMETERS ON THE THERMOPOWER OF A NONDEGENERATE TWO-DIMENSIONAL ELECTRON GAS

Figarova S.R., Mahmudov M.M., Khasiyeva G.N.
Baku State University, Baku, Azerbaijan
mehdimahmudov@bsu.edu.az

The modern molecular beam epitaxy technology with the use of computer control makes to design low-dimensional structures with a wide range of potential profiles. In this work, we study the thermoelectrically power of a nondegenerate two-dimensional electron gas in a complex shape quantum well for scattering of conduction electrons by acoustic and nonpolar optical phonons. The influence of the quantum well parameters, namely, the potential and width of the well, as well as the temperature and charge carrier's concentration on the thermoelectric power is studied.

It is shown that the thermopower of a nondegenerate two-dimensional electron gas nonmonotonically depends on the quantum well

width: for narrow quantum wells (up to 10 nm) its magnitude sharply decreases, and for wide quantum wells, it increases, reaching saturation. The increasing of the quantum well potential leads to the thermopower sharply decreases, which is associated with localization of electrons in the quantum well. In the temperature range 100-400 K, the absolute value of the thermopower increases with increasing temperature (up 15%), while with increasing concentration, it significantly decreases.

RELAXATION TIME FOR INTERBAND AND INTRABAND SCATTERING IN SUPERLATTICES IN A STRONG MAGNETIC FIELD

Figarova S.R., Mahmudov M.M., Qazanfarli R.Kh.
Baku State University, Baku, Azerbaijan
rustam.qazanfarli.xaliq@bsu.edu.az

For the intensive use of low-dimensional electronic systems in nanoelectronics, it is necessary to obtain comprehensive information on the physical characteristics of the systems under consideration. Such information can be obtained by studying electronic transport phenomena in low-dimensional systems. The physical properties of quasi-two-dimensional systems differ significantly from the properties of ordinary isotropic or weakly anisotropic conductors. Various scattering mechanisms of conduction electrons significantly affect the electronic transfer phenomena. Therefore, when studying transport phenomena, it is necessary to take into account all possible scattering mechanisms of current carriers. In quasi-two-dimensional systems, the anisotropy of the structure and energy spectrum of conduction electrons leads to specific features of the scattering mechanisms. Consequently, an accurate determination of the scattering mechanism plays an important role in comparing experimental results with theory.

In the paper, the relaxation time of conduction electrons for the scattering on acoustic and polar optical phonons in superlattices in a strong magnetic field is calculated. Has been studied the probability of intraband and interband scattering. It was found that in a strong magnetic

field for scattering by acoustic phonons, intraband transitions prevail, while in scattering by polar optical phonons, interband transitions prevail. It is shown that the relaxation time is proportional to the density of states, which depends on the magnetic field.

EFFECT OF GAMMA RADIATION ON THE PHOTOELECTRİCS PROPERTIES OF p-$CuTlS_2$ SINGLE CRYSTAL

Madatov R.S.[1,2] , Mamishova R.M.[3], Sh.A.Alahverdiyev, Faradjova U.F.[2]
[1] Institute of Radiation Problems, ANAS, Baku, Azerbaijan
[2] National Aviation Academy, Baku, Azerbaijan
[3] Baku State University, Baku, Azerbaijan
rexsane@yandex.ru

The ternary compound $CuTlS_2$ is very promising for the creation of high-performance broadband photo converters of a new generation, as well as elements of semiconductor technology and nonlinear optics. Interest in these compounds is due to their unique properties (absence of an inversion center, high nonlinear susceptibility, etc.). These materials can find practical application in the creation of lasers, light modulators, photodetectors and other opto-, micro- and nanoelectronic devices, controlled by a magnetic field.

In this work, we investigated the electrical and photoelectric characteristics of $CuInS_2$ crystal. The studied p-CuTlS compound was grown at high temperature using the Bridgman–Stockbarger method. The obtained single crystal had a diameter of 1cm, a length of 8cm and a specific resistance of ~ 40 Ω · cm. Crystal structure and lattice parameters of the sample obtained by X-ray analysis method a = 4.08; c = 8.16Å; z = 2 were calculated, and it was determined that the compound crystallizes in tetragonal crystal system.

The size of the studied sample is 2 × 0.5 × 6mm. Measurements were made on a B7-30 universal ampere-voltmeter at a voltage of 0–20V (E ~ 10–10^5V/cm) and a temperature range of 100–300K.

The electrical conductivity and volt-ampere characteristics of the p-$CuTlS_2$ single crystal with specific resistance ρ= 40 Ω·cm and irradiated by

γ-quantum were studied in the range of 100-300 K temperature and 10-10^4 V/cm. During radiation with Φ = 500 krad γ quantum, a decrease in the current is observed, and the transition voltage from the ohmic part to the quadratic part increases. At 1 Mrad of dose, the value of the current increases concerning to the value before radiation and in the I ~ Un dependence, ohmic, quadratic, and sharply increasing of current are observed. At higher values of the radiation dose the regularity I ~ Un is maintained and in this case the value of the current increases depending on the radiation dose. At high radiation doses, the concentration of charge carriers increases due to the predominance of acceptor type defects, resulting increasing the electrical conductivity of the crystal.

ANISOTROPY OF ELECTRICAL CONDUCTIVITY IN $TlInTe_2$-Te SOLID SOLUTIONS

Madatov R.S.[1], Khalilova K.H.[2], Najafov A.I.[2], Mammadov M.A.[1]
[1] Institute of Radiation Problems, ANAS, Baku, Azerbaijan
[2] Institute of Physics, ANAS, Baku, Azerbaijan
a.najafov@mail.ru

$TlInTe_2$ crystals crystallize in TlSe structure type (*I4/mcm*) and have the following parameters: a=8,494 Å; c=7,181Å; c/a=0,845; Z=4; d=7,36 q/cm^3. The chemical bond in $TlInTe_2$ crystals is ionic-covalent. Both $TlInTe_2$ compounds and $TlInTe_2$-Te compounds with 4.0 at.% Te were found to have p-type conductivity and the following specific resistance along the crystallographic axes: ρ∥=795Om.cm; ρ⊥77350 Ohm.cm və ρ∥=1,6 Ohm.cm; ρ⊥1645 Ohm.cm. $A^3B^3C_2^6$ crystals that crystallize in the TlSe structure type are defective crystals, the density of defects in these crystals is 10^{18}-$10^{20}cm^{-3}$. Physicochemical studies show that in the $TlInTe_2$ crystal, the Te anion is 4% soluble, resulting in the formation of solid solutions. In this study, the temperature dependences of the electrical conductivity of the $TlInTe_2$ crystal with the addition of Te were studied and the effect of the electric field on the anisotropy of the electrical conductivity was investigated. The specific electrical conductivity of $TlInTe_2$ and $TlInTe_2$-Te (4 at.%) crystals was studied in the temperature range of 100-300 K and in

the range of 10-10^2 V/cm electric field in the parallel and perpendicular directions to the plane of the chain.

The current-voltage characteristics and electrical conductivity of single-crystal were studied in the temperature range of 100-300 K and a voltage range of 0-5 V.

The effect of the distribution of additive levels in the direction of crystallographic axes in the $TlInTe_2$–Te system on the current-carrying mechanism was studied in the temperature range of 100-300 K and electric field values $E < 10^2$ V/cm.

A comparison of the temperature dependences of the anisotropy ($lg[\sigma_{||}/\sigma_{\perp}]$~f(1/T) of the specific electrical conductivity in the $TlInTe_2$ and $TlInTe_2$-Te crystals shows that the anisotropy of the conductivity in the $TlInTe_2$ crystal is weak with increasing in the temperature range of 100-250 K and sharply increases in the range of 250-300 K. The anisotropy of the conduction does not change in the $TlInTe_2$-Te crystal with increasing temperature in the range of 100-220 K, but increases sharply in the range of 220-300 K.

Analysis of the obtained results shows that the stoichiometric excess of the additive atom in the crystals with a chain structure allows to purposefully control the anisotropic properties of materials, and this method can be used in the development of fast conversion systems.

INVESTIGATTION OF ELECTROPHYSICAL PROPERTIES OF DEEPLY BURRIED AVALANCHE PHOTODIODES

Jafarova E.A.[1], Dovlatov A.A.[2], Aliyeva L.A.[1], Aliyev R.A.[3], Tapdygov E.S.[1]
[1] Institute of Physics of ANAS Baku, Azerbaijan
[2]Azerbaijan State Oil and Industry University, Baku, Azerbaijan
[3] Institute for Physical Problems, Baku State University, Baku, Azerbaijan
alihuseyndovlatov@gmail.com

There have been investigated electric characteristics of avalanche photodiodes with deeply buried pixels (MAPD) at different polarities of potential applied to the n-Si substrate.

It is shown that the optimal voltage of a structure with deeply buried pixels is higher than the breakdown voltage. The value of the maximum overvoltage at which the process of stable amplification of the photocurrent occurs is determined by the second inflection point of the volt-ampere characteristics (the first inflection point corresponds to the breakdown voltage and the onset of the avalanche process). An increase in the value of the optimal voltage significantly increases the multiplication factor of free charges, the magnitude of the photocurrent, and increases the energetic resolution of the photocurrent signal.

At the forward bias of MAPD (negative potential is applied to n-Si substrate) the exponential rise of the current with the voltage $U_f < 0.5$ V ($I_d = const \cdot \exp\frac{qU_f}{\beta kT}$, β~1.2) has been observed, what appropriate to diffusion mechanism of current leakage through p-n junction.

MODELING OF THE MAIN COMPONENTS DISTRIBUTION IN Ge–Si CRYSTALS BY A MODIFIED TECHNIQUE

Aghamaliyev Z.A.
Baku State University, Baku, Azerbaijan
zohrabagamaliyev@bsu.edu.az

The problem of obtaining single crystals of solid solutions at industrial scales remains urgent. This circumstance motivates studies aimed at improving and modifying existing methods as well as developing new methods for growing single crystals of solid solutions with a set composition and quality.

In this study, are presented the theoretical basis for growing single crystals of semiconductor solid solutions with a set composition using a modified method of zone melting, and also the results of mathematical modeling of the concentration distribution for the components in Ge–Si crystals grown by this method at different operating parameter values. The purpose of the study is to identify the potential and prospects of the method proposed for growing single crystals of semiconductor solid solutions with a set homogeneous or graded composition.

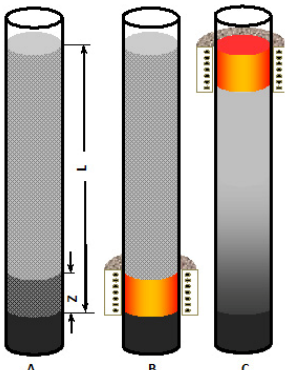

Fig.1 Schematic diagrams of the growth of Ge–Si crystals by modified method of zone melting

The problem of the concentration distribution of components over a Ge–Si crystal grown by modified method of zone melting (Fig.1) has been solved in the Pfann approximation. Analysis of the obtained results clearly demonstrate the potential of modified method of zone melting for obtaining the Ge–Si single crystals with the desired homogeneous and variable compositions in the entire continuous series of solid solutions. In this case, mathematical modeling of the concentration profiles of the components in crystals makes it possible to evaluate the optimal technological parameters (melted-zone length, concentration fractions of Si atoms supplied by the rod and Ge/Si seed material) for obtaining solid solutions with set properties.

It can be state that the method has real prospects for growing bulk single crystals of a wide range of semiconductor solid solutions with a set axial concentration component profile. To provide a single-crystal structure of the Ge–Si solid solutions grown by the method considered, it is necessary to use such technological modes in which, during the entire cycle of crystallization of the melt, the rate of crystal growth for portions both with variable and homogeneous compositions do not exceed the corresponding values of volume of the melt crystallizing per unit of time.

VAPOR SYNTHESIS OF ZnO NANOCRYSTAL-BASED HOLLOW MİCROSPHERES

Jishiashvili A.D., Chirakadze A.A., Shiolashvili, Z.N.
Makhatadze N.K., Gobronidze V.V., Jishiashvili D.A.
Georgian Technical University, V.Chavchanidze Institute of Cybernetics, Georgia
ajishiashvili@gmail.com

The functionality and performance of nanomaterials strongly depend on their morphology. ZnO-based hollow micro- and nanospheres attracted great attention due to their outstanding electrical, optical, catalytic, gas sensing and biomedical properties. This work presents the results of our study on the vapor growth of ZnO-based hollow spheres using Zn,

ZnO and NH_4Cl powder mixtures as source materials. The Scanning Electron Microscopy (SEM), X-ray diffraction, panchromatic cathodoluminescence imaging and Energy Dispersive Spectroscopy (EDS) were used for the characterization of samples. The growth was performed in the evacuated vertical quartz reactor with two temperature zones. In the "hot zone" the source powder was heated by an external furnace up to 600°C. The Si substrate was placed in the "cold zone", at a specified distance above the source, and was heated by thermal convection. After switching on the furnace, the source and substrate temperatures were at first gradually raised within ~30 minutes and then stabilized, reaching 550 and 430C, respectively. At substrate temperatures close to 400°C, mainly the ZnO nanocrystals were formed on the Si surface. At elevated temperatures, the Zn vapor was prevailing, and the deposited material was enriched with Zn. This promoted the formation of Zn suboxides (ZnO_x), which have a low melting point of ~419°C. The layer-by-layer growth of ZnO_x was observed, with a layer thickness between 80-130 nm. The irregular, micrometers size balls comprising ZnO_x layers were produced on the Si surface.

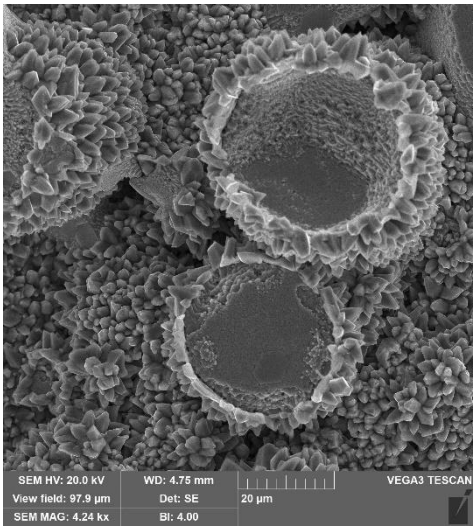

Fig. 1. SEM image of ZnO hollow microspheres grown on Si substrate

After approximately one hour of growth, the source powder was

completely depleted and evaporated. However, the further anneal of the reactor with Si substrate was causing the out-diffusion of Zn from the inner regions of the layered ZnOx balls and oxidation of its surface. As a result, the ZnO micro- and nanocrystals were produced that were covering the whole ball surface. Gradually, the inner part of the ball was depleted of Zn and the hollow microsphere was formed. Fig. 1 shows the example of such hollow spheres.

This work was supported by Shota Rustaveli National Science Foundation of Georgia (SRNSFG) [grant number YS-19-087].

METAL CARBON NANOCOMPOSITES BASED ON HIGH PRESSURE POLYETHYLENE

Mirzoeva N.A.[1], Kurbanova N.I. [1], Zeynalov E.B.[2]
[1] Institute of Polymer Materials of ANAS, Sumgait, Azerbaijan
[2] Nagiyev Institute of Catalysis & Inorganic Chemistry of ANAS, Baku, Azerbaijan
nura_89@bk.ru; ipoma@science.az

The development of nanotechnology opens up new opportunities for extensive research in the field of composite materials. Currently, nanocomposite materials are used as promising polymer materials that can be used in various fields of electronics.

It is known that the use of multi-walled carbon nanotubes as nanofillers significantly improves the characteristics of the resulting materials. The presented work is devoted to obtaining and studying the properties of nanocomposites based on high-pressure polyethylene (PE) with the use of metal-containing nanoparticles stabilized by a polymer matrix and multi-walled carbon nanotubes (MWCNT) as nanofillers.

Nanocomposite polymer materials are obtained by mixing PE with a nanofiller containing nanoparticles of nickel oxide (NPNiO) and MWCNT on laboratory rollers at a temperature of 130-135 ° C for 15 minutes. For mechanical tests, the resulting mixtures were pressed in the form of 1 mm thick plates at 190 ° C and a pressure of 10 MPa for 10 minutes. The ratio

of the initial components (mass.f.): PE / NPNiO / MWCNT = 100 / (0.5; 1.0; 2.0) / (0.01; 0.05; 0.1).

It is shown that the insertion of only MWCNT into the composition of PE leads to an increase in the activation energy of thermo-oxidative destruction, however, it reduces the parameters of mechanical properties. The combined use of MWCNT and nickel oxide nanoparticles contributes to the improvement of both mechanical and thermal properties of composites.

An improvement in the strength, deformation parameters, and also the thermal-oxidative stability of the obtained nanocomposites was revealed, which, apparently, is associated with the synergistic effect of the interfacial interaction of nickel-containing nanoparticles in the PE matrix with MWCNT.

FULLERENE- CONTAINING COMPOSITES BASED ON ISOTACTIC POLYPROPYLENE

Dunyamalieva A. I., Kurbanova N.I.[1], Zeynalov E.B.[2]
[1] Institute of Polymer Materials of ANAS, Sumgait, Azerbaijan
[2] Nagiyev Institute of Catalysis & Inorganic Chemistry of ANAS, Baku, Azerbaijan
dunyamaliyeva89@list.ru; ipoma@science.az

The production and industrial application of polymer nanocomposites is one of the important areas of nanotechnology. Polymer nanocomposites have improved properties compared to conventional polymers and their microcomposites. Prevention of aging of polymer composite materials as a result of long-term use, which occupies a special place in materials science, is one of the important issues.

There is enough data in the literature on the effect of fullerenes on the technological and technical characteristics of polypropylene. The aim of this work was to study the effect of the fullerene mixture $C_{60/70}$, consisting of 85% C_{60} and 15% C_{70} on the structure, mechanical and thermal properties of isotactic polypropylene (PP). Compositions based on isotactic polypropylene (PP) and fullerene mixture (FM) were prepared by mixing in a polymer melt at a temperature of 160-165 ° C and the ratio of

components (wt. p.): PP/FM=100/ (0.02; 0.04; 0.08). To determine the physico-mechanical properties of the obtained compositions, the mixtures were pressed for 10 minutes at a temperature of 190 ° C and a pressure of 10 MPa.

The mechanical and thermo-oxidative properties of the obtained nanocomposites have been studied. It is shown that the insertion of even a small amount of FM into the composition of PP leads to a significant increase in physico-mechanical and thermophysical properties: tensile strength from 31.41 to 32.76 MPa, elongation at break from 34 to 42%, heat resistance from 165 to 235 ° C, which is apparently due to the synergistic effect of the interfacial interaction of fullerene-containing nanoparticles with a polypropylene matrix.

Derivatographic studies have shown that the insertion of fullerene-containing nanoparticles into the polypropylene composition improves the thermal-oxidative stability of the obtained nanocomposites: the activation energy increases from 145.45 to 189.75 kJ/mol. An increase in the thermal stability of PP when adding a fullerene mixture with $C_{60/70}$ is apparently associated with a slowdown in the thermal oxidative decomposition of the polymer due to a decrease in the rate of oxygen diffusion in the presence of a nanofiller.

ADSORBSION AND PHOTODEGRADATION OF ORANGE G DYU BY CoAl LDH /PVA AND COPPER DOPED CoAl LDH/PVA NANOCOMPOSITES UNDER VISIBLE LIGHT

Abdullayeva G., Azizov A., Balayeva O., Buniyatzade I., Mammadyarova S.
Baku State University, Baku, Azerbaijan
ofelyabalayeva@bsu.edu.az

In this work, photocatalytic degradation of Orange G dye was carried out under visible light in the presence of CoAl-LDH/PVA as a catalyst. The conditions for dye degradation were optimized by pH and contact time. The samples were charactezized by ultraviolet-visible spectroscopy, x-ray

powder diffractometer and photoelectrocolorimeter. The photodegradation rate reached a maximum at pH2 (92% at 60 minutes) and reached complete equilibrium.

Wastewater management is a major problem in developing countries due to varying industrial processes satisfying human needs. Orange G (OG) belongs to the class of azo dyes of synthetic origin. It is a form of mono azo and anionic dye, which is soluble in water and stable at any pH.

CoAl-LDH/PVA nanocomposite was synthesized using co-precipitation method. A mixed solution of 0.015 mol Co $(NO_3)_2 \cdot 6H_2O$ and 0.005 mol $Al_2 (SO_4)_3 \cdot 18H_2O$ salts was prepared. The mixed solution was titrated with 0.8 M $NaHCO_3$ and 1.6 M NaOH. For the modification of CoAl-LDH/PVA nanocomposite 0.004 g of $CuCl_2 \cdot 2H_2O$ was added to 10 ml of glycerin and titrated with 10 ml of ascorbic acid. 1.177mol 10 ml of $N_2H_4 \cdot H_2O$ was used as a reducing agent.

For calibration curve, 1,3,5,7,9, 10, 20, 30 and 40 ppm OG azo dye solutions were prepared with distilled water. 0.01 g of nanocomposite and 3 ml of orange substances in different concentrations and pH were used in the experiment. The samples were irradiated during 30, 60 and 300 min under visible light. The efficiency of adsorption and photodegradation was estimated using the following equation:

$$R\ (\%) = C_0 - C_e / C_0 \times 100$$

where C_0 and Ce are initial and equilibrium concentration of OG, respectively. When the sorption efficiency of OG composite at pH3 was 75% the photodegradation reached to 80% at 60 min under visible irradiation (150 watts). The sorption rate at pH2 was lower than at pH3, the photodegradation rate reached maximum at pH2 (92% at 60 minutes). The sorption rate increased after 30 minutes of exposure to copper doped CoAl LDH / PVA nanocomposite (R% = 32%), Cu + composite (R% = 42%). Copper metal nanoparticles are dispersed in the polymer nanocomposite matrix and form an amorphous structure**.** The bandgaps of CoAl-LDH / PVA and Cu dopped CoAl-LDH / PVA were 3.1 eV and 2.8 eV, respectively. The main diffraction peaks for pure CoAl LDH /PVA were observed at 2θ values of 62.1 corresponding to the lattice plane (110). The intensity of this peak decreased to 62.1 by the modification.

SYNTHESIS OF SnS NANOCRYSTALS AND SnS/CdZnS STRUCTURES

Jahangirova S.
Baku State University, Baku, Azerbaijan
sona_aliqizi@mail.ru

Nanocrystalline SnS powder has been prepared using tin chloride ($SnCl_2$) as a tin ion source and sodium sulfide ($Na_2S_2O_3$) as a sulfur ion source on glass substrate by electrochemical deposition at room temperature. The detailed structural and optical properties confirmed the orthorhombic SnS structure and a strongly blue shifted direct band gap (1.74-1.76 eV), for synthesized nanoparticles, after heath treatment. The advanced technology in the electrochemical deposition of thin films of SnS on the surface conductivity CdZnS allowed for the first time a photo converter heterojunctions CdZnS/SnS, showing the possibility to realize high conversion efficiency of solar radiation on the substrates SnS large areas.

Quantum confinement effect in semiconductor nanomaterials has been of special interest during the last decades. Quantum confined semiconductor nanocrystals, which exhibit properties different from bulk materials, are a new class of materials that hold considerable attention for numerous applications in the field of optoelectronics. Modification of molecular design and morphology of such nanostructures provides a powerful approach to control their electronic and optical properties. Among the extensively studied IV-VI semiconductor materials, tin sulfide is very important narrow gap material because of its low toxicity and wide applications as an absorber layer in solar cells, near infrared materials, holographic recording media and solar control devices. The optical properties of SnS vary depending on the synthesizing or fabrication method. In order to obtain nanostructured SnS, the following methods are used: spray pyrolysis of the water solution, chemical vapor deposition, electrochemical deposition, microwave assisted synthesis, mild solution route, modified solution dispersion method, solvothermal process, successive ionic layer adsorption and reaction, hydrothermal synthesis, and molecular beam epitaxy. SnS is an important optoelectronic material. Chemical bath deposition can be used to deposit SnS films. SnS can be deposited in superstrate

or substrate configurations, but the best efficiencies were obtained in the substrate configuration where it is possible to separate between absorber deposition and junction formation.

In this paper we report the preparation, morphological, optical and structural properties of SnS nanocrystals and heterojunction CdZnS/SnS by electrochemical deposition. Depositions were carried out potentiostatically from a de-aerated aqueous solution containing 0.2M solution of tin chloride ($SnCl_4$), $Na_2S_2O_3$ (0.2M). and PVA-400. To optimize the stoichiometry of the deposit, electrochemical baths with different compositions, obtained mixing different volumes of the above-mentioned solutions, were tested. The final pH was about 5, it was obtained adding lactic acid and NaOH (10M). Electrodeposition was performed at a potential of -1.05V vs. saturated calomel electrode (SCE); electrochemical experiments were performed using a PAR potentiostat/galvanostat (model PAR-STAT 2273). The role of PVA is to stabilize the nanostructures preventing them from coagulation.

ELECTRODEPOSITION OF In_2S_3 LAYER FOR SOLAR CELLS

Jahangirova Sona
Baku State University, Baku, Azerbaijan
sona_aliqizi@mail.ru

The electrochemical deposition of In_2S_3 thin films was carried out from an aqueous solution of $InCl_3$ and $Na_2S_2O_3$. The effect of the potential of deposition was studied on the cell parameters of CZS based solar cells. The obtained films depending on the deposition potential and thickness exhibited complete substrate coverage. Maximum photoelectric conversion efficiency of 12.0% was obtained, limited mainly by a low fill factor (65%). Further process optimization is expected to lead to efficiencies comparable to CdZnS buffer layers.

Solar cells based on CdZnS (CZS) chalcopyrite absorbers have reached 20.0% conversion efficiencies at the laboratory scale, using high vacuum processes. However, due to the toxicity of cadmium and the possible gain in current associated with the use of a wider bandgap material, many works are carried out with the aim of developing alternative buffer

layers. The In_2S_3-based material is among the most relevant alternatives. Several techniques, such as sputtering, atomic layer deposition (ALD), evaporation and chemical bath deposition (CBD) have been used to synthesize In_2S_3 thin films on CZS. However, it seems that soft chemical-based deposition techniques such as CBD which do not damage the surface of the absorbers and can provide highly conformal coating are more suitable to get high efficiency Cd-free CZS solar cells. Electrodeposition is a soft technique widely used in industrial processes for large area coating, both in batch and inline systems. This method, more recently applied to semiconductor synthesis, may allow to control the width of the bandgap and the doping level by monitoring solution composition, applied potential, pH and temperature. Moreover, it provides conformal growth with controlled thickness layers. All these advantages yield the method attractive for the synthesis of the absorber, the buffer layers as well as the transparent conductive oxide layer in CIGSe-based solar cells. Even if important works have been done on the electrodeposition of the CZS-based absorbers, very few attempts have been carried out so far to electrodeposit In_2S_3 buffer layers.

The electrodeposition of In-S based layers was carried out using an aqueous solution containing indium chloride (5 mM), sodium thiosulfate (20 mM) as sulfur source and potassium chloride as supporting electrolyte (0.1M). A standard three-electrode setup was used. The reference electrode was a saturated mercurous sulfate electrode (MSE, E°= 0.64V/NHE) and platinum was used as the counter electrode. The deposition was carried out at 60°C.

A preliminary investigation was carried out on molybdenum-coated glass substrates to determine the optimal deposition conditions. In-S layers were then deposited on CdZnS absorbers, Al and glass substrate provided by Würth Solar.

THE STUDY OF SUPRAMOLECULAR ENSEMBLES BASED ON GO NANOLAYERS AND NOVEL AZOMETHINES

Aliyeva G.S.[1], İbrahimli E.R.[1], Mehraliyeva G.E.[1,2], Huseynzadeh A.E. [1], Hasanova U.A.[1], Ismayilov V.M.[1], Yusubov N.N.[1]

[1] Baku State University, Baku, Azerbaijan

[2] Azerbaijan State Oil and Industry University, Baku, Azerbaijan

elvinibraqimli7@gmail.com

Advanced research into chemistry points out compounds or complexes with antimicrobial potential. Schiff bases are one of such compounds. This research aims at the synthesis of a Schiff base and their supramolecular ensembles with nanoscale GO out of fairly common antibiotics which contain B-lactam ring. Substances containing B-lactam rings are currently used as antibiotics, and most of them are distinguished by their effectiveness. Compounds containing B-lactam rings have very simple pharmacology as compared to other agents. Most of them are in parenteral form, have a short half-life.

The main goal is to obtain new biologically active compounds by synthesizing new Schiff bases from the reaction of condensation on the basis of salicylic aldehyde derivatives with B-lactam ring-containing compounds. Supramolecular ensembles of the obtained compounds with GO nanolayers will be obtained. Recently, the use of nanoparticles in pharmaceutical chemistry and targeted drug delivery raises the issue of obtaining supramolecular ensembles with nanoparticles of compounds to be synthesized.

nGO used in components in electronic devices have been used in nanocomposite materials, polymer composite materials, energy storage, biomedical applications, catalysis, and as a surfactant with some overlaps between these fields. In addition, the presence of different functional groups on the surface of graphene oxide ensures that organic molecules are bound by both covalent and non-covalent bonds. It is this feature that expands the field of application of graphene oxide.

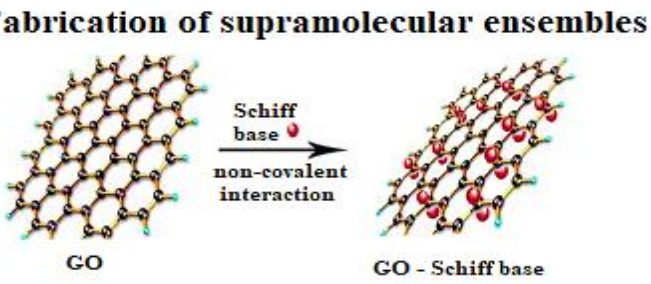

The figure shows a schematic representation of the synthesis of nGOs and the Schiff base. Nowadays, nanolayer graphene oxide (GO) has attracted major interest in the biomedical and pharmaceutical fields. Its individual physical, chemical and biological properties, such as two-dimensional planar structure, high chemical versatility, numerous functional groups, good chemical and thermal stability, inexpensive, extensive surface area, good biocompatibility and high capability of loading drugs by physical adsorption via π-π stacking, make it an excellent carrier for loading and delivery of various therapeutic drugs. In the ongoing research, it is planned to use this property of GO to bind organic molecules with biological activity to nanolayers with non-covalent bonds.

METAL-CONTAINING NANOCOMPOSITES BASED ON ISOTACTIC POLYPROPYLENE AND BUTADIENE–ACRYLONITRILE RUBBER

Kurbanova N.I.[1], Guliyeva T.M.[1], Eyvazova G.M.[2], Aghamaliyev Z.A.[2], Muradov M.B.[2]
[1] Institute of Polymer Materials, ANAS, Sumgayit, Azerbaijan
[2] Baku State University, Baku, Azerbaijan
kurbanova.nushaba@mail.ru; ipoma@science.az

The development of thermoplastic elastomers is a priority direction of studies in the field of polymer materials science. The most promising way to prepare new types of thermoplastic elastomers is blending of elastomers with plastics with simultaneous vulcanization of the elastomer, which leads to high degree of dispersity of the elastomer phase in the materials.

The effect that nanofillers containing copper and zinc oxides stabilized with a maleinized low-density polyethylene matrix and prepared mechanochemical exert on the structure and properties of metal-containing nanocomposites based on isotactic polypropylene and butadiene–acrylonitrile rubber was studied by X-ray diffraction and differential thermal analysis, a scanning electron microscope, as well as dielectric properties.

The filling improves the strength, deformation, and rheological characteristics of the nanocomposites and enhances their resistance to thermal oxidation, which is probably due to the synergistic effect caused by interaction of copper and zinc containing nanoparticles with maleic groups of melanized low-density polyethylene, dielectric properties practically did not change upon the introduction of copper and zinc oxide nanoparticles into the composition.

The nanocomposites based on isotactic polypropylene and butadiene–acrylonitrile rubber can be processed not only by pressing, but also by pressure casting and extrusion, which expands their application field.

The nanofiller containing copper and zinc oxide nanoparticles stabilized by the melanized matrix and prepared mechanochemically show promise as an additive to a compound of isotactic polypropylene with butadiene–acrylonitrile rubber. This favors the creation of the finely crystalline structure of the compound and to the improvement of its properties, which, in turn, expands the possible applications of the nanocomposite in automobile industry, mechanical and electrical engineering, medicine, petrochemical industry, and building.

ON TUNNELING IN MULTILAYER STRUCTURES

Zeynalova Sh.H.
National Aviation Academy, Baku, Azerbaijan
shehla_372@mail.ru

Tunneling is one of the many effects or phenomena occurring in semiconductor multilayer structures. A feature of this effect is the transfer of charge from one layer to another through the p-n junction or dielectric

layer, with the appearance of a sufficiently large current, and the maintenance of this process during the time of exposure to the applied voltage (usually reverse), depending on the size (area and thickness) of the junction and each the adjacent layer, as well as other factors affecting the duration of the phenomenon. Therefore, one of the important directions in the study of multilayer, especially nanostructures, is the simulation of this process under various conditions, taking into account the thickness of the layers, both from a semiconductor and a dielectric.

Currently, there are a number of models describing tunneling. Photo-stimulated tunneling through a three-barrier asymmetric structure with a hyperfine dielectric is considered. On the basis of a simple model, the boundary conditions on the envelope wave functions are obtained in the case of contact of materials with significantly different nature of the electronic spectrum. The study of electron tunneling through thin potential barriers and the analysis of the interaction of these electrons with the energy levels of size quantization in potential wells separating the barriers, which ensures the speed of MIS devices. In order to provide clarity, estimation of the electron wavelength for metal and semiconductor executed.

Thus, the operation of modern high-speed devices is based on the effect of electron tunneling across quantum-dimensional layers, with a sufficiently small thickness, when the quantum-mechanical (wave) properties of an electron are manifested. If, in the early works, the features of the formation of a space charge in the inversion layer near the semiconductor surface were considered, then in the works considered, tunneling in nanometer-scale systems in resonant and near-resonance levels, where the quantum-mechanical nature of quasiparticles is manifested, was studied. In this case, to describe the effect of carrier tunneling transfer matrix method used.

SENSORICS IN POLYMER COMPOSITE MATERIALS

Allahverdiyeva S.Q.
National Aviation Academy, Baku, Azerbaijan
allahverdiyeva77@bk.ru

Partial replacement of aircraft structures with polymer composite materials opens up almost countless opportunities for the development of aviation. The use of polymer-composite materials in the construction of aircraft is one of the strategic and most important directions in the field of diagnostics. Special achievements when using composite materials are predicted not only in the field of strength and reliability of aircraft, but also in equipping aircraft structures with a variety of modern sensors used in diagnostic control.

The adaptive property of polymer-composite materials requires the creation of new diagnostic models and tools that make it possible to detect latent defects in time, adequately respond to the detected defect, monitor the volumetric information received from individual units and housings, and also, after processing it by the on-board computer, prematurely identify the causes of failures and carry out control of the aircraft condition, which will increase the efficiency and reliability of aircraft. The advantage of composite materials consists in combining several materials of different structure into one structure with strictly individual properties. And this leads to the development of new models of control and measuring sensors: it allows to initially build a structure adapted for installation at a specific point of the aircraft structure, i.e. not to select materials that will simultaneously provide the sensor characteristics specified by the technical task and organically fit into the design of the apparatus. This feature of composites plays a key role in the design of automated monitoring and control systems for aircraft systems, where thousands of sensors are required, operating in various aggressive conditions and having different body designs.

Thus, the creation of built-in monitoring systems based on modern sensors in polymer-composite materials without interaction with the external environment will allow to receive and process volumetric information in real working time from units, assemblies and housings, to en-

sure the processing of information on the operating parameters of equipment, as well as the ability to combine sensors into a wireless sensor network, which will increase economic efficiency and ensure the safety of aircraft flights.

PBS/PVA-MG-AL- OH NANOCOMPOSITE AS PHOTOCATALYST FOR MALACHITE GREEN DYE UNDER VISIBLE LIGHT

İbrahimova Kh.A., Azizov A.A., Balayeva O.O., Alosmanov R.M.
Department of Chemistry, Baku State University, Baku, Azerbaijan
khazangul.ibrahimova1994@mail.ru

Metal sulfides are important materials because of their wide applications in optoelectronics and catalysis. Lead sulfide (PbS) as a metal chalcogenide and metal semiconductor has a narrow and direct band gap of 0.4 eV at room temperature. The PbS nanoparticles have vital applications in a nonlinear optical device like absorbers in solar cells, optical information storage, infrared detector, gas sensor, optical amplification, and optical switches, due to the exceptional third-order non-linear optical properties. This paper described PbS nanocomposite based on PVA/Mg-Al-OH layered double hydroxide composite film by a successive ionic layer adsorption and reaction (SILAR) method. The aim of the work is to introduce a new class of polymer-filled nanoparticles with a simple method of preparation and unique photocatalyst properties suitable for sensing behavior. The prepared products were characterized by X-ray powder diffraction analysis (XRD), Scanning electron microscope (SEM), Energy-dispersive X-ray spectroscope (EDS), Fourier transform infrared spectroscope (FTIR), and Ultraviolet-visible spectroscope (UV-Vis). The average size of PbS nanoparticles were determined 4.08 nm and 1.33 nm. The optical band gap of PbS nanoparticles is calculated as 0.47 eV and 0.34 eV. The effect of PbS/PVA-Mg-Al-OH nanocomposite film as a photocatalyst on the degradation of malachite green dye under visible light was investigated. We observed that malachite green was totally degraded at 30 min under visible light. 15 ml of the malachite green dye solution (5 ppm) was used to determine the photocatalytic activity. Some 0.05 g of catalyst was

applied for degradation of 15 ml solution. The samples concentration was determined by UV-Vis spectrometry.

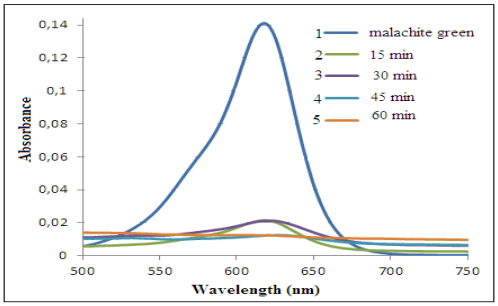

Fig. 1. UV-Vis absorption spectra of 1) malachite green dye and nanocomposite mixed dye under visible light 2) 15 min; 3) 30 min; 4) 45 min; 5) 60 min

SIMULTANEOUS EFFECT OF EXTERNAL FACTORS ON THE DIELECTRIC STRENGTH OF POLYETHYLENE+NANOCLAY NANOCOMPOSITES

Sadygova A.R., Hadiyeva A.A.[1], Asilbeyli P.B.[1], Sadig Kh.O.[2]
[1] Institute of Physics, ANAS, Baku, Azerbaijan
[2] Azerbaijan State Oil and Industry University, Baku, Azerbaijan
arzu-sadigova@mail.ru

When using products obtained from polymers in real conditions, they are exposed to the simultaneously complex effects of mechanical stress, strong electric field and discharge, temperature, humidity, radiation, etc., and in the process of practical application quickly fail (disintegrate). In order to increase the service life of these products and albeit a little prevent their disintegration, polymers-based composites with various additives are used in industry. Composite materials is a system formed by two or more phases that differ in chemical composition and structure.

The results of the study show that the rate of disintegration (the number of broken bonds) in the fragmentation process, which occurs under the simultaneous influence of several external factors, depends on the

changes caused by each factor. By determining the mechanical and electrical durability of these polymers, more wear-resistant materials are selected, and the study of polymer-based composites with various additives is of scientific and practical interest.

In this study, mechanical durability ($\tau_{\sigma E}$) was measured with simultaneous exposure to an electric discharge and electrical durability ($\tau_{E\sigma}$) with simultaneous exposure to a mechanical load for pure high-density polyethylene (HDPE) and HDPE+3,0% nanoclay (NC) composite.

As the mechanical strength was highest at 3,0 % of NC, measurements were performed on pure HDPE and HDPE+3,0% NC nanocomposite. In both samples, the dependence of the mechanical durability logarithm ($\lg\tau_\sigma$) on the mechanical load (σ) was measured under the simultaneous exposure to an electric discharge. The accepted electric discharge voltage is $U = 7 \cdot 10^3 V$ and $U = 9 \cdot 10^3 V$. As a result, the dependence $\lg\tau_\sigma\ (\sigma)$ under the action of an electric discharge in pure HDPE consists of two linear parts. One of them $(\sigma > \sigma^*)$ coincides with the dependence $\lg\tau_\sigma(\sigma)$, which is not affected by the electric discharge, and the other differs in slope $(\sigma < \sigma^*)$. σ^* is the breakdown voltage of the straight line.

At values of mechanical stress $\sigma < \sigma^*$ durability is reduced due to the durability when the discharge is not affected. Then we can write the following expressions from the experimental results.

$$\tau_{\sigma,E} = A_E \exp(-\alpha_E \sigma), \quad \text{if } (\sigma < \sigma^*)$$

$$\tau_{\sigma,E} = A \exp(-\alpha_E \sigma), \quad \text{if } (\sigma > \sigma^*)$$

It can be seen from the observed dependence that another decomposition process arising during an electric discharge is added to the thermal fluctuation decomposition process under the influence of a mechanical load.

In the HDPE and HDPE+3,0% NC nanocomposites, the dependence of the electric durability logarithm on the field strength does not change under the simultaneous exposure to a mechanical load; the dependence $\lg\tau_E \sim f(E)$ is written in the well-known empirical expression:

$$\tau_E = \beta \exp(-\beta E)$$

However, under equal conditions, the simultaneous exposure to a mechanical load causes a decrease in τ_E. The rate of reduction of the dielectric strength of the nanocomposite obtained by the inclusion of 3,0% NC in HDPE is lower than that of pure HDPE. The decrease in dielectric strength is 15% in HDPE and 10% in HDPE+3,0% NC.

ALUMINUM ANODIC OXIDE AS A TEMPLATE FOR FORMATION OF NICKEL NANOWIRES

Karimova A.Kh.
Institute of Physics, ANAS, Baku, Azerbaijan
ayselkerimova00@mail.ru

The aim of the paper is to describe the applications of AAO as a template in metal nanostructures formation and to present the experimental results obtained by us in this field. The basic mechanism of the processes of both anodic oxidation of aluminum as well as electrochemical metal (Ni) deposition in AAO were described. The influence of oxidation parameters on the AAO structure was discussed as well.

Metals in a state of high dispersion currently play an important role in technology. Their chemical and physical macroscopic properties, such as the rate of their reaction with other substances, mechanical properties are significantly different from the bulk metals. Fundamental research and technology development over the last decade have resulted in wider use and implementation of metal-containing materials in a state of high dispersion into the industrial practice.

The fabrication of nanoscale structures has attracted much interest recently owing to their potential use in highdensity magnetic memories, single-electron devices, nanoelectrodes for the direct deposition of nanoparticles from the gas phase, and optical media. The production of nanostructures based on hexagonally arranged porous alumina as a mask or matrix structure is cheaper than that based on traditional methods like nanoscaling using electron beam lithography. To use such an alumina template for new applications of nanostructures, the pores have to be filled

with a conducting or semiconducting material, for example via electrochemical deposition. During electrochemical deposition the growth of nanowires starts at the pore tips and continues in the pore direction from the pore bottom to the pore opening.

The hexagonally ordered porous alumina membranes have been prepared via a two-step anodization process, which is described in detail elsewhere.

The electrochemical anodization of the Al was conducted in a simple homemade two-electrode cell which was provided with electrical motor for intensive stirring of the solution. For fabrication of AAO templates we used 0.4 M oxalic acid solution. The process was conducted under constant cell potential of 40 V at 3–5°C under intensive stirring of solution for 30 min – 2 hours depending on thickness of Al layer.

As a result, we obtained the best nickel filling in the AAO membranes for t of about 5 min. In summary, a highly efficient method for deposition of nickel into ordered nanochannels of porous alumina has been presented. By thinning the barrier layer homogeneously, the porous structure could be kept on the aluminum substrate for the whole process. Our approach to the fabrication of a highly ordered metal nanowire array is inexpensive and very flexible with respect to the size and thickness of the pore structure. In addition, the thickness of the barrier layer and the pore diameter could in principle be varied independently of each other. The use of electrodeposition is well-suited for a uniform deposition in the pores of porous alumina structures, as demonstrated for nickel electrodeposition. Nearly 100% of the pores were filled with nanocrystalline nickel and only a very small fluctuation in growth rate of these nanowires was observed.

NEW LIQUID CRYSTAL NANOCOMPOSITES AND THEIR FUNCTIONAL FEATURES

Bayramov G.M.
Baku State Universitety, Baku, Azerbaijan
qazanfar.bayramov@gmail.com

New colloids with liquid crystal (LC) matrices 5CB (positive dielectric anisotropy) and H37 (negative dielectric anisotropy) and $BaTiO_3$ and $LiNbO_3$ particles have been obtained. In the first case, oleic acid was used as a surfactant. It was shown that the presence of barium titanate particles in the liquid crystal decreases the bleaching temperature, changes the threshold of the Freedericksz effect, and decreases the voltage of electro hydrodynamic instability formation.

First of all, the experimental results are explained by the appearance of local electric fields near polarized ferroelectric particles when an external electric field is applied, as well as a change in the effective viscosity and elastic properties of the liquid crystal, and the existence of additional obstacles (particles) by ions. In this case, the transition of LC molecules from the homeotropic configuration to the planar one requires large and in the opposite direction less efforts than in a pure LC. As a result, the turn-on time of the $BaTiO_3$-5CB colloid decreases, and its turn-off time increases in comparison with pure LC at all applied voltages. The situation is reversed when using a matrix with negative dielectric anisotropy. In this case, the transition from the initial homeotropic orientation of the LC molecules to the planar one is difficult. As a result, the turn-on time of the $BaTiO_3$-H37 colloid increases, and the turn-off time decreases. $BaTiO_3$ particles have a similar effect on the formation of Williams domains in H37.

Observation under a polarizing microscope showed that the addition of $BaTiO_3$ particles to 5CB at a concentration of 1% decreases the transition temperature to the isotropic state from 35.2°C to 32.50°C, and in H-37 - from 61.2°C to 60.1°C.

Samples for obtaining particles of another ferroelectric were pieces of chemically pure lithium-niobate. After grinding in an agate mortar with a small addition of heptane, the resulting powder was separated accord-

ing to the settling time in a column with heptane according to the expression $t=18h\eta/(\rho_1-\rho_2)gd^2$, where h is the column height; η-coefficient of fluid viscosity; ρ_1 and ρ_2 are the specific gravity of barium titanate and heptane; g-acceleration of gravity; d is the cross section of the particles. The final composition was mixed ultrasonically. Observation under a polarizing microscope showed that the addition of $LiNbO_3$ particles to 5CB at a concentration of 1% and 4% decreases the transition temperature to the isotropic state from 35.2°C to 34.60°C and 32.7°C at 1% and 4%, respectively.

The physicochemical and electro-optical properties of the developed LC nanocomposites with various functional features have been investigated.

PLASMONICS FOR SAFETY, SECURITY AND DEFENCE

Illyashenko-Raguin L.N.[1,2], Perevyasko A.M. [2], Petrechenko C.A. [2]
[1] Kharkiv National University of Radio Electronics, Kharkiv, Ukraine
[2] National Academy of the National Guard of Ukraine, Kharkiv, Ukraine
mila.illyashenko@gmail.com

The continued rise in terrorism has created a need for new and innovative applications of photonic technologies in very unconventional ways. They are based on the use of noble metal nanoparticles (NPs). When NPs are illuminated by the light source, they may exhibit a lot of interesting phenomena, including plasmon resonances. They result in resonantly enhanced scattering and resonantly enhanced absorption. Both already proved their usefulness for various civil applications. Resonantly enhanced scattering is useful for applications based on the use of reflected light, such as sensing and imaging. Since absorption results in heat, so that metal NP may become hot enough to fry ill cells of human body, without affecting healthy cells, resonantly enhanced absorption becomes useful for medical treatment of various diseases, especially in such cases when other methods including radio-therapy, surgery, chemotherapy are not able to do so

Plasmon resonance effects depend strongly on size, shape, and material properties of NP. With optimal choice of these parameters it is possible to design NP to be the best suitable for each particular application.

In addition, plasmon effects also depend on properties of that matter, in which NP is situated, that leads to opportunity to use NP in testing for environmental contaminants. The idea is following: when dangerous gas comes to environment, the dielectric permittivity of external environment changes, thus plasmon resonance wavelength of NP will change also. This change is possible to be noticeable. The color of reflected light will change, and new color will correspond to new wavelength of plasmon resonance. Thus by means of the light color reflected by NP, dangerous gases in environment may be detected.

While plasmon effects already found their way into civil defense applications, such as the health care, there are needs to address size, weight, and manufacturing cost issues when NP is designed to be used for sensing under the difficult conditions encountered in military environments. Emerging concepts to use core-shell NPs can support the realization of low-cost solutions, since not whole NP is made on noble metal, rather only its part on the surface of dielectric core. Success however depends on penetration depth of plasmon mode inside the core-shell dielectric-metal NP. In most of cases dielectric core is given, so the size shape and material is not possible to change, and metal is deposed on given core. Thus it needs to know how thick must layer of metal, i.e. metal shell, to provide best possible sensor properties. The set of numerical results includes investigation of these properties, which concerns plasmonic NP sensors within the context of their associated safety, security and defence application.

KINETICS OF FORMATION AND DESTRUCTION OF THE DIELECTRIC GAP ON THE SURFACE OF THE IONIC MATERIAL IN THE EXTERNAL ELECTRIC FIELD

Orbukh V.I., Lebedeva N.N., Eyvazova G.M.
Baku State University, Baku, Azerbaijan
vorbukh@gmail.com

When studying the dielectric spectra of zeolite (a substance with ionic conductivity), an abnormally high value of the dielectric constant was found. This phenomenon, like the monotonic current drop in a constant electric field, is explained by the presence of a dielectric gap on the sample surface. Therefore, it is important to study the features of the dielectric gap in an ionic material. A sample of an ionic material to which an external electric voltage is applied is considered. For definiteness, we will consider a zeolite in which the carriers of the current are positive ions. In the process of current flow, near the anode, a negatively charged (stationary charges) dielectric layer is formed. In order to determine the dependence of this current on time, we consider a plane-parallel plate of an ion-conducting sample. We will proceed from the fact that the boundary (between the already formed part of the dielectric gap and the conducting region) is a plane parallel to the boundaries of the sample.

The process of formation of a dielectric layer is manifested in the movement of the specified boundary towards the cathode. Applying the equation of continuity to positive ions (which pass into the conducting region, thereby increasing the thickness of the dielectric layer), we obtain an equation for the time dependence of the indicated thickness of the charged layer. Based on this result, an explicit expression is obtained for the total current in the circuit, which decreases monotonically to zero (when the process of creating a charged dielectric layer is completed). The current decays exponentially in time, with a time constant inversely proportional to the conductivity and the square root of the external voltage. Let us now consider the destruction of a charged dielectric layer (when the electric voltage is removed and the sample is short-circuited). In this case, in the equations, instead of the voltage, we write zero, and the initial

condition for the gap width is its asymptotic value during the previous exposure in an electric field. As in the previous case, the creation of a dielectric gap, for the case of destruction of the gap, a formula for the total current in the circuit is obtained. The current also decreases as in the previous case, but much more slowly, inversely proportional to the square of time. The time constant is the same as in the previous case.

TEMPERATURE AND SURFACE STATES INFLUENCE ON THE IDENTIFYING OF SCHOTTKY DIODE PARAMETERS

Afandiyeva I. M.[1], Babayeva R.F.[2], Akhundov C.G.[1]
[1]Baku State University, Institute for Physics Problem, Baku, Azerbaijan
[2]Department of Engineering and Applied Science, Azerbaijan State University of Economics (UNEC), Baku, Azerbaijan
afandiyeva@mail.ru

The main aim of this study is two-fold: first, the study of the temperature influence on the functionality of Pd_2Si/n-Si (111) SBDs. Second, the identifying of the surface state role on current transfer. The great interest shown in Pd_2Si/n-Si(111) SBD based on Schottky barriers is caused by the formation of palladium silicide (Pd_2Si) [1,2], which characterized by volume diffusion, the electronic properties of the surface and localized states in the semiconductor band gap. With this aim both the capacitance-voltage $(C-V)$ and conductance–voltage $(G/\omega-V)$ characteristics of Pd_2Si/n-Si(111) SBDs, areas of which about 10^{-6} cm^2 have been investigated in the wide temperature range of 79-360 K, applied bias voltage ± 1V, and with the using of a small sinusoidal test *ac* signal of 20 mV peak to peak amplitude at 500 kHz. On the basis of the temperature dependent characteristics the potential barrier height (Φ_B), the doping degree (N_D), the Fermi energy level (V_n), series resistance (R_s) and surface state density (N_{ss}) were analyzed.

To explain the results has been taken into account the generalized model of the metal-semiconductor contacts with a thin dielectric interlayer. It was revealed, that the value of Φ_B irregular changed (0.46 ÷ 0.69

eV) with the temperature. Such behavior in Φ_B was attributed to the presence of dielectric gap between metal and semiconductor and the influence of surface states and electrons exchanging between surface states and semiconductor or metal under temperature and voltage effects. The voltage dependent profile of R_s was obtained by using Nicollian and Brews method for each temperature [3]. By the using of Hill-Coleman method [4], has been obtained the dependence of surface state density on temperature. The observed changes of investigated parameters with temperature can be attributed to the influence of recharging surface states. The weak dependence of R_s on temperature, which give a peak near 0.1 V, the big value of N_{ss} and minimal value of Φ_B at 240K can be connected with reconstruction and recharging of surface states, the distribution of applied voltage between dielectric interlayer and depletion layer and charge exchange between a surface state with a metal or semiconductor. Due to the influence of temperature and recharging of surface states has been determined the effective value of potential barrier height Φ_{Beff}. Above results can be taken into account in the manufacturing of new multifunctional devices.

THE POTENTIAL BARRIER HEIGHT AND PROFILE OF SURFACE STATES OF Re/n-GaAs SCHOTTKY BARRIER DIODE

Afandiyeva I.M.[1], Babayeva R.F.[2]
[1]*Baku State University, Institute for Physics Problem, Baku, Azerbaijan*
[2]*Dep. of Engineering and Applied Science, Azerbaijan State University of Economics (UNEC), Baku, Azerbaijan*
afandiyeva@mail.ru

The main parameters, performance and reliability of Schottky barrier diodes depend on the choice of contacting materials, their crystal structure, the uniformity of the metal-semiconductor interface. In this study, on the basis of current–voltage $(I-V)$, capacitance–voltage $(C-V)$ and conductance–voltage $(C/\omega-V)$ characteristics of Re/n-GaAs Schottky barrier diodes (SBDs) measured at room temperature the potential barrier height and profile of surface states have been

investigated. Due to some advantage's properties, such as high electron mobility, high voltage electrical breakdown, radiation resistance, electrical resistivity as well as a high dielectric constant the direct-gap semiconductor GaAs is widely used in important element of integrated circuits. On the other hand, rhenium is also an interesting material due to high melting point, chemical resistance, catalytic activity. Usually, rhenium is recommended for the manufacture of thin-film resistors. In addition, there is practically no experimental information in the literature about Re/n-GaAs SBDs.

For the present investigation the diodes were fabricated by using PLD technique. The zero bias BH Φ_{B0} was calculated on the basis of current-voltage characteristic measured at forward and reverse biased regions (±1,2V) which was analyzed by the well-known equation for SBDs with the using the thermionic emission theory (Φ_B =0.6eV). Moreover, series resistance and the ideality factor were obtained as 3.9 Ω and 1.8, respectively. With the aim of the calculate the basic parameters of Re/n-GaAs SBD the capacitance-voltage ($C-V$) and conductance-voltage ($G/\omega-V$) characteristics have been measured in a bias voltage and wide frequency range of -2V÷+4V and from 10kHz to 3000 kHz, respectively. Using the impedance characteristics of SBDs in the frequency range from 10kHz to 3MHz dependence of surface states values N_{ss} on voltage and frequency were evaluated from the low-high frequency capacitance ($C_{LF}-C_{HF}$) and Hill-Coleman methods. The influence of surface states on the electrical parameters of Re/n-GaAs SBDs has been revealed. With the aim of the study the parameters of Re/GaAs the real series resistance of the diode according to a method presented by Nicollian and Brews has been calculated. The changing of R_s with increasing frequency from 3 Ω to 38 Ω have been revealed. The result of analysys for Re/GaAs Schottky diode clearly shows that the contribution of surface state charges decreased at high frequencies, because Nss cannot follow the *ac* signal at high frequencies.

ADSORPTION OF NANOPARTICLES ON THE SURFACE OF PLANT CELLS AND MIGRATION IN THEIR ORGANS

Mustafazade A.A., Ahmadov İ.S.
Baku State University, Baku, Azerbaijan
mustafazadeaysun1@gmail.com

Nanoparticles can enter plants both from its surface organs (mainly in the form of powdered nanoparticles) and from the soil through their roots. In all cases, nanoparticles must be adsorbed on the surface of plant cells in order to be absorbed by plants. On the surface of plants, the adsorbed nanoparticles must first interact with the cuticle, cell wall and plasma membrane. By the electron microscopy it has been identified that nanoparticles can be collected, distributed, localized in any plant structure. Adsorption of Ag, Au and Fe_2O_3 nanoparticles on the surface of pea roots was studied by TEM analysis and preparation of histological preparations. It was found that nanoparticles accumulate in the form of clusters on the cell surface, on the surface of the root after 4 hours. It was observed that the nanoparticles entered the cells after 24 hours.

The nanoparticles that enter the stem cells then migrate to the stem and leaves of the pea plant. In experiments, the migration and localization of nanoparticles in leaf cells were studied. The migration of nanoparticles to the leaves took longer. After the pea seedlings were kept in the nanoparticle solution for 120 hours, samples were taken from their leaves and preparations were made and TEM images were taken. Au nanoparticles accumulate in the leaves of pea plants, which remain in the solution of nanoparticles for a long time. These nanoparticles move from the stem to the leaves and are localized first in the apoplast space and then in the cell wall. Nanoparticles localized in the apoplast pass through the cell wall and are adsorbed on the surface of the plasma membrane. After a while, the nanoparticles cross the plasma membrane and distribute inside the cell. Experiments show that nanoparticles form an important surface in plant cells. Thus, depending on their size, shape and surface load, nanoparticles are adsorbed on different parts of the cell. It has been found that nanoparticles accumulate more in the areas of cells where intensive protein

synthesis takes place. Studies have shown that nanoparticles are first adsorbed on the cell wall in various plant organs, and then on the surface of the plasma membrane. The nanoparticles adsorbed on the cell surface pass through the plasma membrane and are distributed inside the cell.

EXACT SOLUTION OF THE KLEIN–FOCK–GORDON EQUATION FOR THE MODIFIED ROSEN–MORSE POTENTIAL

Aliyeva T.H. [1], Quliyeva G.H.[2]
[1]*Institute for Physical Problems, Baku State University, Baku, Azerbaijan*
[2]*Sumgait State University, Sumgait, Azerbaijan*
aliyevatarana@rambler.ru

In the present work, an analytical solution for bound states of the Klein-Fock-Gordon equation is found for the modified Rosen-Morse potential. To overcome the difficulties arising in the case $l \neq 0$ in the centrifugal part of the Rosen-Morse for bound states, we applied the developed approximation. Analytical expressions for the energy eigenvalue and the corresponding radial wave functions for an arbitrary value $l \neq 0$ of the orbital quantum number are obtained. It is shown that energy levels and eigenfunctions are very sensitive to the choice of potential parameters and orbital and radial quantum numbers.

The Klein–Fock–Gordon (KFG) equation very effectively describes spinless scalar and pseudoscalar particles, and composite particles such as the $\boldsymbol{\pi}$ -meson, the Higgs boson, etc.

In this study, the KFG equations are analytically solved for the Rosen-Morse potential for an arbitrary value of the orbital quantum number $l \neq 0$ using the Nikiforov-Uvarov method.

The modified Rosen–Morse potential is expressed as

$$V(r) = \frac{V_1}{cosh^2(\alpha r)} - \frac{V_2 sinh(\alpha r)}{cosh^2(\alpha r)} \qquad (1)$$

For a scalar $S(r)$ and a vector $V(r)$ potential, the KFG equation in atomic units ($\hbar = c = 1$) in spherical coordinates takes the form:

$$[-\nabla^2 + (M + S(r))^2]\psi(r,\theta,\varphi) = [E - V(r)]^2\psi(r,\theta,\varphi), \quad (2)$$

where M is the rest mass of the scalar particle and E is the energy of the relativistic particle. In Eq. (2) the wave function ψ in spherical coordinates can be taken in the following form:

$$\psi_{nlm}(r,\theta,\varphi) = \frac{\chi_{nl}(r)}{r} Y_{lm}(\theta,\varphi), \quad (3)$$

where $Y_{lm}(\theta,\varphi)$ are the spherical harmonic functions. Substituting the function assigned by expression (3) into Eq. (2), we can rewrite the radial KFG equation as follows:

$$\chi''(r) + \left[E^2 - M^2 - 2\big(MS(r) + EV(r)\big) + V^2(r) - S^2(r) - \frac{l(l+1)}{r^2}\right]\chi(r) = 0. \quad (4)$$

By applying NU method we have obtained energy eigenvalues and the corresponding eigenfunctions for arbitrary $l \neq 0$ states by solving the radial Klein–Fock–Gordon equation for the modified Rosen–Morse potential. Thus energy spectrum defined in this form:

$$M^2 - E^2 = C_2 l(l+1)\alpha^2 - \frac{\alpha^2}{4}\left[2n + 1 - 2\sqrt{(1-4\beta^2) \pm \sqrt{(1-4\beta^2)^2 + 16\gamma^4}}\right] \quad (5)$$

and the corresponding eigenfunctions defined as the follows:

$$\chi(r) = C_{nl}(1+r)^{\frac{1}{4}-\frac{B}{2}}(1-r)^{\frac{A}{2}-\frac{1}{4}}\frac{\Gamma(n+A+1)}{\Gamma(A+1)} \quad {}_2F_1\left(-n, 1+n - \frac{1}{\sqrt{2}}\sqrt{(1-4\beta) + \sqrt{(1-4\beta)^2 + 16\gamma^2}}, 1 - \frac{1}{2}\sqrt{1-4\beta-4i\gamma}\,;\, \frac{1}{2}(1-s)\right) \quad (6)$$

CIRCULAR (LINEAR) POLARIZATION OF THE γ-QUANTUM IN THE REACTION $\mu^-\mu^+ \to H\gamma$

Abdullayev, S.K., Gojayev, M.Sh., Gulayeva, A.K.
Baku State University, Baku, Azerbaijan
sarhaddinabdullayev@bsu.edu.az

The study of the physical properties of the Higgs boson and the study of the mechanism of spontaneous violation of electroweak symmetry is one of the main tasks of future high-energy e^-e^+ and $\mu^-\mu^+$ colliders. The most important interaction constants of the Higgs boson are associated with the vertices $H\gamma\gamma$ and $HZ\gamma$. To measure these interaction constants, the study of the reaction of the associated production of the Higgs boson with a photon at electron-positron colliders [3]. For the production of Higgs bosons, the muon collider has a special advantage, since the effective cross-section of the process $\mu^-\mu^+ \to H$ in the s-channel is $(m_\mu/m_e)^2 \approx 4000$ several times larger than the $e^-e^+ \to H$ reaction cross-section. On the other hand, due to the large mass of muons, synchrotron radiation is several times suppressed than that of electrons.

We investigate the degrees of circular and linear polarization γ-quantum in the process associated production of Higgs boson with photon at muon-antimuon colliders

$$\mu^- + \mu^+ \to H + \gamma \qquad (1)$$

An analytical expression for the differential effective cross-section of the process is obtained within the Standard Model (SM), taking into account the helicities of the muon-antimuon pairs and the circular (linear) polarization γ-quantum.

The differential effective cross-section of the annihilation process of a longitudinally polarized muon-antimuon pair with the associated production of the Higgs boson with a circularly polarized γ-quantum has the form:

$$\frac{d\sigma}{d(\cos\theta_\gamma)} = \frac{\sqrt{2}G_F\alpha_{KED}m_\mu^2}{4s(1-\upsilon^2\cos^2\theta_\gamma)^2}\left\{(1+\lambda_1\lambda_2)\left[\frac{2x}{1-x}\upsilon^2\sin^2\theta_\gamma + (1-x)(1-\upsilon^2\cos^2\theta_\gamma)\right] -\right.$$

$$-s_\gamma(\lambda_1+\lambda_2)[2\upsilon^2\sin^2\theta_\gamma-(1-x)(1-\upsilon^2\cos^2\theta_\gamma)]\Big\},$$

(2)

where $\upsilon=\sqrt{1-4\frac{m_\mu^2}{s}}$ – is the muon velocity, $x=\frac{M_H^2}{s}$ – is the ratio of the squares of the Higgs boson mass to the square of the total energy of the muon-antimuon pair.

For the degree of circular polarization γ-quantum in the reaction (1), the expression

$$P_\gamma(\sqrt{s},\theta_\gamma)=-\lambda_1\cdot\frac{2\upsilon^2\sin^2\theta_\gamma-(1-x)(1-\upsilon^2\cos^2\theta_\gamma)}{(2x/(1-x))\upsilon^2\sin^2\theta_\gamma+(1-x)(1-\upsilon^2\cos^2\theta_\gamma)},$$

(3)

and for linear polarization is

$$P(\sqrt{s},\theta_\gamma)=\frac{2x\upsilon^2\sin^2\theta_\gamma\cos2\varphi_\gamma}{2x\upsilon^2\sin^2\theta_\gamma+(1-x)^2(1-\upsilon^2\cos^2\theta_\gamma)} \quad (4)$$

obtained.

The dependence of these characteristics, as well as the effective cross-section of the process on the departure angle θ_γ and the energy $\sqrt{s}$ of the muon-antimuon pair is studied in detail.

DIELECTRIC FUNCTION AND CRYSTALLINITY OF POLYCRYSTALLLNE FILMS

Aliyeva Y.N., Bagiev E.A., Alizade E.H., Jalili, J.N., Bayramov A.H., Mamedov N.T.
Institute of Physics, ANAS, Baku, Azerbaijan
yeganaaliyeva85@gmail.com

The optical degree of crystallinity based on the imaginary part of dielectric function and the integrated absorption derived from this part are introduced for the films composed of microscopic crystallites. Bruggeman effective medium approximation (BEMA) is used to determine this fundamental parameter, provided that complex dielectric function for single

crystal as reference and for polycrystalline film under consideration is known in a broad spectral range.

Polycrystalline ZnO thin films grown by magnetron sputtering on glass substrates under different oxygen/argon gas mixture (O/Ar ratio 0-6 %) at substrate temperatures 200, 300 and 400oC are examined by room temperature spectroscopic ellipsometry in the photon energy range from 0.74 to 6.5eV to check how the introduced parameters work.

It is shown that in both cases the introduced entities provide information about the spectral distribution of optical crystallinity and, in an indirect way, about the underlying changes in reference crystal structure. At the same time, the degree of crystallinity based on the overall integrated absorption. looks more promising as an optical counterpart of the degree of crystallinity based on the commonly used material constants.

SPIN DYNAMICS (*S* = 1/2 AND *S* = 1) IN HEXAGONAL NANOWIRE SYSTEMS

Tanriverdiyev V.A., Tagiyev V.S., Mustafayev N.B., Ibrahimov I.N.
Institute of Physics, ANAS, Baku, Azerbaijan
vahid_tanriverdi@yahoo.com

In present paper, the behavior of a magnetic superlattice nanotube consisting of mixed spins (1/2 and 1) has been studied within Glauber-type stochastic dynamics. From the analysis of time variations of average magnetization, the different magnetic phases formed in nanotubes with a hexagonal cross-section have been determined.

Stationary solutions of the set of effective-field dynamic equations have been obtained at various values of the interaction parameters, temperature and external magnetic field. It has been found that the considered system consists of several magnetic phases (paramagnetic, ferromagnetic, and nonmagnetic), and there is also a region of their coexistence which depends on the interaction parameters.

PHOTOLUMİNESCENCE PROPERTIES OF GeS:Nd LAYERED CRYSTALS IN ROOM TEMPERATURE

Asadullayeva S.G. [1], Dashdemirov A.O.[2], Alekperov A.S. [2], Jabarov S.H.[3] , Qafarova G.A.
[1] Institute of Physics of the ANAS, Baku, Azerbaijan
[2] Azerbaijan State Pedagogical University, Baku, Azerbaijan
[3]Azerbaijan State Economic University, Baku, Azerbaijan
sasadullayeva@mail.ru

Among the layered crystals, the germanium sulfide compound belonging to the class VI monochalcogenides, is in the center of attention due to its physical properties [1-2] In our present work, for the first time, we have studied the luminescence properties of a GeS layered single crystal alloyed with the Nd + 3 ion. If we look at the literature, we can see that the work on the luminescence properties of the GeS layered single crystal has been less studied than that of the amorphous GeS compound [3-4] For the synthesis of GeS:Nd monocrystals, germanium monocrystals with a special resistance of 50 Ohm cm, sulfur with a purity of "B5" and "Hm-2" neodimum crystals were used. Taking in this stoichiometric proportions, samples of these elements are poured into a quartz ampoule with an inner diameter of 1.0÷2.2 cm, length of 15÷20 cm, and the air inside the ampoule is evacuated to 10^{-3} mm of Hg.
Luminescence spectra were measured at room temperature and shown in Figure

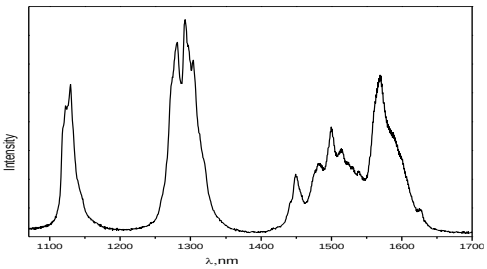

The strong luminescence maxima we observe are due to the internal transitions of the neodymium ion($^4F_{s/2}$ - $^4I_{11/2}$;$^4F_{s/2}$ - $^4I_{13/2}$; $^4F_{s/2}$-$^4I_{15/2}$) .

IMPEDANCE CHARACTERISTICS OF Γ-IRRADIATED $(TlInSe_2)_{1-x}(TlGaTe_2)_x$ SOLID SOLUTIONS

Sardarli R.M., Aliyeva N.A., Mammadov R.A., Rasulova A.A.
Institute of Radiation Problems of ANAS, Baku, Azerbaijan
nuranaalislam@gmail.com

Crystals of the $A^3B^3C^6_2$ family and solid solutions based on them attract the attention of researchers due to the extremely anisotropic crystal structure, instability of the crystal lattice to external influences, these crystals are also promising objects in the production of photoelectric converters, resistance strain gauge, detectors of X-ray and neutron radiation.

This work is devoted to the experimental study of the electrophysical characteristics of single crystals of solid solutions $(TlInSe_2)_{1-x}(TlGaTe_2)_x$, by measuring the total complex conductivity and dielectric relaxation in an alternating electric field.

In the spectral range of 25 ÷ 10^6 Hz, the frequency dependences of the components of the total complex impedance were measured by impedance spectroscopy, and relaxation processes in single crystals of $(TlInSe_2)_{1-x}(TlGaTe_2)_x$ of solid solutions were investigated before and after radiation exposure with a dose of 50 Mrad. It has been found a decrease in the relaxation times in the crystal after exposure to radiation. Using the method of equivalent circuits, the diagrams obtained on the complex plane (Z''–Z') are analyzed. It is shown that after γ-irradiation in single crystals of solid solutions $(TlInSe_2)_{1-x}(TlGaTe_2)_x$ a phase transition occurs with the transition of the system to the superionic state.

The diagrams on the complex plane (Z" –Z'), obtained from measurements after exposure to γ-quanta, are semicircles for one parallel RC – chain and rays in the low-frequency region of the diagrams. These rays in the impedance diagram are most likely related to the diffuse Warburg impedance, which is based on the idea that in the frequency range of the applied sinusoidal signal, the diffusion of carriers does not reach the boundary of the diffuse layer. The transition of the crystal to the superionic state caused by the disordering of the system due to radiation exposure may be responsible for the appearance of the diffuse Warburg impedance.

Earlier in our works, we showed that in crystals of the $A^{III}B^{III}C^{VI}_2$ group, at temperatures above 300K, features associated with the presence of ionic conductivity are manifested. In this case, the Tl^{+1} ions diffusing in the crystal after the transition of the system to the superionic state can be responsible for the presence of the diffuse Warburg impedance in the time-distance curve of the crystal under study, while the factor contributing to the mobility of the Tl^{+1} ions is the defects caused by radiation exposure.

OPTICAL ABSORPTION AND URBACH ENERGY OF $(TLGASE_2)_{1-X}(TLINSE_2)_X$ (X=0÷1,0) SOLİD SOLUTİON

Sardarli R.M., Salmanov F.T., Aliyeva N.A., Mammadov R.A., Rasulova A.A.
Institute of Radiation Problems of ANAS, Baku, Azerbaijan
faminsalmanov1979@gmail.com

$TlInSe_2$ and $TlGaSe_2$ crystal which belongs to the family of $A^{III}B^{III}C_2^{IV}$ compound crystallizes in monoclinic system and $TlInSe_2$ from the same group crystallizes in tetragonal system and lattice periods for $TlInSe_2$ are as a=b= 8,075Å, c=6,847 Å and for $TlGaSe_2$ a=b=10,94 Å, c= 15,18Å, β=100.21, z=16, space group C^6_{2h}-C2/c [1].

The main aim of the research is to study the optical properties of solid solutions of $TlInS_{2(1-x)})Se_{2x}$ system in fundamental absorption range within isomorphic, as well as cation-anion replacement.

Measurement of emission spectrum has been carried out by means of “specord 210 plus” spectrophotometer at 400-1100 nm spectral range and by E⊥C polarization. The measurements have been conducted at room temperature. Measurement accuracy of the spectrometer has been within ±3 nm. According to it, E_g is calculated up to ±0,0004 eV with better accuracy.

Using the reference, the absorption rate can be written as follows

$$\alpha = \frac{1}{d}\ln\left(\frac{(1-R)^2 + \left[(1-R)^4 + 4R^2T^2\right]^{\frac{1}{2}}}{2T}\right)$$

Here *R* is reflection (0,2605 [22]), A-optical density, α-optical absorption rate, and d is the thickness of the sample. The optical absorption rate has been determined by using the value of R at room temperature. Reflection measurements have been carried out in the samples obtained from natural layers by breaking into pieces and thickness of the samples satisfies $\alpha d >> 1$.

Absorption spectrum of solid solutions of $(TlGaSe_2)_{1-x}(TlInSe_2)_x$ (x=0÷1,0) system has been studied at room temperature. According to experimental results, at 300K temperature the absorption rate is 10 cm^{-1} and 110 cm^{-1} in solids of $(TlGaSe_2)_{1-x}(TlInSe_2)_x$ (x=0÷1,0) system and 7 cm^{-1} and 50 cm^{-1} in solids of $(TlGaSe_2)_{1-x}(TlInSe_2)_x$ (x=0÷1,0).

For the studied $(TlGaSe_2)_{1-x}(TlInSe_2)_x$ solid solution samples it has been determined direct and sidewise optical absorption energy transition of band gap. These transitions are obtained from extrapolation of low fragmentary part of direct line to the values of $\alpha^2=0$ and $\alpha^{1/2}=0$ using dependences ($\alpha^{1/2}$-$\hbar\omega$) and (α^2-$\hbar\omega$), respectively.

As it is seen from the dependence of absorption rate on photon energy, the linear absorption varies significantly in mixtures comparing with $TlGaSe_2$ and $TlInSe_2$ in the studied solids.

It has been determined the dependence of direct and sidewise band gap width on concentration from reflection and transmission spectra in 400-1100 nm spectral region at room temperature in solid solutions of $(TlGaSe_2)_{1-x}(TlInSe_2)_x$ system. It has been established that, with increasing concentration in solid solutions of $(TlGaSe_2)_{1-x}(TlInSe_2)_x$ system the band gap width also increases.

THE PROPERTIES OF ELECTROCONDUCTIVITY IN TlSe SINGLE CRYSTAL IRRADIATED WITH γ-QUANTA

Gahramanova S.M., Aliyeva N.A., Mammadov R.A., Dadashova S.D.
Institute of Radiation Problems of ANAS, Baku, Azerbaijan
Samireqehremanli00@mail.ru

TlSe single crystal belongs to the class of A^3B^6 type semiconductor compounds and is obtained in chain (tetragonal) modification [1, 2]. Parameters of tetragonal TlSe structure are a=b=8.02 Å, c=6.79 Å, Z=8 D_{4h}^{18}–14/mcm [3].

Herein, the properties of the conductivity of TlSe semiconductor crystals in the temperature range of 100-300K were studied and the conductivity mechanism was analyzed within the Mott approximation [4,5]. The effect of γ-quanta on these properties has also been studied.

Electroconductivity measurements were carried out by four-probe method, in the directions perpendicular and parallel to the tetragonal "c" axis, in a nitrogen cryostat, in the mode of quasi-stationary continuous heating (cooling) of the crystal at a speed of ≈0.1 K/min. Electroconductivity measurements were performed on a digital immitance E7-25 measuring device.

Temperature dependences of the electroconductivity of TlSe crystals irradiated at the doses of 0, 25 and 75 Mrad were studied in Arrhenius coordinates. An increase in the conductivity was observed in the studied TlSe crystal with increasing radiation dose. The presence of two parts in the change of specific conductivity in $\sigma_{\perp,11}$(T) dependences is typical. The high-temperature (180÷260 K) angle of this dependence is exponential. In this temperature range, the conductivity of heat-excited (activated) carriers in the permitted band is predominant. With a decrease in temperature, a rapid decrease in the concentration of additive carriers is observed, ie the temperature regions below 180 K for the studied solid solutions are the freezing regions of the charge carriers. In [6], the smooth change in the inclination of the curve is characteristic for the hopping conductivity on localized cases in the ($T^{-1/4}$) dependence of lgσ observed during the study of $A^3B^3C^6_2$ group crystals. The high sensitivity of the electrical conductivity value to temperature changes is typical for the materials under study. At the coordinates shown in the TlSe crystal, the experimental

points converge along a straight line. This fact proves that in the studied materials, the transportation of charge in the temperature range of 180÷260K is carried out by the bounce of charge carriers on localized cases located in a narrow energy band near the Fermi level. In this case, the electroconductivity is described by the known Mott relation [4]:

$$\sigma \sim \exp\left[-\left(T_0/T\right)^{1/4}\right], \quad T_0 = \frac{\beta}{kN_F a^3}$$

here, N_F is the density of localized states around the Fermi level, *a* - is the radius of localization of state around the Fermi level, *k* - is the Bolsman constant, *β* - is a number depending on the size of the issue.

For the studied TlSe crystal, the density of localized states around the Fermi level was $N_F = 1.52 \cdot 10^{18}$ $eV^{-1} \cdot cm^{-3}$ for 0 Mrad; the energy difference of the localized states was $\Delta E = 0.101$ eV for 0 Mrad and the length of the bound was $R = 1.15 \cdot 10^{-6}$ cm for 0 Mrad.

IMPURITY-DEFECT LUMINESCENCE IN ZnSe:Fe IN THE NEAR INFRARED RANGE

Abbasov I.I[1],Musayev M.A. [1],Nuriyeva S.G.[2], Huseynov J.I. [3], Gavrishuk E.M. [4], Askerov D.J.[1], Aliyeva L.A. [5], Ragimov R.Sh. [2]
[1]Azerbaijan State Oil and Industry University, Baku, Azerbaijan
[2]Baku State University, Baku, Azerbaijan
[3]Azerbaijan State Pedagogical University, Baku, Azerbaijan
[4]Institute of Chemistry of High-Purity Substances of the RAS, Nizhny Novgorod, Russia.
[5]Institute of Physics of the NAS of Azerbaijan, Baku, Azerbaijan
ibrahimabbasov179@gmail.com

Recently, interest has grown in wide-gap semiconductor structures doped with transition metals as an active medium for mid-IR lasers, since there are many practical applications in this range, such as gas analyzers, medicine, optical communication, etc. In this work, the spectral composition of the luminescence of two ZnSe samples doped with an iron impurity

was investigated using a Varian Cary Eclipse spectrofluorometer in the range of 0.7-1 μm at room temperature. Fe film was deposited to both sides of the CVD (chemical vapor deposition) ZnSe samples by electron beam evaporation, then diffusion doping was performed during HIP (hot isostatic pressure) treatment. Diffusion doping in the first sample was carried out at 1000 atm, 1150^0C for 72 h, and in the second at 1000 atm, 1250^0C for 76 h. The maximum concentration of iron impurities, determined from the absorption edge shift in the ZnSe:Fe samples, is $7.27 \cdot 10^{18}$ cm^{-3} and $9.83 \cdot 10^{18}$ cm^{-3}, respectively.

The excitation of the samples was initially carried out by light with a wavelength λ_{ex}=620 nm, and in the luminescence spectrum the maxima in the first sample were observed at wavelengths of 697 and 824 nm, and in the second sample only at 825 nm and equidistant maxima with LO repetition. The excitation spectrum of peaks at 824 nm in the samples covers the wavelength range of 600-680 nm and is more efficiently excited with light λ=604 nm. The mechanism of radiative recombination, which forms emission lines in the spectral range of 0.7-1 μm, is associated with intracenter radiative transitions of the iron atom, included in the complex defect as Fe^{2+}.

IMPURITY-DEFECT LUMINESCENCE IN ZnSe:Cr IN THE NEAR INFRARED RANGE

Abbasov I.I.[1], Musayev M.A. [1], Nuriyeva S.G.[2], Huseynov J.I. [3], Gavrishuk E.M. [4], Askerov D.J.[1], Aliyeva L.A. [5], Ragimov R.Sh. [2]
[1]Azerbaijan State Oil and Industry University, Baku, Azerbaijan
[2]Baku State University, Baku, Azerbaijan
[3]Azerbaijan State Pedagogical University, Baku, Azerbaijan
[4]Institute of Chemistry of High-Purity Substances of the RAS, Nizhny Novgorod, Russia.
[5]Institute of Physics of the ANAS, Baku, Azerbaijan
ibrahimabbasov179@gmail.com

Recently, interest has increased in the study of the effect of transition metals, including Cr^{2+} and Fe^{2+} ions, on the electronic structure of zinc chalcogenides. Interest in these impurities was related mainly to the fact

that they can be used to reduce the luminescence yield in the visible region of the spectrum and to improve the use of these materials as a working medium for IR lasers with a wide tuning band and the ability to operate at room temperature (at T = 300 K) due to the formation deep energy levels in the forbidden zone. In the given work, the spectral composition of luminescence of two CVD (chemical vapor deposition) ZnSe samples doped with chromium admixture was investigated using a Varian Cary Eclipse spectrofluorimeter in the range of 0,7-1 μm at room temperature. A Cr film was deposited on both sides of the CVD ZnSe samples by electron beam evaporation, followed by diffusion alloying in the process of HIP (hot isostatic pressure) treatment. Diffusion doping in the first sample was carried out at 1000 atm, 1150^0C for 66.5 h, and in the second at 1000 atm, 1150^0C for 26 h. The maximum concentration of chromium impurities, determined from the absorption edge shift in the ZnSe:Cr samples, is $6.1 \cdot 10^{19}$ cm^{-3} and $4.65 \cdot 10^{19} cm^{-3}$, respectively.

The excitation of the samples was initially carried out by light with a wavelength λ_{ex}=620 nm, and in the luminescence spectrum the maxima in both samples were observed at wavelengths 697 nm and 824 nm, and in the second sample its LO or 2LO phonon repetitions (713 nm, 731 nm) were added to the maximum at 697 nm. The excitation spectrum of the maxima at 824 nm in both samples is different: in the first it has a peak at 604 nm, and in the second it covers the wavelength range of 586-675 nm from several maxima. In both samples, it is more efficiently excited by light with λ=604 nm. The mechanism of radiative recombination, which forms emission lines in the spectral range of 0.7-1 μm, is associated with intracenter radiative transitions of the chromium atom, included in the complex defect as Cr^{2+}.

MAGNETIC PROPERTIES OF THE DILUTED MANGANITE SYSTEM $La_{1-C}Sr_CMn_{1-Y}Zn_YO_3$

Eremina R.M.[1], Yatsyk I.V.[1], Shustov V.A.[1], Seidov Z.Y.[2,4], Krug von Nidda H.A. [2], Badelin A.G.[3], Karpasyuk V.K.[3], Najafzade N.J.[4], Ibrahimov I.N.[4], Abdinov J.Sh.[4]

[1] Zavoisky Physical-Technical Institute, Federal Research Center "Kazan Scientic Center of RAS", 420029 Kazan, Russia

[2] Experimental Physics V, Center for Electronic Correlations and Magnetism, University of Augsburg, 86135 Augsburg, Germany

[3]Astrakhan State University, 414056 Astrakhan, Russia

[4] Institute of Physics, ANAS, Baku, Azerbaijan

reremina@yandex.ru

Hole-doped lanthanum manganite compounds $La_{1-c}Sr_cMn_{1-y}Zn_yO_3$ (c+y=0.15; y=0.025, 0.05) have been investigated by means of x-ray diffraction, magnetic susceptibility, magnetization, and ESR measurements. The magnetic measurements show that $La_{0.875}Sr_{0.125}Mn_{0.975}Zn_{0.025}O_3$ and $La_{0.9}Sr_{0.1}Mn_{0.95}Zn_{0.05}O_3$ undergo a ferromagnetic phase transition below T_c=185K and 156K, respectively. To describe the temperature dependence of the ESR parameters above the magnetic ordering transition, it is suggested that in the paramagnetic phase ferromagnetically correlated regions are formed. In the spectrum of magnetic resonance these regions behave as superparamagnetic particles. Using the theory of Raikher and Stepanov for superparamagnetic particles, the analysis of the temperature dependence of the magnetic resonance linewidth was performed. This work was partially supported by the Deutsche Forschungsgemeinschaft (DFG) within the Transregional Collaborative Research Center TRR 80 "From Electronic Correlations to Functionality", project no. 107745057 (Augsburg, Munich, Stuttgart). The work of I.V. Yatsyk, V.A. Shustov, R.M. Eremina was supported by the RFBR grant 18-52-06011. The work of Z.Y. Seidov, M.J. Najafzade, I.N. Ibrahimov and J. Abdinov was supported by the Science Development Foundation under the President of the Republic Azerbaijan Grant EIF-BGM-4-RFTF-1/2017-21/03/1-M-03.

ELECTRICAL AND GALVANOMAGNETIC PROPERTIES OF CHALCOGENIDE SPINEL CONTAINING $Ni_{0.25}Cu_{0.05}Fe_{0.70}Cr_2S_4$

Ahmedov A.I.
İnstitute of Physics of ANAS, Baku, Azerbaijan
susenahmedli@gmail.com

Electrical and galvanomagnetic studies were carried out at low temperatures, which showed that $Ni_{0.25}Cu_{0.05}Fe_{0.70}Cr_2S_4$ is a semiconductor ferromagnet. The ferromagnetic Curie temperature T_C ($T_C \approx 225$ K) was determined. It was found that the anomalous Hall coefficient R_a is three orders of magnitude higher than the normal Hall coefficient R_0, and that both coefficients take on a maximum value around the Curie temperature. Then they drop sharply. As in the case of substances with spontaneous magnetization, in this substance EMF Hall increases sharply linearly in the field of technical magnetization.

The temperature dependence of the electrical conductivity σ of the compound $Ni_{0.25}Cu_{0.05}Fe_{0.70}Cr_2S_4$ indicates a semiconductor type of conductivity. The coefficient of thermal EMF decreases with increasing temperature, and its slow growth begins in the region of magnetic transformation. In this case, the thermal EMF α around T ~ 130K changes sign from positive to negative. The effect of a magnetic phase transition on charge transfer in the ferromagnet $Ni_{0.25}Cu_{0.05}Fe_{0.70}Cr_2S_4$ has been found.

PROTECTIVE EFFECT OF HYDROGEN PEROXIDE IN THE HEMOLYSIS OF ERYTHROCYTES MEDIATED BY SILVER NANOPARTICLES

Voinarovski V.V., Vcherashniaya A.V., Martinovich G.G.
Belarusian State University, Republic of Belarus
voynarovskiy@bsu.by

The formation of reactive oxygen species (ROS) is an important phenomenon in cellular respiration, since it results in a wide range of physiological and pathophysiological consequences. A moderate increase in the concentration of oxidants activates defense mechanisms, due to which the balance of the formation and utilization of ROS is maintained, and an imbalance leads to cell damage and the development of diseases.

Metal nanoparticles capable of catalyzing redox processes change the balance of ROS formation and utilization in cells and, thus, can regulate biological processes. In the presented work, the mechanisms of action of exogenous hydrogen peroxide on the structural stability of erythrocytes during hemolysis induced by silver nanoparticles have been investigated.

The transmission of the redox signal to intracellular targets, taking into account the catalytic properties of nanoparticles, is a complex chain of interrelated events, the theoretical description of which is possible using multifactorial models. As a result of the research, a mathematical model was developed that links the characteristics of nanoparticles, transport and metabolism of hydrogen peroxide, the state of the antioxidant system of erythrocytes, metabolic activity of cells, the redox state of hemoglobin and the structural stability of membranes. As a result of numerical modeling, it was found that the change in the balance of oxidized forms of hemoglobin induced by hydrogen peroxide at a concentration of 10 - 500 μM can lead to an increase in the structural stability of the erythrocyte membrane. The results were confirmed in experiments on erythrocyte hemolysis induced by silver nanoparticles.

Erythrocytes were isolated and washed by centrifugation at 1500 rpm in phosphate buffered saline. The kinetics of erythrocyte hemolysis was measured using a Solar CM-2203 spectrofluorimeter (SOLAR, Belarus) by recording the optical density of the cell suspension ($3 \cdot 10^7$ cells / ml) at

a wavelength of 640 nm. Hemolysis was initiated by adding silver nitrate at a concentration of 50 μM and / or silver nanoparticles obtained from silver nitrate by the "green synthesis" method at a concentration of 250 μM. It was shown that silver nanoparticles exhibited lower toxicity in comparison with silver nitrate solution. It was found that at a hydrogen peroxide concentration of 10 - 500 μM, a decrease in hemolyzed cells is observed upon destruction by silver nanoparticles and silver nitrate; at higher concentrations of hydrogen peroxide, an inverse relationship is observed.

Thus, as a result of theoretical and experimental studies, it was shown that hydrogen peroxide at a concentration of 10 - 500 μM is able to activate the adaptive mechanism of erythrocytes, due to an increase in the number of membrane-bound methemoglobin, which increases the structural stability of the membrane and reduces the number of cells destroyed by silver nanoparticles.

SIMPLE SYNTHESIS METHOD OF TIN DIOXIDE NANOPARTICLES FOR GAS SENSING APPLICATION

Ahmadova D.A, Musayeva N.N.
Institute of Physics, ANAS, Baku, Azerbaijan
sedefahmadova@gmail.com

Metal oxides (mainly tin oxide) have been studied for many years and are used in the electronics industry (gas, temperature, humidity sensors, batteries, transistors). This is due to their electronic structure, chemical and mechanical stability, and their sensitivity to the environment. Tin dioxide (SnO_2) based sensors, which can detect a variety of gases, are used in domestic and industrial applications since many years. For this reason, improving their sensory properties remains a priority.

Such sensors represent a simple principle of operation based on changes in electrical properties as a result of oxidation processes on the surface of the gaseous medium to be detected. The most important characteristics of sensors are sensitivity, selectivity, response, and fast recov-

ery time. Since the sensitivity of the sensor is related to the processes occurring on the surface of the material on which it is formed, it is assumed that the sensitive element's surface area increasing will lead to an increase of the sensor's sensitivity. The optimal way to increase the surface area is to reduce the size of the oxide particles.

For this purpose, in this work, nanosized particles of SnO_2 are synthesized by a simple Sol- gel method. After mixing $SnCl_2 \cdot 2H_2O$ and isopropyl alcohol (C_3H_8O) at 100°C for 40 minutes, the resulting solution was stored at room temperature for 24 hours. The solution, which completely turned into a gel during this period, it was then thermal treated at 400°C for 2 hours. The powder was analyzed by X-ray diffraction, scanning electron microscopy (SEM), IR and Raman spectroscopy methods. The size of the obtained tetrogonal nanocrystalline nanoparticles is 13 nm, which is determined by the Scherrer equation, and the results were confirmed by SEM observation images. The nanocrystals were studied by Raman scattering and IR spectroscopy. Taking into account the influence of the synthesis method on the optical transitions of this a broadband n-type semiconductor, were analyzed the optical properties of the obtained SnO_2 nanocrystals.

FORMATION OF SUPERSTRUCTURE-BASED SOLID SOLUTIONS IN $TlIn_{1-x}Sn_xSe_2$ FILMS

Panakhov M.M.[1], Alekperov E.Sh.[1], Gahramanov N.F.[1], Garayev E.S.[1], Nazarov A.M.[2], Farzaliyev S.S.[2], Sadraddinov S.A.[1]
[1]Baku State University, Baku, Azerbaijan
[2] Institute of Physics, ANAS, Baku, Azerbaijan
alekperoveldar@mail.ru

Nowadays certain semiconductors entering into $A^{III}B^{III}C_2^{VI}$ system compound group are recognized to be the most perspective material in the field of optoelectronics. Occurrence of superstructural phases and number of different modifications in these semiconductors entering to the $A^{III}B^{III}C_2^{VI}$ system leads to the new physical properties. The$TlInSe_2$ sem-

iconductor compounds have a chainlike and to some extend to an anisotropic crystalline structure of tetragonal system with lattice parameters of a=0,8075nm, c=0,6847nm.

In this paper the results of investigation of the effect of impurity with different content of tin on the $TlInSe_2$ compound are presented. Impurity implantation is carried out onVUP-5 installation by simultaneous thermal deposition of Sn and $TlInSe_2$ on the KCl and NaCl substrates in a vacuum under 10^{-5} Pa pressure being in the interval from room temperature to 403 K and preliminarily covered with carbon film. According to thermographic studies of $TlIn_{1-x}Sn_xSe_2$ films the continuous series of substitutional solid solutions are formed upon solution of Sn impurity in $TlInSe_2$. The obtained films of 40 nm thickness were investigated by the method of diffraction of high energy electrons on EMR-102.

The change in the structure and concentrations of defects of crystalline lattice being elementary exciters of atomic subsystem is observed by interpretation of the obtained diffraction patterns of electrons. Depending on the impurity concentration (x) the superstructural phase of $TlIn_{1-x}Sn_xSe_2$ composition (x= 0.02 ÷ 0.09) has four and five-fold increased lattice periods (a, c) relatively to the initial phase of $TlInSe_2$ compound with the space group of symmetry (SGS) D_{4h}^{18}–I4/mcm: $a_{ss}= 5a_0= 4.1453$ nm; $c_{ss}= 4c_0= 2.9658$ нм. According to the law of reflection extinction of diffraction patterns the observed new structure of $TlIn_{1-x}Sn_xSe_2$can be related to SGS $P4_2 – C_4^3$ or $P4_2/m – C_{4h}^2$.

Thus, the epitaxial relationships between NaCl substrate and superstructural phases of $TlIn_{1-x}Sn_xSe_2$ films were established. It is determined that a single elementary cell of $TlIn_{1-x}Sn_xSe_2$ superstructural phase conjugates with seven cells of NaCl substrate. Wherein the relative inconsistency of parameters of conjugating lattices is 4.8 %. It is revealed that the temperature of formation of single crystal solid solution on the basis of superstructural phase of $TlIn_{1-x}Sn_xSe_2$ film corresponds to T=557 K. Depending on the impurity concentration the temperature of formation of perfect films of solid solution decreases from 2.8 % down to 5.3 %. Between monocrystalline film of superstructural phase$TlIn_{1-x}Sn_xSe_2$ and NaCl following epitaxial relationships observed: (001) [100] $TlIn_{1-x}Sn_xSe_2$// (100) [110] NaCl. Elementary cell periods of solid solutions on the base of superstructural phase approximately linearly depend on the concentration

x=0.02 ÷ 0.09 except x=0.04 ÷ 0.06. Thus, an impurity Sn promotes formation of solid solutions on the base of $TlIn_{1-x}Sn_xSe_2$ superlattice as well as has allowed a strictly manipulation with the parameters of thin epitaxial films of superstructural phases.

KINETICS OF CRYSTALLIZATION OF AMORPHOUS $TlIn_{1-x}Sn_xSe_2$ FILMS OBTAINED IN AN ELECTRIC FIELD

Alekperov E.Sh.
Baku State University, Baku, Azerbaijan
alekperoveldar@mail.ru

In present paper a phase transition in amorphous films $TlIn_{1-x}Sn_xSe_2$ (x=0.02÷0.09) of ~30 nm thickness at their thermal treatment and located on substrates of fresh cleaved KCl, NaCl and KJ at a temperature of 353K is considered. The investigated film, obtained by the thermal method in a vacuum of $4x10^{-5}$ Pa, under the influence of an external E = 3000 V · cm^{-1} electric field appeared in the peculiar carbon capsule, was completely insured against oxidation and re-evaporation during transfer to the column of electronograph and further thermal processing. The phase transition upon kinetics of crystallization of amorphous $TlIn_{0.93}Sn_{0.07}Se_2$ films was studied on an EMR-102 electron diffraction device with electric recording of the intensities of diffraction lines.

At first three diffuse lines $S=4\pi\sin\theta/\lambda$ = 21.23; 34.91; 51.83 $нм^{-1}$ are observed on the kinematic electronogramm indicating the phase transition process in the film at 439K. In the kinematic electron diffraction patterns in which the regions of both amorphous and crystalline phases are traced, also are seen the changes in intensities and line widths of the growing crystalline phase obtained at various time instants and temperatures of 413K, 439K, and 470K respectively. Instantaneous crystallization of the amorphous $TlIn_{0.93}Sn_{0.07}Se_2$ films was observed at threshold temperature of 485K. Intensities of diffraction lines (200), (211), (321), (400), (420), (422), (442) were determined as a function of annealing time upon the analysis of micro-photogram using the blackening curve. Isotherms of

crystallization were plotted on the basis of temperature-temporary dependences of crystallization by taking into account the change in intensities of the diffraction lines of the growing crystalline phase. It was determined the growth parameter corresponding to m=3 for the new formed constitutes. The activation energies for amorphous $TlIn_{0.93}Sn_{0.07}Se_2$ films obtained in an electric field and without external effects (E = 0) were determined on the basis of the plotted curves and are presented in the table.

Compounds	Electric field strength E ($V \cdot cm^{-1}$)	Activation energy		
		E_{tot} (kcal / mol)	E_p (kcal / mol)	E_z (kcal / mol)
$TlInSe_2$	0	47.35	16.32	14.71
$TlIn_{0.93}Sn_{0.07}Se_2$	0	49.85	16.03	17.79
$TlIn_{0.93}Sn_{0.07}Se_2$	3000	44.92	14.43	16.06

The observed effect of an electric field leads to an increase in the rateof crystallization process, a decrease in the temperature of phase transformations as well as values of activation energies.

DIELECTRIC HYSTERESIS IN SUBMICRON BARIUM TITANATE PARTICLES

Imamaliyev A.[1], Ganizade G.[1], Humbatov S.[2]
[1]Instiute of Physics, Azerbaijan National Academy of Science
[2]Baku State University
rahimoglu@mail.ru

In this work, the dielectric properties of monodisperse submicron (200 nm) barium titanate ($BaTiO_3$) particles are investigated. To prevent strong aggregation of polarized $BaTiO_3$ particles, the surfaces of these particles were coated with oleic acid. Analysis of the capacitance-voltage (CV) characteristics of barium titanate thin film in the voltage range from -20 V to +20 V allows us to reveal some patterns. As in a bulk crystalline sample of $BaTiO_3$ the dependence of the dielectric constant on the electric field shows a hysteresis behavior. The coercive field is one order of magnitude

higher (10 kV/cm) compared to bulk samples (1.5 kV/cm). Saturation of the dielectric constant is achieved at the electric field of 15 kV/cm. From the saturation value of the dielectric constant, the spontaneous polarization of 200 nm barium titanate particles was estimated: Ps=0.003 C/m^2). This is two orders of magnitude less than bulk samples of $BaTiO_3$ (0.26 C/m^2). An explanation of the results is presented on the basis of the well-known core-shell model.

ACTIVATION PARAMETERS OF BASIC FLOW IN WATER-ETANOL-UREA SYSTEMS

Masimov E.A., Pashayev B.G., Hajiyeva S.N., Aliyev L.P.
Department of physics, Baku State University, Baku, Azerbaijan
p.g.bakhtiyar@gmail.com

Recent studies have shown that inversion of the concentration-dependent isotherms of some physicochemical parameters found in practice for aqueous solutions of a number of substances is observed. For example, in the curves of adiabatic compression in water-ethanol solution and concentration molar volume of ethanol in solution, the molar fraction of ethanol is observed minimum at the $x_{inv}^{\beta_s} = 0.06$ and $x_{inv}^{\overline{v}} = 0.07$values, respectively and the first maximum of molecular light scattering intensity is observed at $x_{max}^{R} = 0.09$. Researchers claim that a quasi-crystalline or clathrate-like (ice-like structure of 100-150 water molecules) structure is formed at the concentration at which the inversion is observed. Thus, initially, the structure of water increases with increasing concentration of ethyl alcohol and becomes maximally structured at a value corresponding to the inversion point of the concentration. Unlike ethyl alcohol, urea destroys the structure of water at all concentrations, i.e. the effect of urea on the structure of water is the same as the effect of temperature. Since the water-ethanol-urea system is always present in living organisms, especially in humans, the study of this system is of great interest. In the presented work, the dynamic viscosity and density of water-ethanol, water-

urea, water-ethanol-urea systems at different temperatures and concentrations were measured. Using the results from practice, consideration of temperature and concentrations of viscous flow activation parameters ($\Delta G_\eta^{\neq}$, $\Delta S_\eta^{\neq}$, $\Delta H_\eta^{\neq}$), and the parameters calculated based on the change in the structural features of the solution was analyzed. It has been found that for water-ethanol systems, as the concentration of ethanol increases, $\Delta G_\eta^{\neq}$ is increasing, $\Delta H_\eta^{\neq}$ and $\Delta S_\eta^{\neq}$ parameters first increase and then decrease, and this dependence is manifested at all temperatures studied. Also, as the temperature increases, the maximum, i.e. the inversion point, does not shift, and the ascending-descending character of $\Delta H_\eta^{\neq}$ and $\Delta S_\eta^{\neq}$decreases. At all temperatures considered for water-urea systems, $\Delta G_\eta^{\neq}$ increases with increasing urea concentration, while $\Delta H_\eta^{\neq}$ and $\Delta S_\eta^{\neq}$ parameters decrease. Since the viscosity of the viscous flow activation characterizes the structural changes in the solution, based on the $\Delta S_\eta^{\neq} = f(x)$dependence, we can say that ethanol has a structural effect on water up to the molar part $x \approx 0.15$, after this concentration has a structural destructive effect, and urea has only a destructive effect on the water structure. As a result of our research, it was found that in water-ethanol-urea systems (x_{et} = 0.05), as in water-urea systems, $\Delta G_\eta^{\neq}$ increases with increasing concentration of urea in solution, and $\Delta H_\eta^{\neq}$ and $\Delta S_\eta^{\neq}$ parameters decrease. In these cases, the maximum does not shift with increasing temperature, and the inversion in the $\Delta S_\eta^{\neq} = f(x)$ corresponds to the molar fraction $x \approx 0.15$. Based on the results obtained, we can say that the effect of urea on the structure of water-ethanol systems, and the effect of ethanol on the structure of water-urea systems is analogous to the effect on the stricture of pure water.

DETERMINATION OF HYDRATION NUMBER OF POLYMERS

Pashayev B.G. [1], Rajabov M.R.[1], Orujova N.F. [2]
[1]Baku State University, Department of Physics
[2]Azerbaijan Technology University, Department of General and Applied Physics
p.g.bakhtiyar@gmail.com; nilufarorujova@gmail.com

The structural characteristics of aqueous solutions of polymers are mainly described by the conformation, size, hydration, etc. of the polymer macromolecule. Since all biological processes take place in water, the study of hydration of macromolecules of biologically important polymers is an interesting and important issue. The concepts of hydration are used to describe the interactions between a solvent and a solution. According to some authors, the process of hydration allows to clarify the general physical view of the effect of various substances on the structure of water. In the process of hydration, some polymer macromolecules keep the water molecules around them relatively strong, while others are relatively weak. The process of hydration in polymer solutions generally characterizes the energy and structural changes that occur.

Polyethylene glycol of different fractions (1000, 1500, 3000, 4000 and 6000) was used as a polymer. Hydration number of polyethylene glycol was determined on the basis of experimental values of the density of aqueous solutions of polyethylene glycols in the temperature range 293.15-323.15 K and the concentration of 0-0.001 molar fraction. To determine the hydration number

$$N_h = \left(\frac{1-x}{x} + \frac{M_2}{M_1}\right)\left(1 - \frac{\rho_1}{\rho}\right)$$

expression was used. Here x is the molar fraction of the polymer in solution, M_1 is the molar mass of water, M_2 is the molar mass of the polymer, ρ1 is the density of water, and ρ is the density of the solution. Calculations show that the hydration number of polyethylene glycol is almost independent of the concentration. We assume that this result is acceptable in the form of liquid solutions. Therefore, we can assume that hydration

number in liquid solutions does not depend on the concentration. It was found that the hydration number of polyethylene glycol increases with increasing molecular weight and decreases with increasing temperature. The change in the hydration number depending on the molecular weight and temperature can be explained as follows. As the molecular weight increases, the volume of the polyethylene glycol macromolecule increases and the voids inside the molecular mass increase and the number of oxygen atoms in the polyethylene glycol monomer, which form hydrogen bonds with water molecules, also increases, resulting in an increase in the number of hydrations. As the average kinetic energy of the thermal motion of the molecules increases with increasing temperature, the hydrogen bond is unable to hold the water molecules in a hydrated macromolecular wash, resulting in a decrease in the hydration number and an increase in the number of free water molecules. It should be noted that during the hydration process, water molecules not only combine with polymer macromolecules, but also compete for water molecules to form hydrogen bonds with polymer macromolecules. This process is characterized by the maximum hydration energy of the polymer macromolecules, which makes the resulting conformation more likely than other conformations that may occur.

PROPERTIES OF THE PP+METAL OXIDE NANOCOMPOSITE BEFORE AND AFTER INFLUENCE ELECTROTHERMAL POLARIZATION

Ibrahimova H.S.[1], Shirinova H.A.[2], Hadiyeva A.A.[1], Yahyayev F.F.[1]
[1]Institute of Physics of the National Academy of Sciences of Azerbaijan, Baku, Azerbaijan
[2]Baku State University, Baku, Azerbaijan
Hicran90@rambler.ru

The development of modern technology requires the advancement and study of the properties of new composite materials. One of the most interesting and promising materials is polymer-based materials. Since the issue of the interaction between fillers and matrices is quite multifaceted,

the development of the production technology of polymer-based composite materials is one of the actual brunches of materials science.

It is known that various morphological forms of supramolecular structure are taking place in polymer composites depending on the kinetics of the crystallization process, determined by external conditions. In this work the thermophysical properties of PP+ ZrO2 nanocomposites before and after electro-thermal polarization were investigated. Polymer nanocomposites were produced by introducing ZrO_2 nanoparticles into the polymer solution. The size of the nanoparticles was about 20-30 nm. The hot-pressing method was used for the production of the nanocomposite samples at melting temperature of the polymer and under the 15 MPa pressure for 3min. The thickness of films was about 70-100mkm. Three modes of crystallization were chosen for the regulation supramolecular structure of the polymer nanocomposites. In fast cooling mode, polymer melt was cooled by the speed of 20-35deg/sec. During nitrogen quenching, the melted nanocomposite was immersed into the liquid nitrogen and cooled at a rate of about 150-250deg/sec. During slow cooling mode, the melted nanocomposite cools under the pressure until room temperature. In this case, the cooling rate is 0.03 deg/sec.

The samples were exposed to electro-thermal polarization at different values of the electric field strength. For polarization, the films are heated up to the polarization temperature, and during 1 hour stay at this temperature under the electric field. Then polarized samples are cooled to room temperature without removing the field.

DSC data were obtained on a NETZSCH DSK 204 F1 Phoenix heat flux calorimeter. It was found that after exposure to the ETP in the thermogram of all the nanocomposites a new endo max is observed in the temperature range of 100-130º. It became clear that more thermostable samples are the nanocomposites obtained by slow cooling mode. The thermal stability of the samples was obtained through slow cooling mode explained by the local destruction of inter-spherulite areas after ETP. It can be assumed that with slow cooling of the samples, the contact between adjacent lamellas is weakened. The samples obtained by slow cooling mode have a higher degree of strength than the samples obtained through other modes of crystallization. Therefore, higher energy is required for their thermal destruction. Samples with a small-spherulite structure have higher stability. Nanocomposites obtained by nitrogen

quenching are in a nonequilibrium state and rapidly crystallize upon heating. These samples contain a small number of regions with an ordered structure and possibly defective crystallites.

DIELECTRIC PROPERTIES OF $MnGaInTe_4$ CRYSTALS IN AN ALTERNATING ELECTRIC FIELD

Niftiyev N.N.[1], Mammadov F.M.[2], Muradov M.B.[3]
[1]Azerbaijan State Pedagogical University, Baku, Azerbaijan
[2]Institute of Catalysis and Inorganic Chemistry named after M. Nagiyev, ANAS, Baku, Azerbaijan
[3]Baku State University, Baku, Azerbaijan
namiq7@bk.ru

In this work, we present the results of investigations of the frequency and temperature dependences of the real and imaginary parts of the constants in $MnGaInTe_4$ crystals at alternating current. $MnGaInTe_4$ crystallizes in a trigonal lattice (space group I-42m, a = 6.10293 Å, c = 12.1766 Å). Capacitance measurements were carried out using E7-20 digital immittance meters (frequencies $25 \div 10^6$ Hz). In fig. 1 shows the dependences of the real part of dielectric constants (ε') on frequency for $MnGaInTe_4$ crystals at different temperatures (T, K: 1- 295.6, 2-313, 3-333, 4-353, 5-363). It can be seen that an increase in ε' is observed with increasing temperature. An increase in ε' is associated with an increase in the concentration of defects with increasing temperature. It was found that in the temperature range of $295.6 \div 363$K at frequencies of $10^2 \div 10^6$ Hz, the value of ε'varies in the range of $140 \div 770$. It is seen that the frequency dependence of ε' underwent significant dispersion.

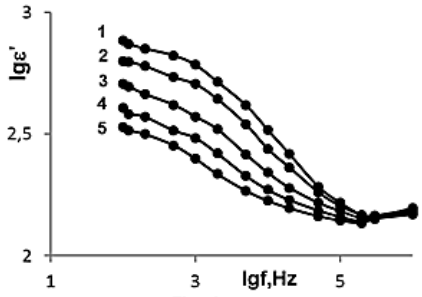

Fig. 1.

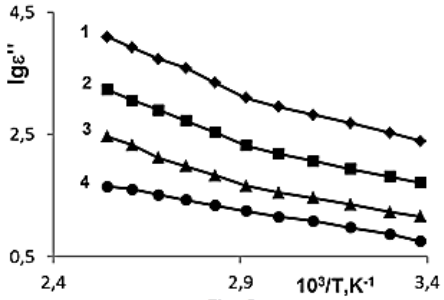

Fig. 2.

In fig. 2 shows the temperature dependences of the imaginary part of the dielectric constant (ε'') of $MnGaInTe_4$ crystals at alternating current at different values of the frequency (*f*, Hz: 1- 10^3, 2-10^4, 3-10^5, 4-10^6). At a high frequency (given 4), one linear section is revealed on the dependence lgε'' from от $\frac{10^3}{T}$. The activation energy was determined from the slopes of this dependence, the value of which was 0.22 eV. In the frequency range $10^3 \div 10^5$ Hz (data 1 - 3), the dependence $\lg\varepsilon'' \sim \frac{10^3}{T}$ consists of two straight lines with different slopes. The slopes of these dependences were used to determine the activation energies, the values of which in the low-temperature region vary in the range of 0.30–0.22 eV, and in the high-temperature region, this is the range of 0.54–0.43 eV. It follows from this that the magnitude of the activation energy is a function of frequency. The frequency dependence of the activation energy can be explained using the hopping mechanism [1]. It is also known that the temperature dependence of the electrical conductivity in $MnGaInTe_4$ crystals has an activation character. This means that in the $MnGaInTe_4$ compound, conductivity is characterized by zone-hopping mechanisms.

MOLECULAR MECHANICS SIMULATION OF CONFORMATIONAL BEHAVIOR OF ANTICANCER AAP-H PEPTIDE

Agaeva G.A. Agaeva U.T., Godjaev N.M.
Institute for Physical Problems, Baku State University, Azerbaijan
gulshen@mail.ru

It is known that some marine organisms possess antithrombotic, antitumor, and antibacterial activities. The bioactive substances of these marine organisms have played important roles in the development of innovative medicines. Prostate cancer (PCa) is one of the most common malignancies of the male urinary system and is also the leading cause of cancer-related death in men]. The anticancer peptide AAP-H is a pentapeptide from the sea anemone *Anthopleura anjunae* with an amino acid sequence Tyr-Val-Pro-Gly-Pro. The results of numerous studies indicated that AAP-H peptide was nontoxic and exhibited antitumor activities in prostate cancer DU-145 cells in vitro and in vivo. For determination a mechanism of action of this pentapeptide and to investigate its structure-function relations is required the knowledge of the conformational specificity and flexibility of backbone and side chains of molecule allowing a rational design of functional groups acting selectively at their receptor level. The conformational behavior of AAP-H peptide and conformational dynamics of its side chains at the present article have been investigated by molecular mechanics method, which allow to determine a whole set of energetically preferred conformers of peptide molecule. The sequential method was used, combining all low-energy conformations of constitutive residues. The conformational potential energy of a molecule is given as the sum of the independent contributions of dispersion, electrostatic, torsional interactions and hydrogen bonds energies. The detailed analysis of the conformational flexibility of AAP-H peptide was founded the limited quantity of stable conformers. The obtained results have shown that the stable conformers of pentapeptide have tendency adopt a beta-turn structure. The obtained results and discussion lead to the following conclusions: (I). molecular mechanics simulation in polar condition confirm

the small flexibility of the sequence of AAP-H peptide; (II). the β-turn conformation on C-terminal tetrapeptide segment of peptide was more stabilized by dispersion interactions between residues. The conformational analysis helped reveal a number of special features of spatial arrangement of these drug-based pentapeptide. The determined stable structures of AAP-H peptide may be used as the basis for the design of further selective agonists.

PHOTOLUMINESCENCE OF Nd^{3+} DOPED $CdGa_2Se_4$ AND $ZnGa_2Se_4$

Mamedova I., Nabiyeva A., Kerimova T., Abdullayev N.
Institute of Physics, ANAS, Baku, Azerbaijan
**irada_mamedova@yahoo.com*

The study of the radiative characteristics of wide-gap semiconductors makes it possible to create various optoelectronic devices on their basis. The introduction of rare-earth activators makes it possible to obtain efficient luminescence with a sufficiently high quantum yield. Compounds $A^2B_2^3C_4^6$ are characterized by bright luminescence, high photosensitivity, significant values of the band gap ~ 2.4 - 4 eV, which is of interest for use as a matrix for doping with rare earth elements. It should be noted that there is a small number of works in which the results of a study of the luminescence characteristics of $A^2B_2^3C_4^6$ compounds using REEs as activators are presented. In this work, as a matrix for doping with Nd^{3+} ions, we used $CdGa_2Se_4$, and $ZnGa_2Se_4$ compounds that are representatives of ternary semiconductors of the $A^2B_2^3C_4^6$ group.

Samples for measurements were synthesized from the starting components Zn, Cd, Ga, and Se taken in a stoichiometric ratio in graphitized quartz ampoules. An impurity of the rare earth element Nd was introduced during the synthesis. X-ray diffractometric studies were carried out on a Bruker D8 Advance instrument. Lattice parameters a = b = 5.571 Å, c = 10.759 Å, c / a = 1.931. CdGa2Se4 and ZnGa2Se4 crystallize in a tetragonal structure (space group S_4^2). The photoluminescence spectra were measured on a Nanofinder 30 confocal laser microspectrometer (Tokyo

Instr., Japan). A femtosecond tunable Ti-doped sapphire laser (Spectra Physics, USA) with a second harmonic wavelength of 400 nm and a maximum power of 10 mW and a Nd: YAG laser with an output radiation wavelength λ = 532 nm were used as a source of exciting light.

In the photoluminescence spectra of $ZnGa_2Se_4$: Nd^{3+} and $CdGa_2Se_4$: Nd^{3+}, narrow lines were found in the spectral range 880-928 nm. Comparison with the literature [1, 2] and tabular data on the frequencies of electronic transitions in the neodymium atom suggests that these bands with split lines are related to the intracenter luminescence of the Nd^{3+} ion. These lines are laser in nature due to radiative transitions between the $^4F_{3/2} \rightarrow {}^4I_{9/2}$ levels. The half-widths of all lines observed in the PL spectrum of ZnGa2Se4: Nd^{3+} and CdGa2Se4: Nd^{3+} are in within of 1–2 nm.

The work was done with the financial support of the Foundation for the Development of Science under the President of the Republic of Azerbaijan (Grant No. EIF-BGM-3-BRFTF-2 + / 2017-15 / 02/1).

THE ROLE OF OSMOTIC PRESSURE IN BIOLOGICAL SYSTEMS

Aliyeva K.N.
Baku State University, Baku, Azerbaijan
konul.aliyeva27@mail.ru

Osmosis occurs due to the fact that water molecules have the advantage of passing through the membrane. Osmotic phenomema are well understood in terms of equilibrium thermodynamics as well as in a statistical-mechanical context; however, neither of these approaches provides a strictly continuum-mechanical understanding of the dynamic mechanism underlying osmotic phenomena. Thus, Dainty wrote that "few phenomena are so well understood thermodynamically or so ill understood kinematically as the osmotic flow of solvent through a semipermeable membrane.

Whenever a solute movement is blocked by the membrane it will transfer momentum to it and, therefore, generate pressure on it. Since the velocity is the same as that of a free molecule, the pressure will be the same as the pressure of an ideal gas of the same molecular concentration.

Hence, the osmotic pressure π, is given by van't Hoff formula, which is identical to the pressure formula of an ideal gas:

$$\pi = cRT \quad (1)$$

The chemical and physical nature of the membrane determines its ability to allow for preferential transport of solvent (water) over solute (salt ions).The rate of water passage through a semipermeable membrane is defined in Equation 2:

$$Q_w = (\Delta P - \Delta P_{osm}) * K_w * S/d \quad (2)$$

where Q_w is the rate of water flow through the membrane, ΔP is the hydraulic pressure differential across the membrane, ΔP_{osm} is the osmotic pressure differential across the membrane, K_w is the membrane permeability coefficient for water, S is the membrane area, and d is the membrane thickness. This equation is often simplified to:

$$Q_w = A*(NDP) \quad (3)$$

where A represents a unique constant for each membrane material type, and NDP is the net driving pressure or net driving force for the mass transfer of water across the membrane. Osmosis is a reversible thermodynamic process. That is, the direction of water flow through the membrane can be reversed at any moment by proper control of the external pressure on the solution. Contrary to that, mixing a teaspoon full of sugar in a cup of tea is an irreversible thermodynamic process of sugar diffusion within water. There is no way to reverse the process at any given moment and unmix the sugar back to the spoon. Reversibility is a fundamental idea of thermodynamics. Osmosis is a reversible process, while sugar diffusion in water is not.

Diffusion is an irreversible process. In order to produce drinking water from seawater, by reverse osmosis, the pressure p of the salty water should be increased above the osmotic pressure, so that clean water will cross the semi-permeable membrane and accumulate at its other side.

CHARACTERIZATION OF SN DOPED ZNS THIN FILMS SYNTHESIZED BY CBD

Jafarov M.A., Kazımzadə A.H., Nasirov E.F., Jahangirova S.A.
Baku State University, Azerbaijan
maarif.jafarov@mail.ru

ZnS and *Sn* doped ZnS thin film was deposited on well treated microscope glass slide substrates as substrate treatment plays an important role in deposition of thin film by CBD process. The substrate cleaning steps involved overnight keeping in chromic acid followed by rinsing in distil water and ultrasonic cleaning in equivolume acetone and alcohol for about 20 minutes. The glass substrates were lightly rubbed before immersion for better adherence and dipped vertically in the bath solution. 80 ml 0.2 M zinc acetate [$Zn(CH_3COO)_2.2H_2O$] and 160 ml 0.2 M thiourea [$(NH_2)_2CS$] was added and stirred properly at room temperature. Then 0.66 M tri-sodium citrate as complexing agent was mixed properly in the solution. After that, ammonia solution was added to make the pH 11 of the bath. The substrates were immersed in the bath solution for 24 hours and a white colored film with a faint shadow of blue appears over the surface of the substrate. To obtained *Sn* doped *ZnS* thin film, 0.1 M tin chloride ($SnCl_2$, $2H_2O$) was added in proper ratio with the solution. In this process ZnS, 2.5% ZnS: Sn and 5% ZnS Sn*:* thin films were prepared. Film thickness measured using gravimetric weight difference method was approximately ~1300 nm for ZnS and ~1400 nm for 5% ZnS: Sn*.*

The phase identification and crystalline properties of undoped and doped samples were studied by X-ray diffraction (XRD) method employing a Bruker x-ray diffractometer with Ni-filtered CuK_α *radiation*. The Transmission electron microscopy investigation was carried out using Tecnai F30 microscope operating at 200 kV accelerating voltage. The optical absorption measurements were carried out using a Schimatzu dual beam UV-Vis spectrophotometer. The spectrum was recorded by using a similar glass slide as reference and hence the absorption due to the film only was obtained. The band gap of the films was calculated from the absorption edge of the spectrum. The absorbance coefficient increases with increasing *Sn* doping for the entire wavelength range. Increase of absorbance implies decrease of transmittance

which might be due to enhanced thickness due to *Sn* incorporation. Band gap energy was derived from the mathematical treatment of the data obtained from the absorbance vs. wavelength spectrum for direct band gap ZnS using Tauc's relationship. The sharp absorption edge corresponding to the band gap confirms the good quality of the films. The band gap energy increases from ~3.69 eV for ZnS to ~3.90 eV for 5% ZnS: Sn indicating a blue shift. Incidentally the band gap of tin sulphide is much lower than that of zinc sulphide and thus incorporation of tin should have caused red shift in band gap.

Dependence of photoluminescence spectra of ZnS films on the excitation wavelength has been investigated. A redshift has been observed with increase of excitation wavelength which may be due to different contribution of excitonic emissions and their phonon replicas. The intensity of the peaks decreases with excitation wavelength.

STRUCTURAL ANALYSIS OF VAL-TRP DIPEPTIDE

Rahimzade S.G., Akverdieva G.A.
Institute for Physical Problems, Baku State University, Baku, Azerbaijan
sararahimzada@bsu.edu.az

The Val-Trp dipeptide is effectively used in the treatment of hypertension, chronic kidney and heart disease. Despite the interest in the pharmacological activities of this dipeptide up to the present no theoretical studies of its structural characteristics have been reported yet.

The present study of Val-Trp dipeptide has been performed using molecular mechanics framework, followed by AM1 and PM3 quantum chemical methods. The geometry and energy parameters, dipole moment, HOMO and LUMO energies, energy gap (ΔE) were calculated for stable structures of the title molecule. The results showed that conformations with folded and extended form of backbone are realized for this molecule. The qualitative and quantitative differences of the most stable conformations of two characteristic shapes of this dipeptide were evaluated.

The stability of dipeptide is found to be very sensitive to the positions of the side chains of the aminoacid residues. It was revealed that the folded conformation is stabilized by formation of hydrogen bonds between the hydrogen related by the peptide bond with the nitrogen atom of the main chain of Trp residue and two oxygen atoms of the C-terminal carboxyl group, and the extended conformation is stabilized by formation of hydrogen bonds between the terminal amine cation and the oxygen related by the peptide bond with the carbon of the main chain of Val residue. The results showed that both characteristic structures of dipeptide have large energy gap, that indicate this dipeptide is a hard molecule. The calculations identified the different features of the electronic structure of two characteristic favorable conformations of Val-Trp dipeptide. The conformational differences cause the electron redistribution, and consequently, affect the electron population, the orbital energies and, as result, the effective charges on the atoms. The redistribution of charges as a result of folding of the peptide chain leads to a decrease in the dipole moment.

It is concluded that the both used quantum chemical methods are sensitive to the changes in the charge distribution on atoms and as result to the changes in the dipole moments, depending on the conformational rearrangements of the peptide chain of the investigated molecule.

SPATIAL STRUCTURE OF THE EXORPHINC MOLECULE

Agayeva L.N. [1], Abdinova A.A. [2], Akhmedova S.R. [3], Akhmedov N.F. [1]
[1]matter structure departament, Baku State University, Baku, Azerbaijan
[2]Azerbaijan State Pedagogical University, Baku, Azerbaijan
[3]Azerbaijan Technical University, Baku, Azerbaijan
leylanamiq@mail.ru

We have investigated the structural and functional organizations of the opioid peptides enkephalins, endorphins, endomorphins, dynorphins, neoendorphins and adrenorphins, and we are currently investigating the spatial structure of molecules of rubiscolins, soymorphins and casomorphins. This work is a continuation of our previous research.

The molecule was calculated using the theoretical conformational analysis method. The potential function of the system is chosen as the sum of non-bonded, electrostatic and torsion interactions and the energy of hydrogen bonds. Nonvalent interactions were assessed by Lennard-Jones potential. Electrostatic interactions were calculated in a monopole approximation according to the Coulomb's law using partial charges on atoms. The conformational possibilities of the exorphin C molecule were studied under the conditions of the water environment.

The energy of hydrogen bonds was estimated using the Morse potential. The three-dimensional structure of the exorphin - C molecule (Tyr1-Pro2-Ile3-Ser4-Leu5-OH) was investigated based on the low-energy conformations of the corresponding amino acid residues. The calculation results show that the conformations of eight shapes eeef, efee, efef, efff, eeff, effe, eeee and eefe fall into the relative energy range of 0–3 kcal/mol. The energy of non-valence interactions in low-energy conformations changes in the energy range (-18.2) - (-15.7) kcal/mol, electrostatic interactions (-0.4) - (1.7) kcal/mol, torsion interactions (3.1) - (4.5) kcal/mol. The relative energy range 0 - 5.0 kcal/mol contains 12 conformations of the eeef shape, 10 conformations of the efee shape, 12 conformations of the efef shape, and 15 conformations of the efff shape. The global conformation of the exorphin-C molecule is the $B_3BB_{22}R_{12}R_{32}$ conformation of the eeef shape. The conformation is advantageous in terms of non-bonded and torsion interactions. Effective di- and tripeptide interactions appear in this conformation, Tyr1 effectively interacts with the dipeptide fragment Pro2-Ile3, the contribution of which is (-9.5) kcal/mol, also Ile3 with Ser4 and Leu5, which contributions are (-4.7) kcal/mol and Ser4-Leu5 (-2.8) kcal/mol. The $B_3RB_{32}B_{32}B_{31}$ conformation of the efee shape has a relative energy of 0.1 kcal/mol. In this conformation, Tyr1 effectively interacts simultaneously with all subsequent amino acid residues, which contribution is (-12.7) kcal/mol, also Pro2-Ile3 with Ser4-Leu5, which contribution is (-7.4) kcal/mol. The $B_3RB_{32}R_{32}R_{31}$ conformation of the efef shape also has a relative energy of 0.1 kcal/mol; it differs from the previous conformation in the shape of the Ser4 and Leu5 backbones. Therefore, the energy contribution of amino acid residues to the total energy is almost the same as the previous conformation. The $B_3RR_{12}R_{32}R_{31}$ conformation of the efff shape has a relative energy of 1.8 kcal/mol, is advantageous in

terms of non-valence interactions, and not favorable in terms of electrostatic interactions. In this conformation strong interactions of the Tyr1 residue with the Pro2-Ile3-Ser4-Leu5 residues arise.

INFLUENCE OF A HIGH-FREQUENCY ELECTRIC FIELD (50 HZ) ON BLOOD PLASMA WITH THE PATHOLOGY OF B-THALASSEMIA

Dadashov M.Z.
Institute of Biophysics of the NAS of Azerbaijan, Baku, Azerbaijan
mursald@mail.ru

b-thalassemia is one of the hereditary hemoglobin pathologies in the world, and 17% of newborns are born with this pathology. Up to 3.4% of babies with such pathologies end their lives in the first 5 years, while others need regular blood transfusion and taking of iron-containing drugs during their lifetime. In some regions of the ourRepublic frequency of the gene carriers of this disease is more than 20%. According to the Ministry of Health, about 300 children are born with homozygous thalassemia (thalassemia major) pathology every year in our republic, and currently the number of patients with such b-thalassemia is about 1800, and the number of people registered with this disease is increasing year by year. One of preventive measures is the protection of the population from adverse environmental factors of anthropogenic origin, since adverse environmental factors cause oxidative stress in organisms. Resistance to oxidative factors in people with thalassemia is less pronounced than in healthy people, and in these people, there is an autoxidation of hemoglobin, lipid peroxidation, protein oxidation, lysis of erythrocytes, etc. violations are associated with oxidative stress. Low-frequency electromagnetic waves (ELF EMF) generated by anthropogenic origin, covering of industrial frequency (50/60 Hz) power lines, electrical devices and wireless irradiators in homes and workplaces are one of the unfavorable environmental factors as a result of the rapid development of energy and tele-radio-communication technologies. It is shown that these waves cause oxidative stress in erythrocytes, mitochondria, liver, kidneys, and nerve cells, causing leukemia in

young organisms. The "depth“of the resulting oxidative diversion depends on the frequency, intensity, duration of exposure, characteristics of the affected cells and other factors. Lipid peroxidation, protein oxidation, superoxydismutase (SOD) and catalase activity of antioxidant enzymes in plasma were studied in blood plasma samples (10 samples) of practically healthy and (10 samples) people with homozygous B-thalassemia affected by 50 Hz high voltage EMS 10 and 20 kV/m intensities for 2 hours. Measurements were made on the SF-46 spectrophotometer. Blood samples were taken from the Research Institute of Hematology and transfusion. In the statistical calculations, the average value and standard deviations were determined and compared using the t-student method. Statistical validity was taken as $p<0.05$. The results showed that in patients with thalassemia, plasma samples are more sensitive to peroxidation at 1-and 2-hour exposures, which manifests itself in a higher MDA content compared to healthy people, a more significant rise after a 2-hour effect is observed by ~22%. The same situation is also observed in the increase in carbonyl groups in plasma proteins, this indicator demonstrates higher indicators at 2-hour exposure than in healthy human blood samples, which indicates that thalassemia plasma proteins are more susceptible to oxidative damage caused by the action of the electric field. Activity of catalase increase in insufficient, and activity of SOD statistically significant difference was not observed. The obtained results show that low-frequency EMF is dangerous to human health, as well as these effects are more harmful for patients with thalassemia.

EVOLUTION OF POLARIZED MUON-PHOTON SHOWER IN CRYSTALS WITH THE ACCOUNT LINEAR POLARIZATION OF γ − QUANTA AND LONGITUDINAL POLARIZATION OF MUONS

Rajabov M.R.
Baku State University, Baku, Azerbaijan
m_rajabov@mail.ru

Modern accelerator technology and existing modern muon detectors allow interesting non-elastic electromagnetic interaction of high-energy electrons, muons and $\gamma-$quanta with atoms and nuclei of matter.

When high-energy charged particles and $\gamma-$quanta pass through matter, In addition to separate acts, they give birth to shower structures under certain conditions. These shower structeres are continuously directed jets of various particles, such as, charged particles in solid and qas meters, muon-photon shows in amorphous and crystal environments, nucleon cascades in nuclear matter. Electromagnetic showers resulting from interactions of high energy particles with atom nuclei in crystal environment are main source of electron, positron and photon beams of high energy and also are excellent tool for investigation of matter structure and electromagnetic particles with atom nuclei in crystal environment properties of nuclei.

This article is devoted to a theoretical study of the development of a muon-photon shower with the account the linear polarization of quanta and helicities of muons, which is directly related to the problem of radiation protection of superconducting magnetic systems of accelerators of new types. Analytical expressions that we obtained for the distribution of shower leptons and $\gamma-$quanta are

$$P(E_0,E,t)=\frac{V\,exp(\,sy-\lambda t)}{s\sqrt{-2\pi\lambda^{''}t+1/s^2}}$$

$$\Gamma(E_0,E,t)=\frac{W\,exp(\,sy-\lambda t)}{s\sqrt{-2\pi\lambda^{''}t+1/s^2}}$$

here s-is Laplas-Mellin parameter, E_0, E- are initial and current energies of shower particles, t is depth of penetration, V, W, y –are some functions of depending on s, initial energy of particles and initial conditions.

BACKWARD BREMSSTRAHLUNG OF MUONS WITH ACCOUNT THE OF POLARIZATION PARTICLES AND RECOIL EFFECTS

Rajabov M.R.
Baku State University
m_rajabov@mail.ru

The processes of bremsstrahlung of polarized electrons and photo-production of $\mu^+\mu^-$ — pairs on nuclei are the main sources of polarized photon, muon beams.

These processes are successfully adopted for the study of the electronic structure of nuclei and hadrons. In the processes under consideration, part of the energy and momentum of an incident high-energy electron (or $\gamma -$ quanta) can be transferred to the target nucleus, which can lead to the excitation of nuclei, change the distribution of the charge and magnetic moment of the nucleus, cause changes in the spectrum of gamma quanta and lepton pairs, and affect the polarization characteristics particles.

Along with direct bremsstrahlung, the process of inverse bremsstrahlung of a muon on nuclei can be used to study the electromagnetic properties of nuclei and hadrons.

This article is devoted to the study of the backward bremsstrahlung of a muon on nuclei, with account the polarization of the particles and the recoil energy. The reaction probability has the following form:

$$dW = A(F_0 + \lambda_1\lambda_2 F_1 - \xi\lambda_1 F_2 - \xi\lambda_2 F_3)$$

Here A is some factor depending on the inelastic structure function of the nucleus and the recoil momentum, the helicities of the initial and final muons and the Stokes parameter for the photon, Fi (i = 0,1,2,3) are the partial functions.

THE INVESTIGATION OF OPTICAL CHARACTERISTICS OF $Ni_{1-x}Zn_xFe_2O_4$ NANOPOWDERS

Sadıgova A.A., Alıyeva Sh.N., Mehdıyev T.R.
Institute of Physics, ANAS, Baku, Azerbaijan
a.elesgerqizi@mail.ru

The optical and UV-VIS luminescent spectra of $Ni_{1-x}Zn_xFe_2O_4$ ferrite nanopowders with x = 0;0,25;0,4;0,5;0,6;0,75;1,0 were investigated in 4000-50 cm^{-1} and 200-700 nm at room temperature with Vertex 70V (Bruker, Germany).. The features of the diffuse reflectance spectra of $Ni_{1-x}Zn_xFe_2O_4$ ferrites were analyzed by the Kramers-Kronig procedure.

The infrared spectra of all studied ferrite $Ni_{1-x}Zn_xFe_2O_4$ compositions are shown in fig 1. When analyzing the obtained spectra, it was found that their profiles have a complex structure and when changing the composition of the composition, not only a shift is noticeable, but also splitting into spectral components. The temperature in all the studies was equal to 300K.

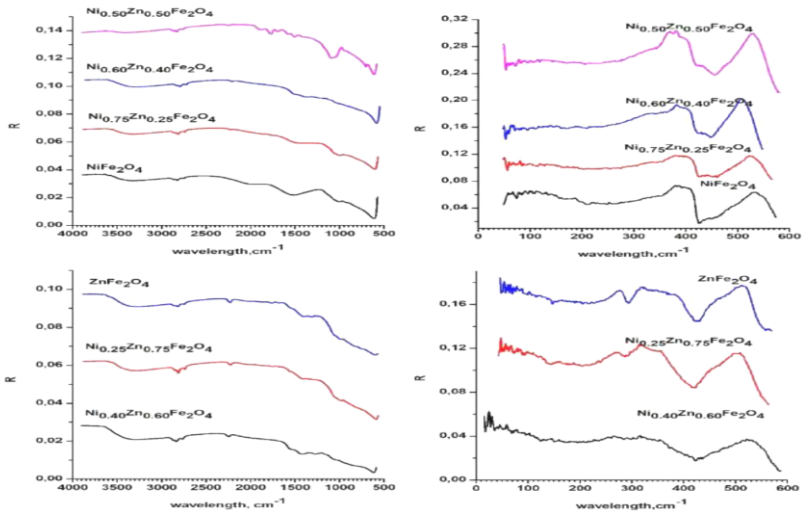

Fig. 1. Diffuse reflection IR spectra of $Ni_{1-x}Zn_xFe_2O_4$ ferrites in 4000-700cm^{-1} and in 600-50cm^{-1}.

KINETICS OF IV→III POLYMORPHOUS TRANSFORMATION IN $Rb_{0,95}Cs_{0,05}NO_3$ SINGLE CRUSTAIS

Kazimova A.F.
Institute of Physics, ANAS, Baku, Azerbaijan
aygun-kazimova-1981@mail.ru

The crystal growth velocity of III-modification on temperature at IV→II transformation in $Rb_{0,95}Cs_{0,05}NO_3$ single crystals is measured by optical microscopy. It is shown that crystal growth velocity of III-modification in the dependence on temperature at empiric formula $\upsilon=(-0.49\Delta T+0.563\Delta T^2-0.0018\Delta T^2)\cdot 10\text{-}2$cm/sec where $\Delta T=T_{trans}+T_0$. The activation energy of transformation process IV→III which is equal to E=23,72 kcal/mol has been calculated.

The investigation results of morphology and crystal growth kinetics at polymorphous transformations in rubidium and cesium nitrates are given in work Cleaver B. and J.F. Williams. On the base of obtained data the new modification in investigated crystals has been revealed. As a result of investigations, the community of crystal growth mechanism of new modification inside matrix one in rubidium and cesium nitrates.

According data at enough high pressures the high temperature phases I and II of rubidium nitrates disappear and III phase stays as a high-temperature one. Thus, I and II phases disappear from solid solutions of cesium nitrate in rubidium nitrate at cesium salt concentration ~25mol%.

We are planning the series of investigations on morphology and kinetics of crystal growth for revealing of mechanism of polymorphous transformations in solid solutions of cesium nitrate in rubidium nitrate and the present work is dedicated to the one of such problems. This work is dedicated to investigation of kinetics of crystal growth of III modification as temperature function at IV→III transformation in $Rb_{0,95}Cs_{0,05}NO_3$.

GENERATION OF ULTRAHIGH FREQUENCY IN GAAS-TYPE SEMICONDUCTORS

Hasanov E.R.[1], Alimova T.A.[2]
[1]Baku State University
[2]Physical Institute, ANAS, Baku, Azerbaijan
turkan5@list.ru

The current oscillations in an external electric field in GaAs-type two-valley semiconductors for the first time are studied by Gunn. On the basis of this effect the energy generators were constructed. The energy radiation of a super high frequency ($\omega \sim 10^9 - 10^{11}$) occurs at the certain value of the dc electric field. The critical values of an electric field at which the energy radiation begins, are found in many works, including [2]. The Gunn Effect mechanism is investigated in [1, 2]. The authors of these works point out that in GaAs and InP with increasing of the external electric field the charge carriers with smaller energies are passed into high – lying energy band.

When the number of the charge carriers exceeds any certain magnitude, a sample conductivity is decreased and a negative differential conductivity takes place:

$$\frac{dl}{dE} = \sigma_d$$

I is a current density and E is an intensity of an external field.

The carrier number in the lower valley will be equal to any part f of the full carrier number (N).

$$n = f(E)N, \text{ here } f(E) = \frac{m-1}{m-1\left(\frac{E}{E_0}\right)^m}$$

A parameter m is finded from experiment [3]. Ultrahigh frequency generation

$$I = I_1 + I_2$$

where I_1 and I_2 are the current densities in the first and second valleys

In the absence of the external fields the carrier concentrations in the valleys are $n_2 << n_1$, and $I_2 << I_1$. Then for total current we have

$$I = e\mu E - en\mu_1[EH] + ed\nabla n + eD[\nabla nH], \vec{I} = \partial(H_x, H_0, E_0)\vec{E}$$

With taking into account (4) on can write the equation (5) in the form:

$$\frac{\partial^2 R}{\partial t} + {\omega_0}^2 R = r\Phi\left(R, \frac{\partial R}{\partial T}\right), R = \frac{N_1}{N_0}, r = \frac{\omega_0}{k_x U_0} \ll 1$$

Applying the Bogolyubov – Mitropolsky method it is easy to find the current oscillation amplitude in the first approximation.
It follows from the calculations that the following inequalities are satisfied $H_1 < H_0 < H_2$

$$\text{Where, } H_1 = \frac{\sqrt{2m}}{m-1} H_x; \quad H_2 = H_x \frac{U_0}{k_x D}\left[\frac{\varepsilon m k_x U_0}{\sigma_0 (m-1)}\right]^2$$

That wave frequency $\omega_0 = \left[\frac{\sigma_0 k_x U_0 (m-1)}{m\varepsilon}\right]^{1/2} x$ decreases with increasing H_0.

MINIMAL COUPLING CONSTANT OF ρ MESON-Δ BARYON INTERACTIONS IN THE AdS/QCD SOFT WALL MODEL AT FINITE TEMPERATURE

Nasibova N.A.
Institute of Physics, ANAS, Baku, Azerbaijan
n.nesibli88@gmail.com

As known, QCD is a theory of strong interaction. AdS/QCD correspondence provides a scheme to solve strongly coupled gauge theories like QCD. Holographic QCD or AdS/QCD models are widely applied to predict the phenomenological quantities and to investigate other strong interaction problems in particle physics. It has hard- and soft- models. We have used the thermal soft-wall model. in the present work to study the temperature dependence of $g_{\rho\Delta\Delta}(T)$ coupling constant. We have studied this process corresponding zero-temperature limit. First of all, we have considered the soft-wall model with a thermal dilaton field as follows:

$$\Phi(z, \ T) = K(T)^2 z^2, \tag{1}$$

Where

$$K(T) = k * (1 + \Delta_T) \tag{2}$$

$$\Delta_T = -\frac{N_f^2 T^2 - T^2}{12 N_f F^2} - \frac{N_f^2 T^4 - T^4}{144 N_f^2 F^4}\,. \tag{3}$$

Here *F=0.087* is chiral decay constant, N_f *=3* is the number of quark flavors and scalar parameter *k=383*.

2. *ρ meson -Δ baryon minimal coupling constant.*

Meson-baryon coupling constant $g_{\rho\Delta\Delta}\,(T)$ is obtained from the action by including the thermal dilaton field. The corresponding action is given as follows [4]:

$$S = \int d^5x\ e^{-\Phi(z,T)}\sqrt{g}\,L \tag{4}$$

Here $\sqrt{g}$ is determinant of Schwarzschild metric. The minimal term of Lagrangian $\mathcal{L}^{(0)}_{\rho\Delta\Delta}$ is defined as below:

$$\mathcal{L}^{(0)}_{\rho\Delta\Delta} = \bar{\Psi}_1^{\nu}\Gamma^{\mu}V_{\mu}\Psi_{1\nu} + \bar{\Psi}_2^{\nu}\Gamma^{\mu}V_{\mu}\Psi_{2\nu} \tag{5}$$

The corresponding Lagrangian is taken into account in the action, then the expression of $g_{\rho\Delta\Delta}\,(T)$ takes the following form:

$$g^{\,y/d}_{\rho\Delta\Delta}(T) = -\int_0^{\infty}\frac{dz}{z^2}V_0(z,T)\left[\left|f_{1L}^{(n)}(z,T)\right|^2 + \left|f_{1R}^{(n)}(z,T)\right|^2\right] \tag{6}$$

Here, $V_0(z,T)$ is profile function of vector meson is defined as follows:

$$V_0(z,T) = \sqrt{\frac{2\Gamma(n+1)}{\Gamma(n+m+1)}}K_T^{m+1}z^{m+\frac{1}{2}}e^{-\frac{K_T^2 z^2}{2}}L_n^m(K_T^2 z^2), \tag{7}$$

m is defined *m=N+L-1, N* is the number of partons of the meson, *L* is the orbital angular momentum. So, for *ρ* meson m=1.

$f_{1L/1R}^{(n)}(z,T)$ are the left- and right- profile functions of fermions at finite temperature in Eq. (6) and defined as follows:

$$f_n^{L,R}(z,T) =$$

$$= \sqrt{\frac{2\Gamma(n+1)}{\Gamma(n+m_{L,R}+1)}} K_T^{m_{L,R}+1} r^{m_{L,R}+\frac{1}{2}} e^{-\frac{K_T^2 z^2}{2}} L_n^{m_{L,R}}(K_T^2 z^2). \qquad (8)$$

Where for baryons m_L=1 and m_R=2.

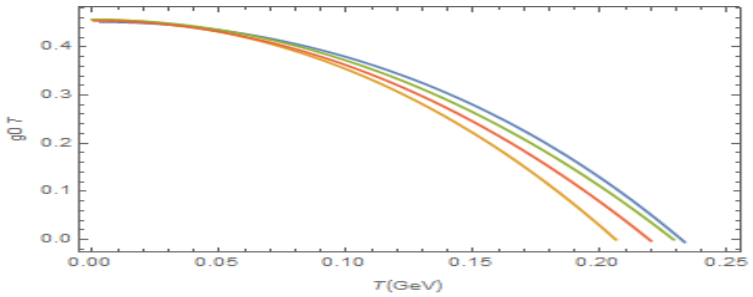

Fig. 1. The temperature dependence of $g^0_{\rho\Delta\Delta}(T)$ for N_f=2, F=87 MEV (blue), N_f=3, F=100 MEV (green), N_f= 4, F=130 MEV (red), N_f= 5, F= 140 MEV (yellow).

DEUTERON PROFIL FUNCTION IN HARD-WALL MODEL OF ADS/QCD

Huseynova N.J., Mamedov Sh.A.
Baku State University, Baku, Azerbaijan
nerminh236@gmail.com

One of two stable isotopes of hydrogen is Deuterium (D), which also is known as a heavy hydrogen. The nucleus of a deuterium atom, called a deuteron consists of one proton and one neutron, whereas the far more common Protium has no neutrons in the nucleus. Deuterium is destroyed in the interiors of stars faster than it is produced. Deuterons are formed chiefly by ionizing deuterium (stripping the single electron away from the atom) and are used as projectiles to produce nuclear reactions after

accumulating high energies in particle accelerators. A deute-ron also results from the capture of a slow neutron by a proton, accompanied by the emission of a gamma photon.

In this work, deuteron is studied in the framework experimental and theoretical approaches of elementary particle physics. We study profile function of deuteron in hard-wall model of the Anti-de Sitter (AdS)/Quantum Chromodynamics (QCD), where the confinement and chiral symmetry breaking propers of QCD and finiteness condition of the 5D action is constructed by cut off the AdS space at Infrared boundary.

We present profile function of the deuteron in the framework of hard-wall AdS/QCD mo-del. First, we construct an effective bulk action, which describes the interaction for free deuteron fields. Guided on this action according to classical field theory, we write Lagrange-Euler equation for the free deuteron field. Appling Kaluza-Klein decomposition from the Euler-Lagrange equa-tion we obtain an equation over the additional coordinate for the deuteron wave function. Having solved the equation of motion we find profile function for the deuteron in the framework of hard-wall model of AdS/QCD.

CONTENT

Printed: 14.12.2021
Volume 13.75 p.s.. Amount 150

Baku State University publising hause.
www.bsu.edu.az
Baku., ac. Z. Khalilov. 33
Tel: (+99412) 538 87 39 / 538 50 16
e-mail: bdumetbee@gmail.com